MODELING OF THE SOLAR RADIATION OUTPUT IN THE DEMOCRATIC REPUBLIC OF CONGO

By

Lusamba Yangindu Dieudonné

Submitted

to

The University Of South Africa

College Of Science, Engineering And Technology

School Of Engineering

Department Of Electrical Engineering And Smart Systems

A dissertation submitted in partial fulfillment of the requirement for the degree of Master of Engineering at the University of South Africa

Master of Engineering in Electrical Engineering

Supervisor: Professor Mbuyu Sumbwanyambe

Johannesbourg, South Africa

April 2026

MODELING OF SOLAR RADIATION OUTPUT IN THE DEMOCRATIC REPUBLIC OF CONGO

Abstract

The Democratic Republic of Congo is not only a geological contrast but also an energy contrast, as it possesses a great hydroelectric potential capable of satisfying its own needs and those of many African countries. However, according to the most optimistic studies, the electrification rate in the Democratic Republic of Congo is less than 19%. Photovoltaic solar energy therefore represents a viable solution to help meet national energy needs. Accurate knowledge of solar irradiance is essential for proper sizing and optimization of photovoltaic systems.

This study aims to establish general statistical models to predict solar irradiance (kWh/m²/day) as a function of sunshine duration (h/day) for any province of the Democratic Republic of Congo. Global solar irradiance data were obtained from RETScreen through the Renewable Energy Atlas of the DRC, while sunshine duration data were collected from the European Centre for Medium-Range Weather Forecasts. Five models (linear, quadratic, cubic, logarithmic, and exponential) were developed using the least squares method and validated using normalized statistical errors (NMAE, NMBE, NRMSE), the Nash–Sutcliffe efficiency criterion (NS), and the coefficient of determination (R^2).

Two scenarios were analyzed: scenario 1: excluding the provinces of Nord and Sud Kivu, and scenario 2: including these provinces.

By excluding these provinces, the quadratic and cubic models explained 88% and 93% of the relationship between annual average sunshine duration and solar irradiance, respectively. Including them reduced performance, with $R^2 \approx 0.70$, indicating that additional climatic variables may be required. A national sunshine duration heat map identifying four main exposure zones was also produced, supporting photovoltaic planning across the Democratic Republic of Congo.

Acknowledgement

I am very grateful to Lord for allowing me to conduct this study and completed that. I sincerely thank my promoter, Professor Mbuyu Sumbwanyambe, who accepted to supervise this work. I discovered in him a very attentive supervisor, who knows how to combine patience and roughness. I also thank Professors Edmond Phuku Phuati and Jean-Marie Tshitenge from the Department of Physics at the University of Kinshasa, who kindly agreed to discuss several scientific aspects of this study with me.

I am sorry of the death of Professor Paul Luhumbu Luwembo. I am grateful to him for encouraging me to start doctoral studies.

I thank Doctor Athanase Mulumba Bitakavula who, while I was looking for a promoter, guided me on the path of Professor Sumbwanyambe.

My thanks to pastor Yvan Ngalamulume for his disposal to guide me in correcting.

My brother Michel Ilunga Yangindu was a great support to me for several formalities related to my registration at the University of South Africa. I am very grateful to him.

To Astrid Kanyeba Yangindu, my loving wife and to my children: Samuel Ilunga Yangindu, Débora-Julianna. Betu Yangindu and Faveur-Divine Kanyeba Yangindu, I also say thank you for their encouragement.

Thanks to my parents Liévin Ilunga Yangindu and Victorine Kabimanya, for their encouragement. My thanks brothers Danny Bapebabo, Georges Mukeba, Boniface Wakuteka, Etienne Kamba, Séraphin Lukusa and my sister Marthe Njiba.

Pastor Florent Musiteki, my pastor, encouraged me to do the Master's and break into the path of knowledge. I am entirely grateful to him.

Chapitre 1 Contents

List of figures

List of tables

Nomenclature

D_n	Rank occupied by any day of the year
$\bar{H}$	Horizontal global solar radiation for a day completely covered [by the cloud]
$\bar{H}_c$	Global solar radiation for a cloudless sky
$\bar{H}_0$	Solar radiation outside the atmosphere
I_{bn}	Direct irradiation on a normal surface
I_{bT}	Direct irradiation on a surface of inclanation ß
I_{dh}	Irradiation received on a surface inclined at an angle β
k	Ratio between the horizontal global solar radiation received during a day
$\bar{S}$	Daily sunshine duration
$\bar{S}_0$	Extrterrestrial daylight hours
T_L	Link Turbidity
τ	Atmospheric transmittance

Acronyms

AASD	Annual Average of Sunshine Duration
AA	Anual Average
AU	Astronomical Unit
ADPI	Agence pour le Développement et la Promotion du Projet grand Inga
CIMO	Commission for Instruments and Methods of Observation
CTS	Calculation Time Step
ECMWF	European Centre for Medium Range Weather Forecasts
GHI	Global Horizontal Irradiation
GSI	Global Solar Irradiation
ITCZ	Intropical Convergence Zone
LCOE	Levelized Cost of Electricity
MAE	Mean Absolute Error
MASD	Monthly Average of Sunshine Duration
MBE	Mean Bias Error
PMA	Province Monthly Average
RE	Relative Error
RSME	Root Quare Mean Error
SD	Sunshine Duration
SI	Solar Irradiation
SMA	Site Monthly Avrage
SMFT	Start of Meteorological File Time
SNEL	Société National d'Electricité
UNDP	United Nations Development Program
WMO	World Meteorological Organization

CHAPTER 1: GENERAL INTRODUCTION

1.1 Background

In the Democratic Republic of Congo (DRC), the energy needs are predominantly derived from the hydropower through the Congo river. This generation constitutes approximately 85% of the total energy consumption. Note that in this other forms of energy though being generated are not as consumed as hydro power. Against all the other forms of energy generation, that is Biomass, solar, wind and the rest, hydro Electricity accounts for only 15% of the overall energy mix, with a 19.1% share in urban areas and a mere 1% in rural areas [1]. This disparity highlights the significant energy access gap between urban and rural populations. The country primary electricity provider, which is the "Société Nationale d'Electricité" (SNEL), is responsible for 93% of the total electricity and energy supply within the DRC. Most of this electricity is generated from hydropower, mainly sourced from the Congo River and other rivers across the country. Despite the substantial hydropower potential, the electricity access rate remains critically low, particularly in remote areas where grid extension is challenging.

With an annual population growth rate of 3.2% [2], the demand for energy is anticipated to increase proportionally, placing even greater pressure on the already fragile energy infrastructure. The country's hydroelectric generation, transmission, and distribution networks are severely strained, and without major investments in modernization, the situation is unlikely to improve. In rural regions, where grid expansion is unfeasible in the short term, communities often rely on biomass-based energy sources, particularly firewood and charcoal. However, the overexploitation of biomass contributes to deforestation, soil degradation, and increased greenhouse gas emissions, further exacerbating environmental challenges in the DRC.

Considering that only 15% of the energy demand is currently met by electricity, it is highly improbable that SNEL will be able to bridge this gap within the next 5 to 10 years. The financial resources required for large-scale infrastructure expansion far exceed the capabilities of both SNEL and the Congolese government. Therefore, alternative Renewable Energy Technologies (RETs) that do not depend on traditional grid connections must be explored.

One promising approach is the development of micro-hydropower stations, which could harness the vast but underutilized hydroelectric potential available in the DRC. However, given

the country's vast geographical size of 2,345,410 km², a significant portion of the population remains unconnected to the existing grid. For these isolated regions, solar energy emerges as a viable alternative, offering decentralized, clean, and sustainable power solutions that could help alleviate the ongoing energy crisis.

1.2 Definitions of Key Solar Terms

To ensure clarity and consistency in the analysis and discussion of solar resources across the DRC, the following definitions are adopted throughout this study. These definitions cover the key solar parameters relevant for solar energy assessment, physical analysis, and photovoltaic system planning. These definition are summarized in Table 1.1.

Table 1.1: Key Definitions of Key Solar Terms

Term	Definition	Unit / Notes
Solar Radiation	Total energy emitted by the Sun across the full electromagnetic spectrum, reaching the top of the atmosphere or the Earth's surface.	W/m²
Solar Irradiance (SI)	Instantaneous solar power per unit area on a surface perpendicular to Sun rays; measures the intensity of solar radiation at a specific moment.	W/m²
Solar Irradiation (Solar Energy)	Total solar energy received per unit area over a time period; the temporal integration of irradiance, indicating solar resource availability.	kWh/m², MJ/m²
Direct (Beam) Radiation	Portion of solar irradiance traveling straight from the Sun to the surface without atmospheric scattering.	W/m²
Diffuse Radiation	Solar irradiance scattered by molecules, aerosols, or clouds, arriving at the surface from all directions.	W/m²

Term	Definition	Unit / Notes
Global Horizontal Irradiance (GHI)	Total irradiance on a horizontal surface, combining direct and diffuse components; key for PV system design.	W/m²
Sunshine Duration (SD)	Number of hours when direct irradiance exceeds a threshold (typically 120 W/m²), providing a practical measure of solar availability.	hours/day
Albedo (Surface Reflectivity)	Fraction of incoming solar radiation reflected by a surface, affecting net radiation at ground level.	Dimensionless (0–1)
Atmospheric Opacity / Transmissivity	Opacity: fraction of solar radiation absorbed or scattered by the atmosphere. Transmissivity: fraction reaching the ground.	Dimensionless (0–1)
Photovoltaic (PV) Yield	Electrical energy generated per unit of incident solar irradiation on PV panels; essential for solar resource assessment.	kWh/kWp

1.3 Problem statement

Photovoltaic solar energy presents a promising solution to address the persistent electrification deficit in many households across the DRC. However, designing and optimizing photovoltaic systems requires accurate solar radiation data, which is not readily available for all locations. As a result, there is a critical need for reliable models to estimate solar radiation based on accessible data. Currently, no model exists that can simulate solar radiation for any province of the DRC with sufficient accuracy.

A central research question of this study is whether daily sunshine duration can effectively predict solar radiation across all DRC provinces. Existing literature on solar radiation for the country is limited and generally provides only broad mappings of sunshine, offering basic indications of solar potential across provinces. There is a clear gap in models that simulate solar radiation at specific sites using average annual or monthly sunshine duration data.

This study seeks to address this gap by developing statistical models capable of predicting the yearly mean of global solar radiation on a horizontal plane for any province in the DRC. In addition, it aims to create a map of yearly mean sunshine duration and analyze its spatial variation across the country. Understanding this mapping provides a foundation for interpreting daily sunshine characteristics and guides further investigation into the factors that influence solar radiation variability.

By tackling these challenges, the study offers a practical approach to support solar energy planning and the deployment of photovoltaic systems, particularly in regions where ground-based solar measurements are scarce or nonexistent.

1.4 Research gap

Previous studies have developed linear and nonlinear models to estimate global solar radiation from sunshine duration, including the Angstrom–Prescott model [3, 4], the quadratic model of Ögelman [5], and the exponential model of El-Metwally [6]. These models have been widely applied in several African countries such as Algeria [7, 8, 9], Nigeria [10], Chad [11], and Cameroon [12].

However, most of these models are developed for specific climatic zones and rely on locally calibrated coefficients. Their direct application to the DRC remains questionable due to its vast geographical extent, equatorial positioning, and heterogeneous climatic conditions [13, 14, 15].

Although the 2014 Renewable Energy Atlas of the DRC provides a spatial description of solar potential [13], no generalized statistical model has been developed to establish a national relationship between sunshine duration and global solar radiation across all provinces. This gap justifies the present study.

1.5 Objectives of study

The main objective of this study is to improve the design and sizing of solar photovoltaic (PV) systems in the DRC by establishing a reliable statistical relationship between global solar irradiation (GSI) and daily sunshine duration (SD) for all provinces. Accurate estimation of

solar irradiation is essential due to the country's vast geographical extent and heterogeneous climatic conditions, providing a practical and cost-effective approach to solar resource assessment, especially in remote and underserved areas [13, 14].

The specific objectives are as follows:

i. Predict global solar irradiation across the DRC using provincial daily sunshine duration data.

ii. Analyze correlations between daily sunshine duration and key meteorological variables, including humidity, rainfall, maximum temperature, and minimum temperature, to identify factors significantly influencing solar irradiation.

iii. Develop a national map of annual mean sunshine duration, which will serve as a reference for solar resource distribution and as a tool to guide future research and planning for PV system deployment.

iv. Validate statistical models using normalized errors (NMAE, NMBE, NRMSE), Nash–Sutcliffe efficiency (NS), and the coefficient of determination ($R^2 \geq 0.7$) [16] to ensure predictive accuracy and applicability across all provinces.

By achieving these objectives, the study will provide both theoretical insights into solar irradiation variability in the DRC and practical guidance for engineers, policymakers, and researchers in designing, optimizing, and deploying photovoltaic energy systems nationwide.

1.6 Methodology

This study adopts a quantitative approach aimed at establishing statistical relationships between the annual mean SD (independent variable) and the annual mean GSI (dependent variable) for each province of the DRC [17].

SD data (1999–2019) are sourced from the European Centre for Medium-Range Weather Forecasts (ECMWF) [14], while SI data are obtained from the RETScreen database [13]. These reliable secondary sources cover the entire territory of the eleven former provinces, ensuring comprehensive representation of the different climatic zones.

Given the scarcity of direct solar irradiation measurements, SD is used as a proxy variable to estimate irradiation levels. The raw data undergo pre-processing to ensure accuracy and consistency, including handling missing values, detecting outliers, and normalization where necessary.

At the provincial level, the weighted mean SD ($\bar{S}$) is calculated by considering administrative subdivisions (districts, territories, cities) to accurately reflect territorial variability [18, 19, 20]. The calculation follows the formula:

$$\bar{S} = \frac{\sum A_i S_i}{\sum A_i} \tag{1.1}$$

where A_i represents the area of the subdivision and S_i its annual mean SD.

For statistical analysis, MATLAB is used to develop five models: linear, quadratic, cubic, logarithmic, and exponential. Local coefficients are determined by comparing the relationships obtained with models available in the literature. Model performance is evaluated using the coefficient of determination ($R^2 \geq 0.7$), along with normalized error metrics: NMAE, NMBE, NRMSE, and the Nash–Sutcliffe efficiency (NS) [21, 22].

Two scenarios are considered:

— Sceanrio 1: Excluding the Grand Kivu provinces to avoid biases due to particular climatic conditions.
— Sceanrio 2: Including all provinces to assess the effect of regional variations on model performance.

Figure 1.1. Workflow of the proposed methodology used to estimate global solar radiation from sunshine duration across the provinces of the DRC.

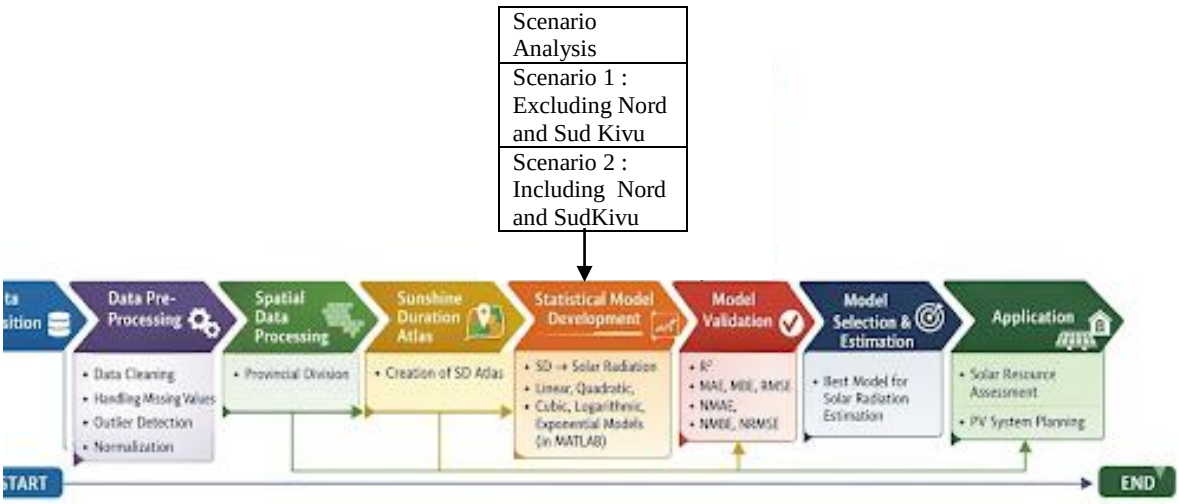

Figure 1.1: Workflow of the proposed methodology

The overall methodological framework adopted in this research is summarized in Figure 1.1. describes the sequential process from data acquisition and preprocessing to statistical modelling, validation, and application for photovoltaic energy planning.

1.7 Approach, Hypotheses, and Significance

1.7.1 Approach

This study establishes a statistical relationship between the annual mean daily sunshine duration ($\bar{S}$) and the annual mean global solar irradiation ($\bar{H}$) on a horizontal surface for all provinces of the DRC. The approach accounts for regional variations to ensure precise estimates across the entire territory.

1.7.2 Testable hypothesis:

Main Hypothesis (Solar Irradiation): Daily SD is the primary factor influencing the GSI incident on a horizontal surface. Other meteorological factors (humidity, temperature, cloud cover) are considered secondary [21, 23].

1.7.3 Significance of the study

This study offers a dual significance, encompassing both theoretical and practical dimensions. From a theoretical perspective, it provides robust statistical models to understand

the spatial and temporal variability of SI in the DRC. These models compensate for the lack of direct measurements and enrich the literature on solar resource assessment [13, 14, 23].

On a practical level, this study enables photovoltaic system designers to simulate annual SI for any province, improving the sizing and optimization of installations. The models also support energy planning and policymaking for the deployment of renewable energy in remote areas.

The combination of a rigorous statistical modeling, validation through normalized indicators, and regional analysis ensures that the results are reliable, applicable, and scientifically sound for solar energy assessment and planning in the DRC.

1.8 Positioning of the Present Work with respect to Prior Publications

This dissertation builds upon preliminary work presented in IEEE PowerAfrica Conference (PAC 2024). While those publications introduced initial findings on SD–GSI relationships, and some spatial and climatic factors influencing SD in the DRC, they were limited in scope and geographical coverage. This study advance prior works by explicitly integrating spatial heterogeneity into the modeling framework, resolving the apparent paradox of Sud Kivu, where high SD coincides with comparatively low global solar irradiation, and by demonstrating how the resulting models inform PV system planning and energy deployment strategies across the 11 former provinces of the DRC.

These results call into question the validity of uniforme SD-GSI parameterizations at the national scale and highlight the nevessity of spatially adaptive modelling frameworks for reliable solar energy planning in tropical regions. As such, this dissertation should be regarded as the complete and consolidated version of the research, offering a deeper and more rigorous scientific contribution.

1.9 Structure of the study

This dissertation is organized into six chapters, following a logical and coherent progression from contextual analysis to statistical modeling and validation, in accordance with the research objectives.

Chapter 1 introduces the general background of solar energy assessment in the DRC. It presents the research problem, identifies the existing research gap, formulates the study objectives, and outlines the methodological approach. This chapter establishes the theoretical and scientific framework of the study and clearly defines the hypothesis guiding the research.

Chapter 2 reviews the relevant literature on the estimation of global solar radiation from sunshine duration. It presents classical empirical models, including linear and nonlinear formulations, and discusses their applicability in different climatic contexts. This review provides the theoretical foundation for the statistical modeling developed later in the study.

Chapter 3: Spatial Characterization of Sunshine Duration and Solar Potential in the DRC
This chapter describes the spatial distribution of annual mean sunshine duration and solar potential across the national territory. It provides a geographical overview of solar resource availability and establishes the spatial context necessary for statistical modeling. The analysis highlights regional contrasts and identifies the main patterns of solar potential across provinces.

Chapter 4: **Spatial and Climatic variables influencing Sunshine Duration in the Democratic Republic of Congo**
This chapter examines the main spatial and climatic factors affecting SD across the DRC, focusing on Longitude, Maximum and Minimum temperatures, relative humidity, and rainfall. Correlation coefficients were established between each of these factors and the annual SD, providing a quantitative assessment of how they influence solar exposure in each province. These results form a critical foundation for developing reliable solar irradiation models in the following chapters.

Chapter 5: Statistical Modeling and Validation of the SD–SR Relationship
This chapter constitutes the scientific core of the dissertation. It presents the statistical models developed to establish the relationship between SD and GSI. Linear and nonlinear formulations are introduced, and the least squares method is applied to determine model coefficients. The performance of the models is evaluated using statistical indicators such as the coefficient of determination (R^2), MAE, MBE, RMSE, and Nash–Sutcliffe efficiency. Two modeling scenarios are analyzed to assess the robustness of the results. The chapter emphasizes methodological rigor, and concision, focusing on model performance and validation.

Chapter 6: General Conclusion and Perspectives

This final chapter synthesizes the main findings of the study and provides a response to the research problem and objectives. It discusses the scientific and practical contributions of the established models, identifies the limitations of the study, and outlines perspectives for future research in solar resource assessment and photovoltaic system optimization in the DRC.

1.10 Summary

The chapter 1 establishes the scope of the research by clearly defining its context and specifying the research problem. In view of the critical energy challenges in the DRC, where biomass dominates energy consumption and electricity access remains severely limited, particularly in rural areas, the study addresses this issue through the exploration of Renewable Energy Technologies (RET), with particular emphasis on photovoltaic solar energy.

Beyond the general energy context, this chapter identifies the scientific gap related to the limited availability of reliable solar resource assessment models adapted to the DRC. It therefore formulates precise research objectives aimed at establishing a statistical relationship between annual mean SD and annual mean GSI. This ensures that the research remains focused, coherent, and scientifically grounded.

The chapter also presents the working hypothesis and provides a detailed description of the methodological approach adopted in the study. It explains the tools used to collect, preprocess, and analyze data, as well as the statistical framework guiding the modeling process. This rigorous methodological foundation ensures the development of credible and validated solar irradiation models.

Finally, this chapter outlines the overall structure of the dissertation, ensuring a logical progression from contextual analysis to spatial assessment and statistical modeling. Each subsequent chapter builds upon this foundation and gradually leads to the establishment and validation of models for estimating annual mean global solar irradiation incident on a horizontal surface across the provinces of the DRC.

CHAPTER 2: LITERATURE REVIEW

2.1 Introduction

This chapter presents a critical review of the principal models used to estimate GSI, with particular emphasis on regression approaches based on SD. Rather than merely presenting general solar energy concepts, this chapter examines the theoretical foundations, methodological assumptions, statistical structures, and practical limitations of existing models. The objective is to evaluate their scientific robustness and their applicability to the climatic and geographical conditions of the DRC.

The review is structured in three complementary parts:

(i) the theoretical foundations related to solar geometry and extraterrestrial radiation,
(ii) regression models developed for estimating GSI on horizontal surfaces from SD data, and
(iii) a brief review of models used to estimate SI on inclined surfaces for photovoltaic applications..

Beyond a descriptive synthesis of previous works, this chapter seeks to identify methodological inconsistencies, geographical limitations, and gaps in spatial calibration. Particular attention is given to the transferability of regression coefficients across climatic zones. This analytical perspective is essential in order to justify the development of location-specific statistical models adapted to the spatial heterogeneity of the DRC.

2.2 Regression Models for Global Solar Irradiation on Horizontal Surfaces

2.2.1 Classification of solar radiation models

According to references [7, 13], solar radiation models can be systematically classified into three main categories: time-series and regression models, artificial intelligence models, and physically derived radiative transfer models, each reflecting different levels of complexity and data requirements.

Regression models constitute the methodological core of this study due to their simplicity, interpretability and Moderate data requirements.

Artificial intelligence models may offer high predictive performance but require large, high-quality datasets and advanced computational infrastructure [24, 25]. Physically derived models require detailed atmospheric inputs rarely available at national scale in developing countries.

However, regression models are inherently location-dependent, and their coefficients must be calibrated locally [26, 27].

2.2.2 Sunshine duration–based models

Numerous empirical and semi-empirical models have been developed to estimate global or diffuse SI on a horizontal surface using meteorological variables such as cloud cover, temperature, precipitation, relative humidity, and sunshine duration, or combinations of these parameters. Among these variables, SD has historically received particular attention due to its strong correlation with surface solar radiation and the relative availability of long-term sunshine records in many meteorological stations.

This section focus exclusively on models that describe GSI as a function of SD. This focus is motivated by practical and methodological considerations: in regions such as the DRC, long-term radiometric measurements remain scarce, whereas SD data are more widely available and sufficiently reliable. Hence, SD–based models constitute a parsimonious yet operationally robust framework for estimating GSI in data-limited environments

From a physical standpoint, variables such as cloud cover, relative humidity, and precipitation are known to directly affect the SD recorded at a given location [1, 13, 21]. Therefore, daily SD can be interpreted as an integrated indicator of atmospheric transmissivity. Several empirical studies confirm strong correlations between SD and GSI [28, 29, 30] justifying its use in empirical models.

However, the family of SD-SI empirical models presented in Equation (2.5)-(2.9) constitutes a progressive refinement of the functional relationship between SD and GSI on a horizontal surface [31, 32]. Beyond their mathematical formulation, each model embeds specifc physical assumptions that directly affect their suitability for PV system design and energy yield estimation [33].

2.3.2.1. The Angström–Prescott formulation

One of the earliest and most widely used models is the Angström equation [3], which expresses global solar radiation as a fraction of extraterrestrial radiation, modulated by the ratio of actual to maximum possible sunshine hours:

$$\frac{\bar{H}}{\bar{H}_C} = k + (1-k)\frac{\bar{S}}{\bar{S}_0} \tag{2.1}$$

In equation (2.1), the coefficient k is approximately 0.25, and the variables are defined as:

- H : average global solar radiation on a horizontal surface
- Hc : average solar radiation under clear-sky conditions
- n : measured daily sunshine duration
- N : maximum possible sunshine duration (astronomical day length)

2.3.2.2. Clearness index and modifications

The ratio between measured global radiation and extraterrestrial radiation, called the clearness index, quantifies the atmospheric transmissivity. Prescott [4] introduced a modified Angström model incorporating empirical coefficients a and b to improve adaptability to local climatic conditions:

$$\frac{\bar{H}}{\bar{H}_0} = a + b\frac{\bar{S}}{\bar{S}_0} \tag{2.2}$$

Here, a reflects baseline atmospheric transparency, while b describes the sensitivity of global radiation to SD. These coefficients vary across regions, a ranges from 0.06 to 0.44, b from 0.19 to 0.87 [34], highlighting the need for site-specific calibration, especially in tropical and equatorial climates [35]. This model represents a first-order linear transfer function between normalized SD and normalized GSI [31].

The linear formulation provide first-order estimate of available solar energy, suitable for pre-feasibility studies and large-scale solar maping [33], it enables rapid estimation of annual PV yield (kWh/kWp) in data-scarce regions such as the DRC. However, this linear formulation may underestimate peak irradiance conditions, leading to potential bias in inverter sizing and storage planning [36].

2.3.2.3. Latitudinal corrections

Glover and McCulloch [37], proposed a latitude-dependent modification, multiplying a by cosφ:

$$\frac{\bar{H}}{\bar{H}_0} = a\cos\varphi + b\frac{\bar{S}}{\bar{S}_0} \tag{2.3}$$

This introduces a geometrical correction reflecting solar declination effects, although for a fixed site, the term becomes constant, reducing the model to a form similar to Prescott:

$$a\cos\varphi = \hat{a} \tag{2.4}$$

Then, the model expressed in Eg.(2.2) is reduced to a form similar to Prescott as in Eq. (2.5) :

$$\frac{\bar{H}}{\bar{H}_0} = \hat{a} + b\frac{\bar{S}}{\bar{S}_0} \tag{2.5}$$

Such refinements improve global applicability but do not resolve regional coefficient variability.

2.3.2.4. Higher-order and nonlinear extensions

To capture potential nonlinearities, several extensions have been proposed such as:

1. Quadratic term by Ögelman [5] [10]

$$\frac{\bar{H}}{\bar{H}_0} = a + b\frac{\bar{S}}{\bar{S}_0} + c\left(\frac{\bar{S}}{\bar{S}_0}\right)^2 \tag{2.6}$$

The introduction of a quadratic term accounts for non-linear atmospheric effects, particulary the interaction between cloud cover variability and radiation transmission [32]. It

reflets the fact that increases in SD do not translate linearly into irradiation gains, especially under partially cloudy conditions.

The Equation (2.6) improves estimation of mid-range irradiance regimes, which are critical for daily PV production profiles. In addition, this Equation enhances accuracy in battery storage sizing, where errors in intermediate irradiance levels can accumulate significantly. Finally, this model is particularly relevant for tropical climates such as the RDC where interaction between high atmospheric humidity, persistent cloud cover,and strong convective activity induces non-linear responses in SI.

2. Cubic term by Bahel et al. [38] :

$$\frac{\bar{H}}{\bar{H}_0} = a + b\frac{\bar{S}}{\bar{S}_0} + c\left(\frac{\bar{S}}{\bar{S}_0}\right)^2 + d\left(\frac{\bar{S}}{\bar{S}_0}\right)^3 \tag{2.7}$$

The cubic model captures higher-order atmospheric variability, including complex interactions between cloud thickness, humidity, and solar attenuation. It allows the model to adapt to extreme conditions (very low or very high SD ratios).

This formulation provides high-fidelity estimation of solar resource, essential for bankable PV projects, reduces uncertainty in long-term energy yield predictions. It is particularly useful for regions with strong climatic gradients, as observed across the DRC (See Chapter 3 and 4).

3. Exponetial models – Almorox and Hontoria [25], El-Metwally [39] (2.8–2.9):

$$\frac{\bar{H}}{\bar{H}_0} = a + be^{\left(\frac{\bar{S}}{\bar{S}_0}\right)} \tag{2.8}$$

Or the altenative form :

$$\frac{\bar{H}}{\bar{H}_0} = ae^{(1/\bar{S}/\bar{S}_0)} \tag{2.9}$$

This formulation introduces an exponential response, reflecting threshold behvior in atmopspheric transmissivity. Once a certain level of SD is reached, irradiation increaqes more rapidly due to reduced cloud persistence and improved atmospheric clarity.

The model captures rapid increases in irradiance during clear-sky transitions, critical for peak power estimation; it supports better sizing of inverters and protection systems, which must handle short-duration high-power events, also, this formulation is relevant for operational forecasting and grid integration studies.

4. Logaritkmic model [40]

$$\frac{\bar{H}}{\bar{H}_0} = a + b log\left(\frac{\bar{S}}{\bar{S}_0}\right) \quad (2.10)$$

The logarithmic formulation reflects a diminishing return effect, where increases in SD yield progressively smaller gains in irradiation. This behavior is consistent with saturation effects in atmospheric transmissivity, especially in humid tropical environments.

The logarithmic model is particularly suitable for cloudy and humid regions, where additional SD do not proportionally increase energy yield. It helps avoid overestimation of PV production, improving reliability of energie yield forecasts. However, this relationship is critical for mini-grid design in rural electrification, where overestimation can lead to undersized storage systems reliability issues.

2.3.2.5. Critical synthesis: comparative overview

Collectively

The table (2.1) summarizes the key characteristics, advantages, and limitations of the main SD–based models. This synthesis follows the rigorous standards of critical reviews, enabling a clear understanding of methodological choices and their direct implications for the SD-GSI analysis.

Table 2.1: Key characteristics of the main SD based models

Model	Form	Key Coefficients	Advantages	Limitations	Recommended Application
Angström	Linear: $\frac{\bar{H}}{\bar{H}_0} = a + b\frac{\bar{S}}{\bar{S}_0}$	a, b	Simple, widely used, requires minimal data	Ignores nonlinearity, site-specific calibration needed	Data-scarce environments, first-order estimate
Prescott	Linear: $\frac{\bar{H}}{\bar{H}_0} = a + b\frac{\bar{S}}{\bar{S}_0}$	a, b	Improved regional fit, widely validated	Regional variability, tropical climates require calibration	Low-latitude and mid-latitude sites
Quadratic (Ögelman)	$\frac{\bar{H}}{\bar{H}_0} = a + b\frac{\bar{S}}{\bar{S}_0} + c\left(\frac{\bar{S}}{\bar{S}_0}\right)^2$	a, b, c	Captures nonlinearities, improved R^2	Overfitting risk, less physical interpretability	Tropical regions with convective cloud patterns
Cubic (Bahel et al.)	$\frac{\bar{H}}{\bar{H}_0} = a + b\frac{\bar{S}}{\bar{S}_0} + c\left(\frac{\bar{S}}{\bar{S}_0}\right)^2 + d\left(\frac{\bar{S}}{\bar{S}_0}\right)^3$	a, b, c, d	Captures higher-order effects	Requires larger datasets, may overfit	Tropical/subtropical zones with high variability
Logarithmic	$\frac{\bar{H}}{\bar{H}_0} = a + blog\left(\frac{\bar{S}}{\bar{S}_0}\right)$	a, b	Good for low n/N, smooth response	Nonlinear regression complexity, less intuitive	Hourly estimation, heterogeneous climates
Exponential	$\frac{\bar{H}}{\bar{H}_0} = a + be^{\left(\frac{\bar{S}}{\bar{S}_0}\right)}$ or $\frac{\bar{H}}{\bar{H}_0} = ae^{(1/\bar{S}/\bar{S}_0)}$	a, b	Captures rapid increases at high sunshine duration	Sensitive to outliers, may overpredict	High sunshine-duration regions, tropical DRC

Overall, the literature summarized in Table 2.1 shows that SD-based models remain widely used for estimating global solar radiation, with numerous functional forms proposed to improve model flexibility under different climatic conditions.

2.3.2.6. Implications for SD–GSI modelling

These considerations support the assumption that SD implicitly integrates the combined atmospheric effects influencing GSI. The critical review demonstrates that:

i. Linear models (Angström, Prescott) remain robust for first-order, site-specific estimates.
ii. Higher-order or nonlinear models can improve statistical fit but require careful calibration to avoid overfitting.
iii. Regional and tropical calibration is essential due to convective clouds, high humidity, and rapid variability in [41] sunshine hours.

In the present study, this analysis informs the selection of regression structures for the DRC, guiding the SD–GSI modelling that will underpin the spatial characterization of SD and solar potential in Chapter 3. Higher-order models may improve statistical fit (R^2) but may increase risk of overfitting and reduce physical interpretability, particularly in heterogeneous tropical climates [42].

2.3 Estimation of Solar Irradiation on an Inclined Plane

Extensive scientific literature has addressed the estimation of solar irradiation on inclined surfaces, including isotropic sky models [43] and anisotropic approaches such as the Perez Punctual Source (PPS) [44, 45, 46, 47]and Perez All-Weather (PAW) models. These models, while indispensable for system-level PV and solar thermal design, involve complex corrections for surface orientation, tilt angle, circumsolar and horizon brightening, and local albedo effects. Their application at national or regional scales is constrained by the scarcity of precise local parameters and by the amplified uncertainties inherent to inclined-plane modeling.

In practice, the total irradiation incident on a tilted surface comprises three components: direct beam radiation, sky-diffuse radiation, and ground-reflected radiation. Diffuse radiation modeling ranges from simplified isotropic assumptions to advanced anisotropic formulations (PPS/PAW) [43] [48], which improve realism but primarily impact surface-specific system optimization rather than large-scale solar resource assessment.

For climate-scale solar potential estimation, the critical challenge remains the reliable quantification of GSI on horizontal surfaces. Horizontal irradiation represents the foundational metric for national and regional solar mapping, estimation of photovoltaic energy yield, and integration with SD metrics to capture atmospheric clarity and seasonal variability.

The integrated SI–SD approach adopted in this study leverages this horizontal reference. While SI quantifies the energy magnitude, SD provides a temporal and atmospheric complement, reflecting cloud persistence, sky clarity, and effective solar exposure duration [26, 27]. This synergy is pivotal for accurate daily and monthly PV yield predictions, capturing intra-annual variability critical for storage sizing and grid integration, and providing a robust, physically consistent basis for subsequent horizontal irradiance modeling in Chapter 5.

In summary, while inclined-plane models remain scientifically relevant for localized PV system design, the horizontal-surface framework offers a methodologically coherent and operationally reliable foundation for large-scale solar resource modeling. By explicitly linking SI to SD, this framework ensures that PV yield assessments are both physically grounded and statistically robust, aligning with the primary objective of the study: establishing predictive models of GSI on horizontal surfaces..

2.4 Critical Synthesis and Identified Research Gap

This review of SD–based models underscores several fundamental insights relevant to SI modelling in tropical regions such as the DRC:

i. The Angström–Prescott framework remains the most widely adopted approach for estimating GSI from SD, providing a robust first-order approximation that balances simplicity and operational applicability.
ii. Empirical coefficients (a, b, c, d) exhibit significant spatial and climatic variability, reflecting local atmospheric conditions, cloud dynamics, and latitudinal influences; consequently, site-specific calibration is essential to achieve reliable estimates.
iii. Higher-order extensions (quadratic, cubic, logarithmic, exponential) can improve statistical performance metrics such as R^2, but may compromise physical interpretability and transferability, particularly under the highly variable convective cloud regimes of equatorial climates.
iv. Most empirical validations of these models have been conducted at single stations or over limited regional scales, limiting their generalizability across broad and heterogeneous climatic zones.

Despite the extensive development and refinement of regression models, several critical gaps remain, particularly in the context of the DRC:

— There is a lack of spatially consistent calibration of Angström–Prescott and higher-order models across all DRC provinces, which is crucial given the country's wide latitudinal and longitudinal span.
— The statistical stability of annual mean SD and its impact on SD–GSI regression coefficients has received limited evaluation.

— Comparative analyses of multiple regression scenarios within a unified national framework remain largely absent.
— Insufficient attention has been given to spatial variability and heterogeneity, which are particularly pronounced in large equatorial countries with diverse topography and microclimates

Given the geographical extent, equatorial positioning, and complex climatic variability of the DRC, the direct adoption of regression coefficients derived from other regions is scientifically questionable. Coefficients calibrated in mid-latitude or arid regions may not adequately capture the combined effects of high humidity, rapid convective cloud formation, and frequent daily fluctuations in SD characteristic of tropical DRC.

These considerations justify the development of a spatially calibrated and statistically validated SD–GSI modelling framework, explicitly accounting for provincial differentiation, local atmospheric conditions, and methodological robustness. Such a framework not only addresses existing empirical gaps but also provides a critical foundation for the spatial characterization of solar potential presented in Chapter 3, ensuring that derived models are both physically meaningful and operationally reliable across the heterogeneous landscapes of the DRC.

CHAPTER 3: SPATIAL CHARACTERIZATION OF SUNSHINE DURATION AND SOLAR POTENTIAL IN THE DRC

This chapter focuses on the spatial characterization of SD and solar potential in the DRC. Due to the vast size of the country, which spans nearly eight degrees of latitude across the Equator and over 19 degrees of longitude, solar potential and SD are unevenly distributed across its territory. Understanding the spatial variability of SD is essential for accurately assessing the solar energy potential and identifying regions suitable for PV energy deployment.

After a brief overview of the country's physical geography, the chapter presents the distribution of SD across provinces, highlighting areas with low, medium, high, and very high solar potential. This information is then combined with energy demand data to evaluate the feasibility of solar energy solutions in different provinces. This chapter is designed to serve as a conceptual and analytical bridge to Chapter 4, which provides a detailed examination of the observed SD data in order to identify the dominant spatial and climatic drivers governing its variability, and to identify the spatial and climatic factors that indirectly control the total solar irradiation received on a horizontal surface. The insights derived from this analysis constitute the foundational basis for the development and calibration of the SD–SI models presented in Chapter 5 for the DRC [49, 50, 51, 52].

3.1 General Information

3.1.1 Physical geography

The DRC is located in Central Africa, within the inter-tropical zone (5°N–13°S latitude, 12°E–31°E longitude) [15]. Covering an area of 2,345,410 km², it is the second-largest country in Africa after Algeria [13]. Straddling the Equator, the DRC occupies a central position between Central Atlantic Africa, East Africa, Sudano-Sahelian Africa, and Southern Africa [15].

The country possesses about 52% of Africa's freshwater reserves and is home to 155 million hectares of natural forests, representing 60% of the Congo Basin forest area [15]. These forests make the DRC a key player in global efforts to reduce greenhouse gas emissions and preserve biodiversity.

In terms of energy, the DRC is rich in natural resources, allowing exploitation of various renewable energy sources, including solar, biomass, hydroelectricity, and wind [13]. Significant reserves of hydrocarbons, including methane gas from Lake Kivu, mineral coal, and geothermal resources, further complement the energy landscape [13].

3.1.2 Renewable energy and solar potential

The distribution of solar potential and SD is not uniform across the DRC. According to the "Atlas of Renewable Energies in the DRC" (2014) [13], the country can be classified into four solar potential zones: low, medium, high, and very high. These zones reflect differences in average solar irradiation and SD, influenced by latitude, altitude, and cloud cover [13, 53].

3.1.2.1. Low Solar Potential Area

A. Location and SI Characteristics:

— Sud Kivu (latitude 1°36'S–5°S, longitude 26°47'E–29°20'E) is the only province in this category [15].
— Average solar irradiation ranges between 3.5 and 4.5 kWh/m²/day [13].
— Main cities: Bukavu, Kamitunga, Baraka, and Uvira [13].

B. Photovoltaic Energy Opportunity:

In 2014, energy demand was estimated at 39.7 MW, while available capacity was only 33 MW [13, 54]. Assuming a 4% annual growth rate, the current energy demand is estimated at 52.2 MW using Equation estlabished by Lusamba-Yangindu et al. [55]. Although the solar potential is the lowest in the DRC, PV systems are feasible, especially in areas difficult to connect to the SNEL grid [13].

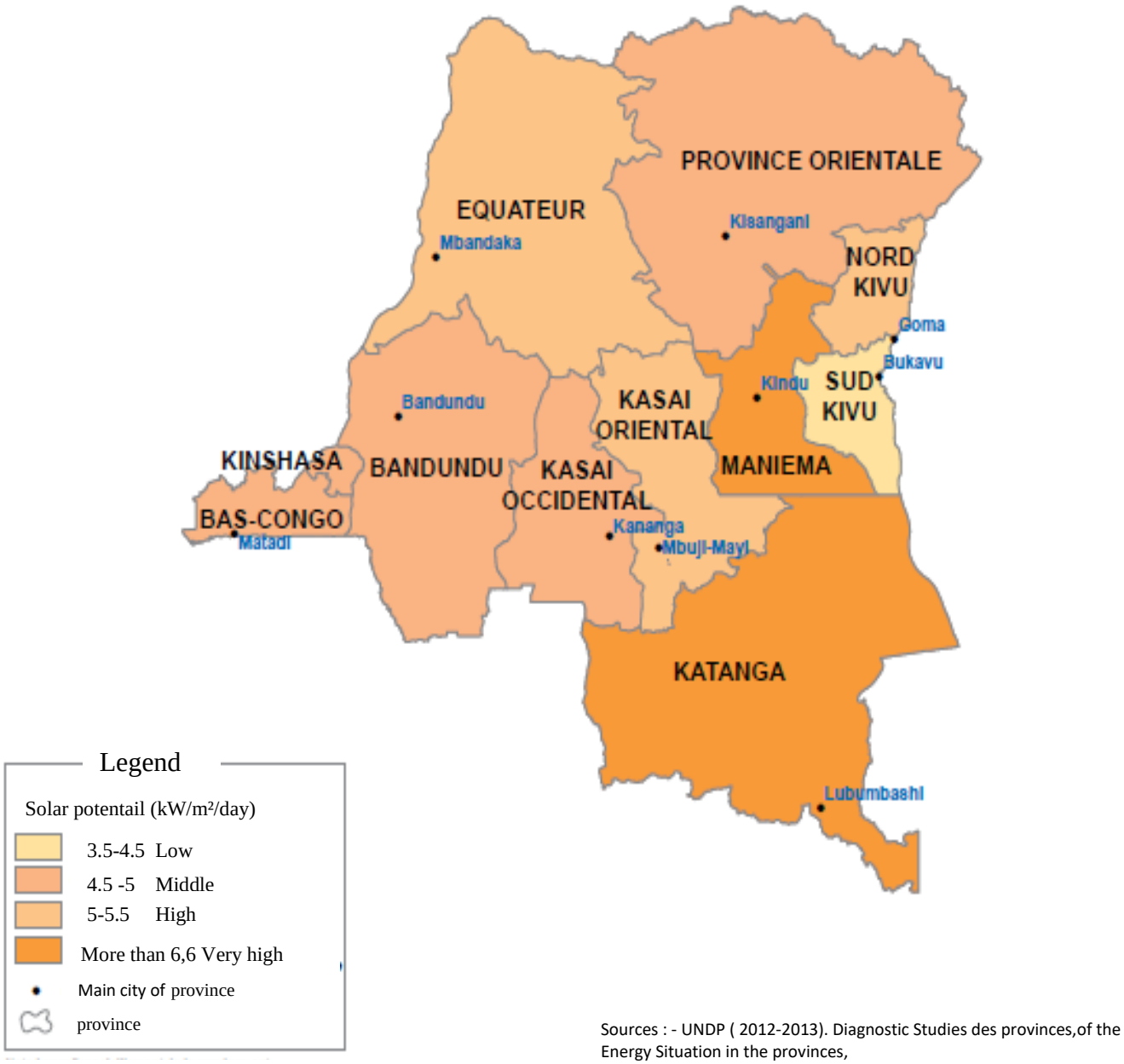

Fig. 3.1: GHI solar resource map of the Democratic Republic of Congo [13]

3.1.2.2. Medium Solar Potential Area

A. Location and SI Characteristics:

Average SI: 4.5–6 kWh/m²/day [13]

Provinces: Kinshasa, Kongo Central, Bandundu, Kasai-Occidental, Province Orientale [13].

B. Photovoltaic Energy Opportunity:

— Bandundu:

- household demand = 356 MW;
- installed capacity = 3.57 MW [13]
- Current demand ≈ 468 MW; projected 2030 demand ≈ 667 MW [55] .
- PV energy can address the supply gap.

— Kinshasa:

- demand = 852 MW; projected 2030 demand = 1,596 MW [13].
- supply = 410 MW;
- PV energy is promising for rural and semi-urban districts.

— Kongo Central:

- SI ~4.5 kWh/m²/day [13].
- PV can supplement rural household energy needs.

— Kasai-Occidental:

- demand = 233 MW (households), 296 MW (all sectors);
- 2030 projected demand = 472 MW (households), 600 MW (all sectors) [13].
- PV could mitigate future energy deficits.

— Province Orientale:

- Electrification rate = 3.6%;
- SI 3.5–5 kWh/m²/day [13].
- PV is a cost-effective solution.

Figure 3.2 presents the projected evolution of energy demand in the DRC based on historical data and growth assumptions

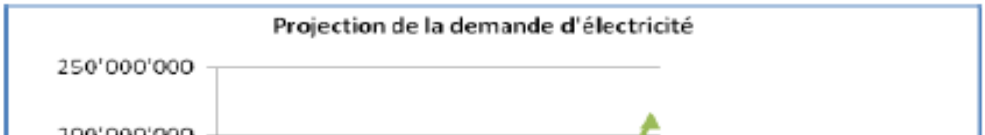

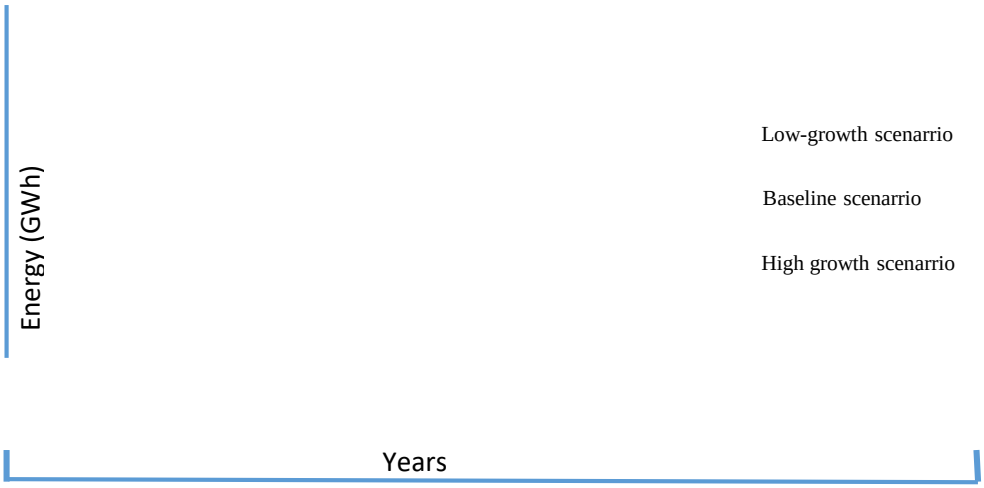

Figure 3.2: DRC projection enery demand [89]

The figure highlights a sustained upward trend in energy demand, driven by demographic growth and increasing socio-economic activities. The widening gap between projected demand and existing generation capacity underscores the structural deficit of the national energy system. This dynamic justifies the integration of alternative energy solutions, particularly decentralized renewable systems such as photovoltaics, to complement conventional supply infrastructures.

3.1.2.3. High Solar Potential Area

A. Location:

- Former provinces of Équateur, Kasai-Oriental, and Nord Kivu [13].
- Average SI: 6–6.5 kWh/m²/day [13].

B. PV Opportunities:

— Kasai-Oriental:

- Household demand (2012) = 303 MW; projected 2030 demand = 614 MW [13].
- Hydropower is unreliable; PV complements energy supply.

— Nord Kivu:

- 2014 demand = 153 MW; projected 2030 demand = 287 MW [13].
- PV viable where grid connection is costly.

— Équateur:

- 2012 demand = 426 MW; projected 2030 demand = 863 MW [13].

3.1.2.4. Very High Solar Potential Area

A. Location:

— Katanga and Maniema [13].

— Solar irradiation >6.5 kWh/m²/day

— Key cities: Lubumbashi, Kolwezi, Likasi (Katanga); Kindu, Lubutu, Punia, Kibombo (Maniema)

B. PV Opportunities:

— Katanga:

- installed capacity(2014) = 567 MW;
- demand = 900 MW; projected 2030 demand >2,100 MW
- PV can meet mining sector needs.

— Maniema:

- Installed capacity = 2.1 MW;
- 2012 household demand = 105 MW; projected 2030 demand >221 MW
- PV is a cost-effective solution.

3.2 Sunshine Duration Characteristics

The theoretical SD is defined as the interval between sunrise and sunset. However, the actual length of the day, calculated from sunrise to sunset, varies throughout the year [56] Theoretical SD assumes an entirely clear sky [57]; increased cloud cover reduces the actual sunshine received [58].. According to the World Meteorological Organization (WMO), SD is

measured as the total time during which direct solar irradiance exceeds 120 W/m², taking into account cloud cover or the proportion of the sky obscured by clouds [50], [59, 60, 61, 62, 63].

Understanding SD is essential for solar energy also for several sectors, including tourism, public health, agriculture, vegetation [49], [61, 62, 64]. The DRC, located on the Equator within the inter-tropical zone, is about half covered by dense forest, mainly in the central basin, while the remainder consists of wooded savannahs, particularly in Kongo Central, Kasai, northern Équateur, Katanga, and Kivu [63]. Its equatorial position results in high annual rainfall [51, 52], generating frequent cloud cover. The dry season, lasting roughly four months, is the period with the clearest skies [63].

Despite its geographic location, which limits seasonal SD variation compared to higher-latitude countries, cloudiness significantly influences observed SD [65, 66], varying across provinces and months. For practical applications, especially in solar energy, only observed SD can reliably convert solar radiation into electrical energy using PV [65] systems. SD thus becomes a key parameter in assessing recoverable energy at any site.

Data on SD from various sites across the DRC were compiled to determine provincial SD characteristics. These include average SD (hours per day or per year), months with minimum and maximum SD, spatial patterns of SD influenced by longitude, temperature, relatve humidity and rainfall. The following section focuses on provincial analysis.

3.2.1 Analysis of sunshine duration by province

3.2.1.1. Bandundu Province

The former Bandundu Province is subdivided into three districts: Kwango, Kwilu, and Maï-Ndombe. SD is analyzed for each district to determine the provincial characteristics. Table 3.1 presents the monthly weighted averages of SD for Bandundu Province, derived from the three districts. Details on the SD of distrcts are provided in Appendix A.

Table 3.1: Weigted MASD for Bandundu Province

Aire (Km²)	89 974	78 219	127 465	Weighted averages
District	Kwango	Kwilu	Mai-Ndombe	in h/day
January	6,4	6,3	6,5	6,4
February	6,5	6,3	6,4	6,4
March	6,2	6,1	6,2	6,2
April	5,5	5,5	5,6	5,5
May	6,5	5,7	5,9	6,0
June	7,6	7,1	6,8	7,1
July	7,8	7,5	7	7,4
August	7,4	6,9	6,5	6,9
September	6,4	5,9	6,1	6,1
October	5,5	5,3	5,8	5,6
November	5,3	5,3	5,7	5,5
December	5,8	5,8	5,9	5,8
Averages	6,4	6,1	6,2	6,2

Source: Compiled from [14].

The aggregated data indicate an annual provincial average of approximately 6.2 h/day. The monthly distribution shows a clear seasonal structure, with maximum values in July and minimum values in November. The relatively narrow range of variation suggests a consistent solar resource across the province.

Figure 3.3 illustrates the overall temporal evolution of sunshine duration at the provincial scale in Bandundu.

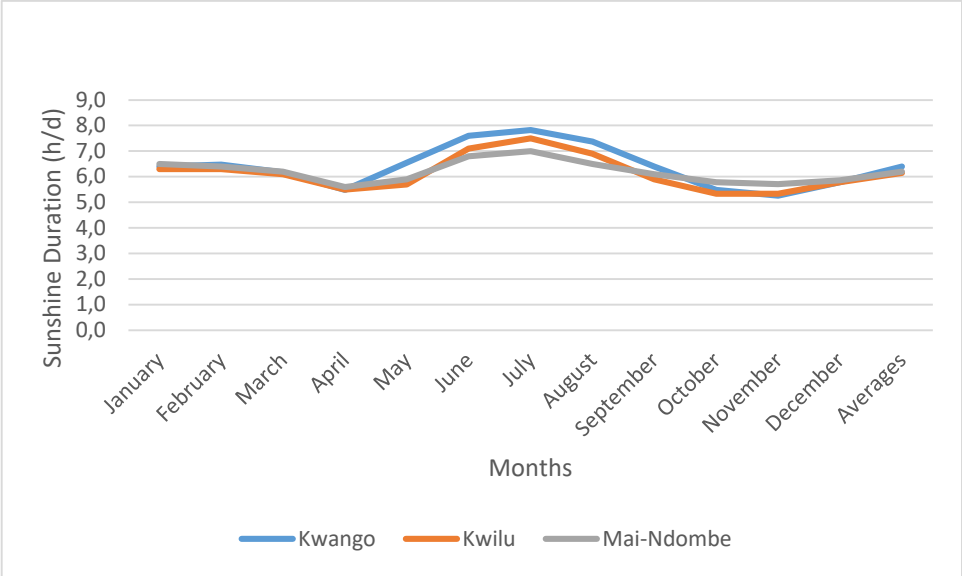

Figure 3.3: Temporal Trend of Monthly SD for Bandundu Province [15].

The figure synthesizes the district-level patterns into a coherent provincial trend, highlighting the strong seasonality of sunshine duration. The alignment of peaks and minima across the province confirms the dominant influence of regional climatic dynamics, particularly cloud cover and rainfall regimes, in shaping solar availability.

The relatively narrow range of annual averages between districts indicates that Bandundu Province benefits from a spatially coherent solar resource, with moderate intra-provincial variability.

A. Key Provincial-Level Analytical Observations

- The average SD of 6.2 h/day confirms that Bandundu Province possesses a moderately high and relatively stable solar resource throughout the year.
- Seasonal variability is essentially governed by cloud cover and rainfall dynamics, rather than astronomical factors, due to the province's inter-tropical location.
- The dry season constitutes a natural peak period for photovoltaic productivity, whereas the rainy season introduces temporary reductions in effective solar input.
- The limited spatial variability between districts suggests that solar energy planning at the provincial scale can rely on relatively uniform baseline assumptions.

B. Implications for Decentralized and Grid-Connected PV Planning

In the context of rural electrification and isolated communities:

— The relatively stable annual SD supports the technical viability of solar home systems (SHS) and mini-grids.
— System sizing should be based on the lowest monthly SD values (≈5.5 h/day) to ensure reliability.
— Battery storage must be dimensioned according to rainy-season conditions rather than annual averages.
— Territories with SD values above the provincial mean (e.g., parts of Kwango) may be prioritized for decentralized PV deployment.

For utility-scale or grid-integrated installations:

— The moderate seasonal amplitude limits long-term production volatility.
— Peak SD during the dry season can complement hydropower generation, particularly when reservoir levels fluctuate.
— The relative homogeneity of SD across districts facilitates provincial-scale solar investment planning and reduces the risk of significant spatial production imbalance.

C. Synthesis for Bandundu Province

The spatial analysis of SD in Bandundu Province demonstrates that:

— The province benefits from consistent and technically exploitable solar conditions.
— Cloud dynamics constitute the primary regulator of seasonal solar variability.
— The observed SD regime is sufficiently stable to justify both decentralized rural electrification initiatives and grid-connected photovoltaic expansion.
— Planning strategies must systematically integrate minimum monthly SD values in order to guarantee long-term technical reliability and economic viability.

3.2.1.2. Province of Equateur

The former Province of Equateur[1] is subdivided into four former districts: Equateur, Mongala, Nord-Ubangi and Sud-Ubangi and Tsuapa. The spatial characterization of SD is presented below

[1] also referred to as Grand Equateur. It should not be confused with the District of Equateur, which constitutes only one component of the former Province of Equateur.

following the same analytical structure adopted for Bandundu Province. The aggregated monthly averages for the four districts are presented in the table 3.2. Details on the SD of distrcts are provided in Appendix B.

Table 3.2: Weigted MASD for Equateur Province

	Equateur	Mongala	Nord Ubangi	Sud Ubangi	Tshuapa	Provincial mens
January	6.7	7.0	7.5	7.4	6,4	7,0
February	6.5	6.7	7.2	7.1	6,2	6,8
March	6.2	6.3	6.8	6.8	5,9	6,4
April	5.6	5.7	6.2	6.2	5,1	5,9
May	5.4	5.4	5.9	5.9	5	5,6
June	6.0	5.6	6.0	6.0	5,8	5,9
July	6.0	5.6	5.9	5.9	6,1	5,9
August	5.6	5.1	5.3	5.3	5,4	5,4
September	5.3	5.0	5.1	5.1	5,2	5,2
October	5.3	4.8	4.8	4.9	4,9	5,0
November	5.1	4.7	5.3	5.1	4,7	5,1
December	6.0	6.1	6.8	6.5	5,4	6,3
Averages	5.8	5.7	6.1	6.0	5,5	5.9

Source: Compiled from [14].

The comparative data reveal a relatively narrow range of annual SD values (approximately 5.5–6.1 h/day), indicating a globally homogeneous solar resource at the provincial scale. However, Nord-Ubangi consistently exhibits slightly higher values, reflecting its more favorable climatic conditions. Figure 3.4 synthesizes the temporal trends of SD across the four districts of Former Equateur.

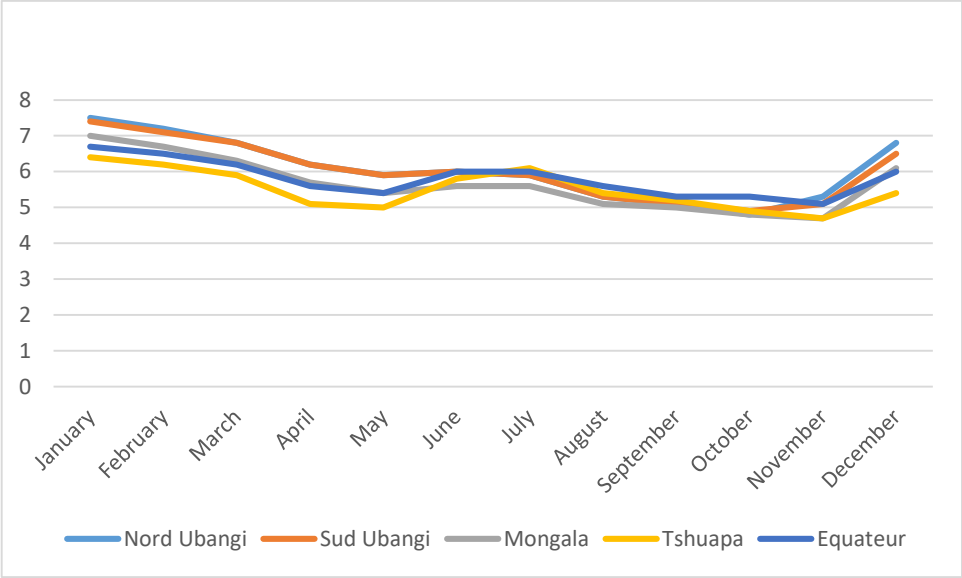

Figure 3.4: Temporal Trend of Monthly SD for Equateur Province

Source : Compiled from [15]

The superposition of district-level curves highlights a strong temporal coherence, with synchronized seasonal peaks and minima. This alignment confirms that large-scale atmospheric dynamics, rather than local geographical differences, primarily govern SD variability across the province.

Based on weighted district averages, the following provincial characteristics are established:

- Annual weighted provincial average SD: 5.9 h/day
- Highest district annual SD: Nord-Ubangi (6.1 h/day)
- Lowest district annual SD: Tshuapa (5.5 h/day)
- Highest SD territory: Bosobolo (6.6 h/day)
- Lowest SD territory: all territories of Tshuapa (5.5 h/day)
- Month of maximum provincial SD: January
- Month of minimum provincial SD: October

The province therefore exhibits a moderate but spatially structured sunshine regime, with a north–south gradient in solar availability.

A. Key Provincial-Level Analytical Observations

— The provincial average of 5.9 h/day confirms that Equateur possesses a moderate but exploitable solar resource.
— The highest SD values are concentrated in Nord-Ubangi, suggesting a spatial gradient associated with forest density and cloud persistence.
— The minimum SD occurring in October–November corresponds to peak rainfall intensity across the province.
— The annual variability remains limited in amplitude compared to higher latitude regions, which is consistent with inter-tropical climatic dynamics.

B. Link Between Sunshine Duration and PV Potential

SD serves as an operational proxy for solar resource assessment, particularly in regions where high-resolution solar irradiance measurements remain limited.

It is also worth noting that:

— An annual average of 5.9 h/day supports the feasibility of decentralized photovoltaic deployment.
— Higher SD values in Nord-Ubangi indicate priority zones for PV investment.
— Seasonal minima in October–November must be incorporated into system sizing to ensure reliability.
— The relatively stable inter-district variability allows provincial-scale planning without major spatial production imbalance.
— Suitable for rural electrification given stable annual SD.
— Battery storage must be dimensioned based on October–November conditions.
— Nord-Ubangi presents favorable conditions for mini-grid expansion.
— Moderate seasonal amplitude reduces long-term production volatility.
— Spatial coherence facilitates regional planning.
— Integration with hydropower should consider seasonal complementarity.

3.2.1.3. Kasaï occidental

Unlike other former provinces, Kasaï Occidental is relatively compact in spatial extent. For this reason, the analysis is not structured according to district subdivision, but rather

conducted directly at the level of major cities and territories. The following locations were considered: Kananga, Tshikapa, Demba, Dekese, Dimbelenge, Ilebo, Kazumba, Luebo, Luiza, and Mweka.

Table 3.3 presents the MASD across selected cities and territories of Kasaï-Occidental.

Table 3.3: Weigted MASD for Kasaï-Occidental (h/day)

Latitude	5°53'32"S	5°30'S	5°33'S	6°25'S	7°12'S	3°27'S	4°19'48"S	4°50'00"S	6°25'00"S
Longitude	22°24'10"E	22°15'E	23°06'E	22°09'E	22°25'E	21+23'E	20°35'14"E	21°34'00"E	20°48'00"E
Area (Km²)	847	14 702	12 881	8 961	13 223	25 175	15 654	13 223	382
Cities	Kananga	Demba	Dimbel.	Kazumba	Luiza	Dekese	Ilebo	Mweka	Tshikapa
January	5.9	5.6	5.9	5.8	5.7	5.8	5.6	5.5	6.0
February	6.0	5.6	5.9	5.9	5.9	5.7	5.7	5.5	6.2
March	5.7	5.3	5.6	5.6	5.4	5.3	5.2	5.0	5.6
April	5.6	5.0	5.4	5.6	5.9	4.6	4.6	4.4	5.4
May	6.1	5.6	6.1	6.4	7.1	5.0	5.0	5.1	6.6
June	7.4	7.1	7.3	7.4	7.7	6.5	6.5	6.7	7.7
July	7.6	7.4	7.6	7.7	7.8	7.1	7.1	7.1	7.8
August	6.6	6.5	6.7	6.7	7.1	6.2	6.2	6.2	7.2
September	5.2	5.3	5.4	5.2	5.6	5.5	5.5	5.4	5.9
October	4.6	4.7	4.9	4.6	4.7	5.1	5.1	4.9	5.2
November	4.8	4.7	4.8	4.7	4.7	4.9	4.9	4.7	5.0
December	5.4	5.0	5.3	5.2	5.1	5.1	5.1	4.8	5.4
Averages	5.9	5.7	5.9	5.9	6.1	5.6	5.5	5.4	6.2

Source: Compiled from [14].

The data reveal a relatively homogeneous spatial distribution of SD, with annual averages ranging narrowly between approximately 5.4 and 6.2 h/d. A clear seasonal pattern emerges, characterized by maximum values during the dry season (June–July) and minimum values during the rainy season (October–November). This limited spatial variability suggests that, at the provincial scale, SD is primarily governed by regional climatic conditions rather than local geographical differences.

Figure 3.5 illustrates the temporal evolution of monthly SD for the different localities of Kasaï-Occidental.

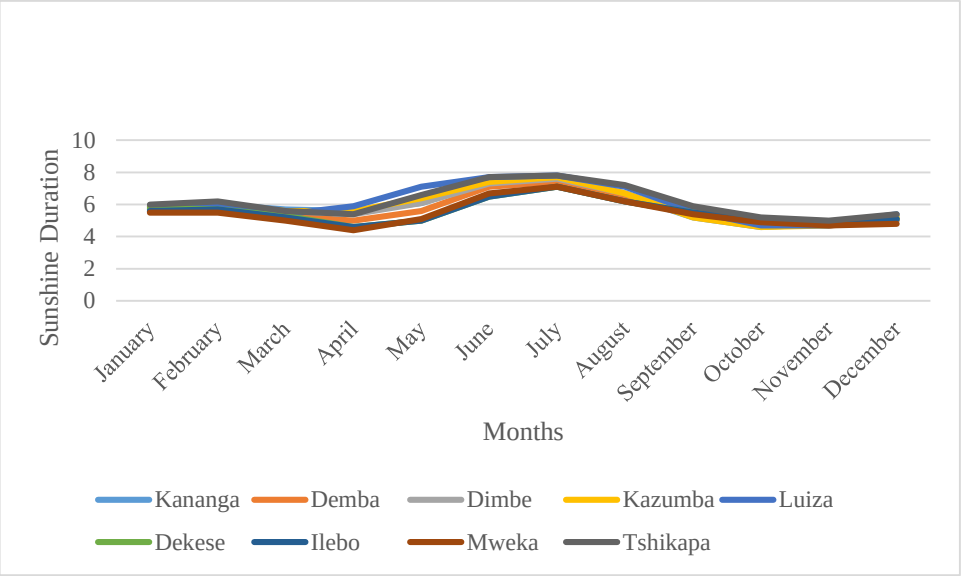

Figure 3.5: Trend of monthly Average of SD for Kasaï Occidental

The superposition of SD curves highlights a strong temporal coherence between locations, confirming the dominance of seasonal climatic forcing. The absence of significant divergence between curves reinforces the reliability of using a provincial average for modeling purposes. However, the observed deviation from the theoretical solar trend suggests the influence of atmospheric factors such as cloud cover and humidity.

A. Key Provincial-Level Analytical Observations

The key provincial-level analytical observations deriverd from preceding analysis are presented below:

- The average SD of 5.7 h/day indicates a moderate but technically exploitable solar resource.
- The dry season (June–August) provides a clearly defined high-production window for photovoltaic systems.
- The rainy season introduces a pronounced but predictable reduction in sunshine duration.
- The relatively limited spatial variability across territories facilitates provincial-scale planning with standardized baseline parameters.

B. Link Between SD and PV Potential

SD provides a robust operational proxy for evaluating solar resource adequacy in the absence of high-resolution irradiance data.

- An annual average of 5.7 h/day supports decentralized photovoltaic deployment.
- The strong seasonal peak in July suggests optimal production conditions during the dry season.
- System design must integrate the minimum monthly SD (≈4.7 h/day) to ensure reliability.
- Territories such as Tshikapa and Luiza may be prioritized for PV development due to their higher annual SD values.

Decentralized systems are particulary relevant for remote and underseved areas, where grid extension remains technically or economically challenging. According to precedent observations:

- The moderate but stable annual SD in Kasaï Occidental supports solar home systems and rural mini-grids.
- Battery storage should be dimensioned according to November conditions.
- Seasonal performance variability must be integrated cinto load forecasting models.

For grid-connected systems, the following key considerations can be highlighted :

- The pronounced seasonal peak during July enhances predictability of dry-season output.
- Complementarity with hydropower resources should be explored.
- Provincial-scale PV deployment is technically feasible due to limited spatial SD dispersion.

3.2.1.1.1 Synthesis for Kasaï Occidental

The spatial characterization of SD in Kasaï Occidental demonstrates that:

- The province possesses a moderate yet reliable solar resource;
- Seasonal variability is primarily cloud-driven;

— Empirical SD patterns diverge from theoretical astronomical expectations, confirming the need for ground-based assessment.
— The SD regime supports both decentralized electrification and grid-integrated photovoltaic expansion, provided that minimum monthly values are incorporated into system design.

3.2.1.4. Kasaï Oriental[2]

The former province of Kasaï Oriental was subdivided in 2015 into three daughter provinces, which are: Kasa-Oriental (new province), Lomami and Sankuru.The spatial characterization of SD is explored at the level of these three new provinces, while maintaining the perspective of the former territorial configuration. The influence of Sankuru, whose large surface area significantly affects the provincial weighted average of MASD is highlighted. The MASD values for the former Kasai-Oriental districts are summarized in Table 3.4. Details on the SD of distrcts are provided in Appendix C.

Table 3.4: Weighted MASD for Kasaï-Oriental (h/day)

Area (Km²=	9 481	56 426	104 331	
Districts	Kasaï-oriental	Lomami	Sankuru	Weigted Averages
January	6,2	5,9	5,9	5,9
February	6,4	6,2	5,9	6,0
March	6,0	5,9	5,4	5,6
April	6,0	6,2	4,9	5,4
May	6,9	7,3	5,2	6,0
June	7,6	7,7	6,5	7,0
July	7,7	7,8	7,1	7,4
August	7,1	7,3	5,8	6,4
September	5,6	6,0	5,4	5,6
October	5,1	5,3	5,1	5,2
November	5,2	5,1	4,9	5,0
December	5,7	5,6	5,1	5,3
Averages	6,0	5,8	5,5	5,6

[2] Unless otherwise stated, in this study, “Province Orintale “ refers to the former Province Orientale. When reference is made to the new province, this will be explicitly specified.

It is observed that the new provinces of Kasaï oriental (9.535Km²) and Lomami (56.426 km²) which represent together 38.7% of the total area of the province, exhibit yearly mean of daily SD equal respectively to 6.0h/d and 5.8 h/d against to 5.5h/d for the district of Sankuru which occupies 104,331Km² or 61.3%. The province's weighted MASD is 5.6 h/d. This finding highlights the influence of Sankuru in the calculation of the weighted average of SD for the whole province.

The curves in Figure 3.6 illustrates the temporal trend of SD for the districts of the former province of Kasaï-Oriental.

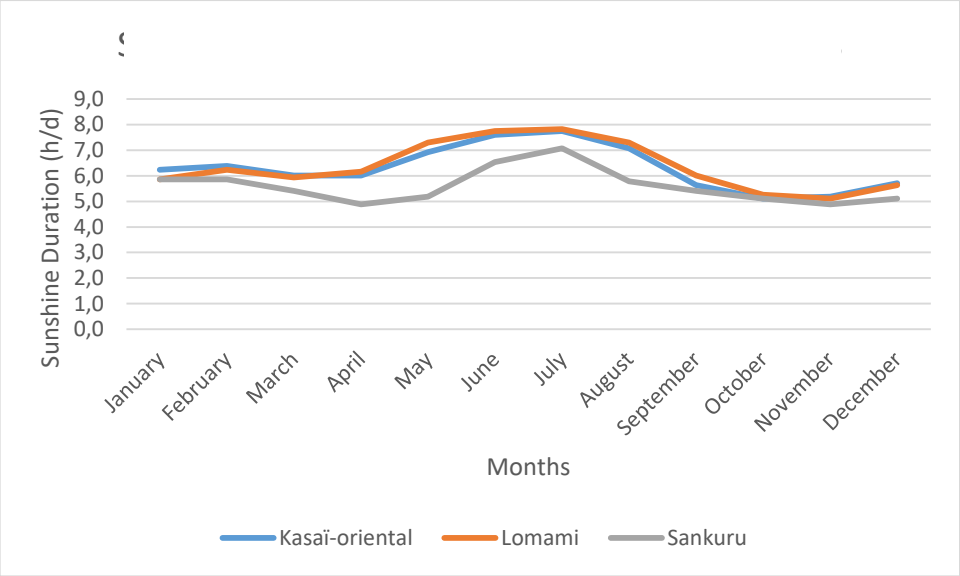

Figure 3.6: Temporal trend of monthly SD for Kasaï-Oriental

The aggregation of all curves highlights the dominant influence of Sankuru, whose lower SD values reduce the provincial weighted average. This demonstrates the importance of spatial weighting in regional solar assessments and confirms that large-area provinces require careful consideration of internal heterogeneity.

A. Key Provincial-Level Analytical Observations

Key provincial-level analytical findings for the former Kasaï Oriental province are outlined as follows:

- A moderate solar availability (5.6 h/day), suitable for PV exploitation.
- The strong dry-season peak (June–July) is consistent across all daughter provinces.

— Sankuru significantly lowers the weighted provincial average due to its large area and lower SD values.
— Spatial heterogeneity is moderate but structurally coherent across the province.
— Cloud cover remains the primary driver of SD variability, rather than latitudinal positioning

From a photovoltaic planning perspective it is noted that:

— An average SD of 5.9 h/day supports decentralized solar electrification strategies.
— Lomami represents the most favorable sub-region for PV deployment.
— Sankuru requires more careful system sizing due to lower SD values.
— The minimum monthly SD (≈4.9 h/day) must guide battery and storage dimensioning for off-grid systems.
— Seasonal predictability enhances production forecasting for grid-connected systems.

3.2.1.1.2 Synthesis for the Former Kasaï Oriental Province

The spatial characterization of Sunshine Duration in the former Kasaï Oriental province demonstrates that:

— The province presents exploitable solar resources with moderate seasonal variability.
— Large-area provinces with lower SD (such as Sankuru) strongly influence weighted averages.
— Empirical SD analysis provides a more realistic planning framework than theoretical sunshine models.
— Both decentralized and grid-connected photovoltaic systems are technically viable, provided that system design incorporates minimum seasonal thresholds.

3.2.1.5. Katanga

Katanga [3] covered a vast southern portion of the DRC. It has since been subdivided into four provinces:Haut-Katanga, Haut-Lomami, Lualaba, Tanganyka.

[3] The former Katanga [3]province, before the 2015 territorial reform

Given its large latitudinal extent and diversified climatic zones, Katanga presents one of the most structurally differentiated SD regimes in the country. The spatial characterization is therefore conducted separately for each daughter province before establishing the weighted synthesis of the former Katanga entity. Table 3.5 presents the MASD across districts of Katanga. Details on the SD of distrcts are provided in Appendix D.

Tableau 3.5: Weighted MASD for Katanga (h/day)

Area (km²)	131 443	108 204	121 308	134 940	Weighted Annual Averages
Months/Districts	Haut Katanga	Haut Lomami	Lualaba	Tnnganyika	
January	6.1	5.6	5.7	6.1	6,0
February	6.1	5.7	6.0	6.4	6,2
March	5.6	5.3	5.6	6.1	5,8
April	6.1	6.4	6.5	6.6	6,5
May	7.4	7.8	7.7	7.5	7,6
June	7.7	7.8	7.8	7.8	7,8
July	7.8	7.8	7.8	7.9	7,8
August	7.9	7.9	8.0	7.8	7,9
September	7.9	7.5	7.8	7.2	7,6
October	7.6	6.5	7.1	6.6	7,0
November	6.6	5.3	5.8	5.9	6,1
December	5.9	5.2	5.2	5.7	5,7
Averages		6.6	6.8	6.8	6,8

Table 3.5 reveals a pronounced seasonal structure in SD across the districts of Katanga, characterized by a clear transition from relatively low values at the beginning of the year to a marked peak during the mid-year period. Beyond this seasonal cycle, the limited inter-district variability suggests a relatively homogeneous regional atmospheric regime, indicating that large-scale climatic controls dominate over local geographical effects. This spatial coherence strengthens the reliability of the weighted averages and supports their use in regional-scale solar resource assessment.

Complementary infomration is provided by Figure 3.7, which illustrates the temporal evolution of MASD across the Katanga province.

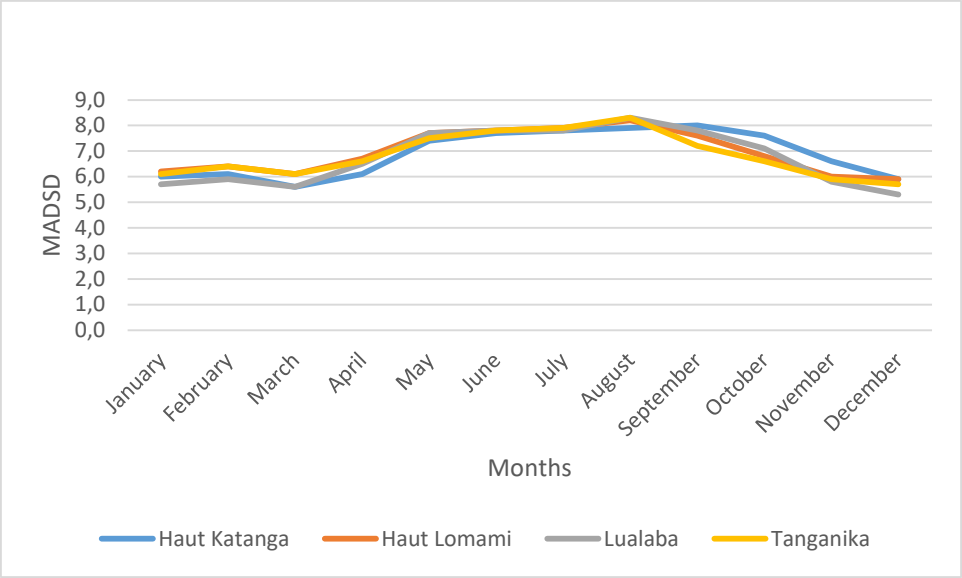

Figure 3.7: Temporal trend of monthly of SD for Katanga

Among all provinces of the DRC, Katanga exhibits the highest annual average SD. In light of this distinctive characteristic, its solar regime is synthesized into three key analytical components; namely the provincial-level analytical synthesis, the relationship between SD and PV potential, and the implications for both decentralized and grid-connected PV systems, which are developed in the following subsec

Provincial-Level Analytical Synthesis

From a provincial-level analytical synthesis perspective, it can be observed that :

- Katanga exhibits one of the most structurally stable and elevated SD regimes in the DRC.
- The dry-season peak is remarkably consistent across all four daughter provinces.
- Spatial heterogeneity remains moderate despite large territorial extent.
- Atmospheric clarity during the austral winter significantly enhances solar availability.
- The SD curves show empirical dominance over purely theoretical astronomical expectations.

The high annual SD (≈6.9 h/day) confirms that the former Katanga region represents a strategic solar development corridor within the DRC.

From a PV planning perspective:

- High dry-season SD enhances generation reliability.

— Minimum monthly SD (≈4.7 h/day) remains sufficiently elevated to support stable PV output.
— Spatial uniformity allows standardized technical sizing across provinces.
— Industrial mining zones (Haut-Katanga, Lualaba) could benefit from hybrid solar integration. Regarding the implications for decentralized PV systems, it is observed that :
— Strong solar availability supports rural electrification via solar mini-grids.
— Storage sizing can be optimized due to relatively high minimum SD values.
— Seasonal predictability reduces performance uncertainty.

With respect to grid-connected systems, it is worth noting that :

— Katanga is suitable for large-scale solar farms.
— Complementarity with hydroelectric resources enhances grid stability.
— Industrial demand centers align geographically with high SD zones.

3.2.1.1.3 Synthesis for Katanga

The spatial characterization of Sunshine Duration in the former Katanga province demonstrates that the region possesses one of the most favorable solar climates in the DRC, seasonal variability is strong but highly predictable, empirical SD data provides robust input for long-term photovoltaic planning, both decentralized and utility-scale PV systems are technically and economically justified.

3.2.1.6. Kinshasa

Kinshasa is divided into four districts. However, unlike the other provinces, the data analysis was conducted for the entire city as a whole. Monthly average SD for Kinshasa are presented in table 3.6.

Table 3.6: MASD for Kinshasa

Months	MASD (h/day)
January	5.1
February	4.9
March	5.2

Months	MASD (h/day)
April	5.1
May	4.4
June	3.9
July	3.9
August	3.2
September	3.5
October	4.4
November	4.9
December	5.2
Average	4.5

Source: Compiled from [14].

SD values are relatively low (~4.4–4.5 h/d), reflecting persistent cloudiness during the long wet season. August represents the annual minimum due to peak cloud cover.

Figure 3.8 shows the temporal evolution of SD for Kinshasa.

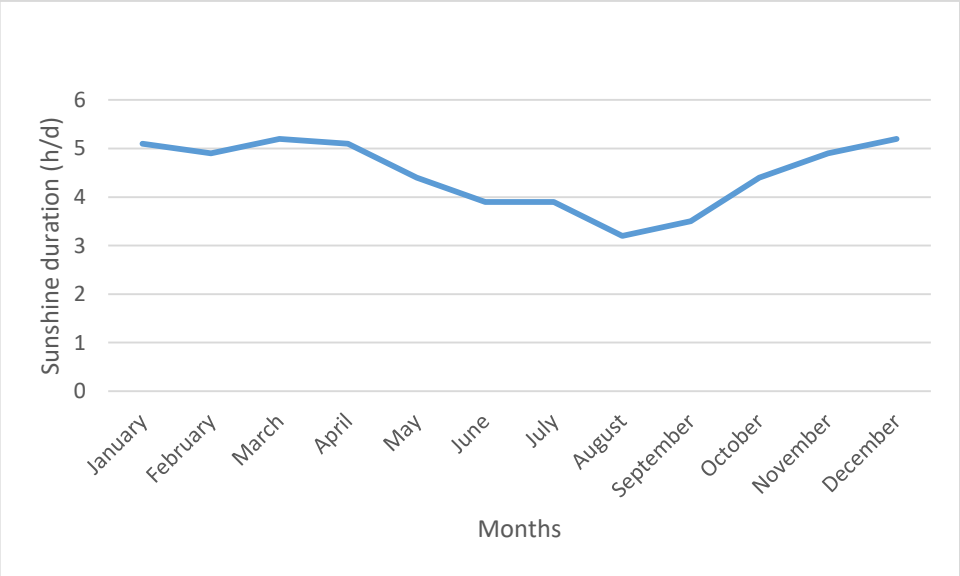

Figure 3.8: Temporal Trend of monthly SD for Kinshasa

Kinshasa exhibits a low yearly average of daily SD, evaluated at 4.5h/d. It is observed that the average monthly of daily SD decreases from March to June, stabilizes from June to July, and then drops again until September before rising again through December

A. Analytical Interpretation

From a climatological perspective, the comparatively modest annual mean SD for Kinshasa (4.4 h/day) can be explained by the combined influence of equatorial atmospheric

dynamics, high relative humidity, and persistent cloud formation processes characteristic of the western part of the DRC.

Kinshasa lies within the humid tropical belt and is strongly influenced by the seasonal migration of the Intertropical Convergence Zone (ITCZ), a low-pressure belt near the equator where the northeast and southeast trade winds converge, leading to intense convective activity and cloud formation. The proximity of Kinshasa to the Atlantic Ocean further enhances moisture advection into the lower troposphere. The resulting high precipitable water content favors frequent cloud development, particularly convective and stratiform clouds, which reduce direct solar radiation and consequently limit sunshine duration. Even during relatively drier periods, residual atmospheric moisture and aerosol concentrations contribute to partial attenuation of incoming solar radiation through scattering and absorption mechanisms.

The maximum monthly SD of 5.2 h/day occurs in March and December, while the minimum monthly SD of 3.2 h/day is recorded in August. This seasonal pattern differs markedly from that observed in southern provinces, where maximum sunshine generally coincides with the dry season (June–July).

In Kinshasa, the occurrence of peak SD in March and December can be associated with transitional climatic phases linked to the northward and southward displacement of the Intertropical Convergence Zone (ITCZ). During these transitional periods, cloud cover may be temporarily reduced compared to peak rainy months, allowing increased sunshine hours. Conversely, the minimum SD observed in August, despite being within the broader dry season of western DRC, can be attributed to:

— The presence of persistent low-level stratiform cloud decks,
— Increased atmospheric stability,
— Maritime air mass influence,
— Possible aerosol loading and mist formation.

These atmospheric conditions can significantly reduce effective SD even when precipitation levels remain relatively low.

The relatively narrow range between maximum and minimum weighted SD values (5.2 h/day and 3.2 h/day) indicates moderate intra-annual variability. From a statistical standpoint, this limited amplitude suggests that Kinshasa experiences a relatively stable but consistently moderate solar regime rather than pronounced seasonal extremes. However, despite this

moderate variability, the overall annual average remains structurally lower than that of eastern and southern provinces, where continentality effects, lower humidity levels, and clearer dry-season skies favor longer sunshine duration.

In radiative terms, the reduced SD in Kinshasa implies:

— Lower cumulative annual GHI,
— A higher proportion of diffuse radiation relative to direct beam radiation,
— Greater atmospheric attenuation due to water vapor content and cloud optical thickness.

These characteristics are critical for solar resource assessment and photovoltaic performance modeling, particularly when distinguishing between technologies highly sensitive to direct irradiance (such as concentrated solar systems) and those capable of efficiently utilizing diffuse radiation (such as conventional photovoltaic modules).

Although Kinshasa exhibits lower SD compared to provinces such as Katanga, its solar potential remains sufficient to support PV systems, particularly, Rooftop PV installations for residential and commercial buildings, Grid-connected distributed generation systems and Hybrid PV systems combined with battery storage.

PV system sizing in Kinshasa must account for:

— Lower average daily solar input compared to high-SD provinces
— Seasonal variability, particularly the reduced SD observed in August
— Urban atmospheric effects, including pollution and humidity

For national energy planning, Kinshasa represents a strategic priority due to its high population density and strong electricity demand. Even with moderate SD values, large-scale rooftop solar deployment could significantly reduce pressure on the national grid and improve energy reliability.

Therefore, while Kinshasa does not belong to the highest solar potential zone identified in section 3.1.2.4, its solar resource remains technically viable and economically relevant for urban PV development.

3.2.1.1.4 Synthesis for Kinshasa

The comprehensive analysis of SD for Kinshasa can be summarized as follows:

— The annual weighted average sunshine duration in Kinshasa is 4.4 h/day, one of the lowest among the analyzed provinces.
— The maximum monthly SD (5.2 h/day) occurs in March and December, while the minimum (3.2 h/day) is observed in August.
— The city shows moderate intra-annual variability but generally lower SD compared to southern and eastern provinces.
— Despite this, solar energy remains viable for PV deployment, particularly for rooftop and distributed urban systems.
— Proper system sizing and consideration of seasonal variability are essential for optimizing PV performance in Kinshasa.

3.2.1.7. Kongo Central

Similar to Kinshasa, Kongo Central is relatively small in geographical extent. Therefore, the SD analysis was conducted without subdividing the province into districts. The data analysis was carried out for the following cities and territories: Banana, Boma, Kasangulu, Kimvula, Madimba, Matadi, Mbanza-Ngungu, and Songolo. Table 3.7 presents SD values across multiple sites in Kongo Central.

Table 3.7: MASD for Kongo-Central

Latitude	5°56'S	5°50'55"S	4°35'S	5°44'S	4°58'S	5°49'03"S	5°16'S	5°42'S	4°58'S	Averages
Longitude	12°21'E	13°03'22"E	15°11'E	15°58'E	15°09'E	13°28'15"E	14°51'E	14°02'E	12°56'E	
Area (Km^2)	4,265	65	4,680	3,371	8,260	110	8,460	3,620	3,099	
January	5.3	4.2	5.0	6.2	4.6	4.0	4.6	3.9	3,5	4,7
February	5.1	4.2	4.9	6.3	4.7	4.0	4.8	4,1	3,6	4,8
March	5.4	4.5	5.3	6.3	5.0	4.3	5.2	4,4	4,0	5,1
April	5.0	4.1	5.0	5.5	4.9	3.8	5.0	4,0	3,6	4,8
May	3.8	2.6	4.4	6.2	4.3	2.6	4.1	2,9	2,3	4,1
June	3.1	1.6	4.1	7.2	4.4	2.0	4.3	2,6	1,7	4,0
July	3.1	1.5	4.2	7.6	4.9	2.1	4.9	3,2	1,6	4,4
August	2.6	0.8	3.3	6.9	3.7	1.1	3.4	1.7	0.8	3.3
September	2.3	0.5	3.5	6.1	3.6	0.7	2.9	1.1	0.5	3.0
October	2.6	1.7	4.4	5.5	3.9	1.8	3.6	2.1	1.6	3.5
November	4.4	3.8	5.0	5.6	4.6	3.6	4.5	3.7	3.1	4.5
December	5.0	4.1	5.0	5.9	4.6	3.8	4.6	3.8	3.2	4.6
Averages	4.0	2.8	4.5	6.3	4.4	2.8	4.3	3.1	2.4	4.2

Wide SD ranges confirm significant spatial variability, reflecting the influence of coastal proximity and topographic diversity while, figure 3.9 compares temporal SD evolution across Kongo Central sites.

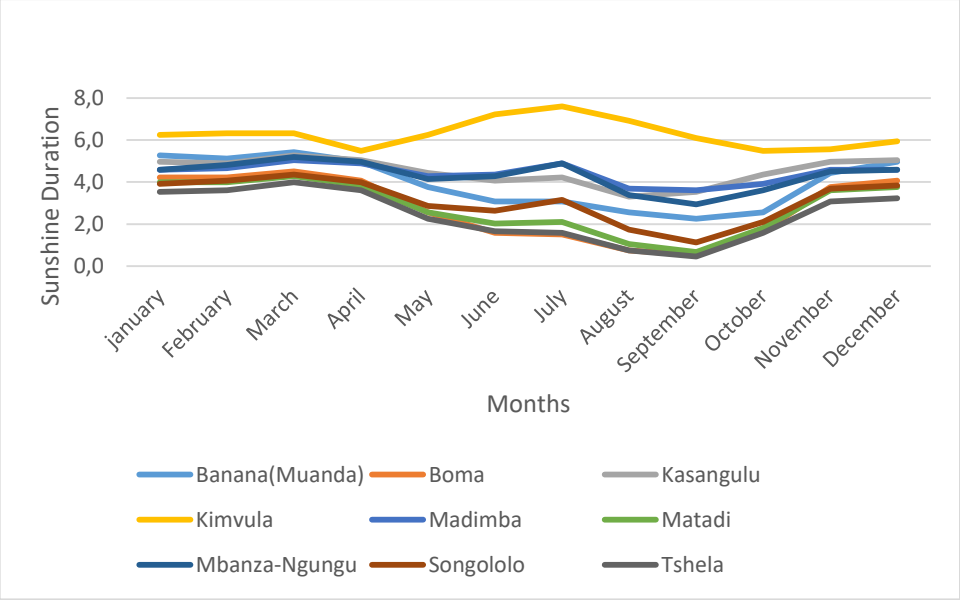

Figure 3.9: Temporal Trend of monthly SD for Kongo Central

The figure reveals deviations from theoretical seasonal patterns, emphasizing the need for localized calibration when modeling solar radiation in coastal areas.

Analysis of the Observed Characteristics

The annual weighted SD for Kongo Central is 4.2 h/day, which is slightly lower than that of Kinshasa (4.4 h/day) and considerably lower than the values recorded in southern provinces. This relatively moderate provincial average reflects the strong maritime and humid tropical influence affecting the western corridor of the Democratic Republic of Congo.

However, a remarkable feature of Kongo Central is the very high spatial variability observed between its territories. The maximum monthly SD reaches 7.6 h/day in Kimvula, while the minimum monthly SD drops to 0.5 h/day in Tshela. This very large monthly amplitude (7.1 h/day difference) indicates strong local climatic contrasts within the province. Such variability may be explained by the differences in altitude and local topography, the orographic cloud formation in certain territories, the proximity to maritime air masses, and the local convective activity patterns.

Kimvula, which records the highest annual mean SD of 6.3 h/day, appears to benefit from more favorable atmospheric transparency and reduced persistent cloud cover compared to other territories. In contrast, Tshela, with the lowest annual mean SD of 2.5 h/day, likely experiences more frequent cloudiness, higher atmospheric moisture retention, or local microclimatic effects that significantly reduce effective sunshine duration.

At the provincial level, the weighted SD maximum is 5.1 h/day, while the weighted minimum is 3.0 h/day, showing moderate intra-annual variability when aggregated across the province. The maximum SD for the province occurs in March, whereas the minimum occurs in September. This seasonal behavior suggests a transitional peak period around March linked to reduced cloud persistence, and a relative solar minimum in September possibly associated with atmospheric stability and residual moisture accumulation.

From a climatological perspective, the coexistence of very high local monthly values (7.6 h/day) and extremely low values (0.5 h/day) within the same province highlights the importance of territorial-scale solar resource assessment rather than relying solely on provincial averages.

The observed characteristics have important implications for PV planning in Kongo Central: It is noted that:

1. The strong spatial heterogeneity means that PV system sizing should be performed at the territorial level rather than using only the provincial weighted average
2. Territories such as Kimvula, with an annual mean SD of 6.3 h/day and monthly peaks of 7.6 h/day, are highly favorable for utility-scale PV plants, grid-connected solar farms and hybrid PV–battery systems with high yield performance.
3. While territories like Tshela, with an annual mean SD of 2.5 h/day and extreme monthly lows (0.5 h/day), require oversized PV arrays, larger battery storage capacity, hybridization with other energy sources (diesel, hydro, or biomass),and more conservative performance ratio assumptions.
4. With a provincial weighted SD of 4.2 h/day, Kongo Central remains suitable for decentralized rooftop PV systems, particularly in urban centers such as Matadi and Boma. However, system optimization must account for seasonal dips, especially around September.

Overall, while Kongo Central does not present uniformly high solar potential, certain territories offer very strong solar opportunities, making the province strategically interesting for targeted solar investments.

3.2.1.1.5 Synthesis of Kongo centrals

The overall findings of SD study for Kongo Central can be summarized as follows:

- The annual weighted SD of Kongo Central is 4.2 h/day.
- Strong spatial variability exists between territories.
- The highest monthly SD (7.6 h/day) and highest annual mean SD (6.3 h/day) are recorded in Kimvula.
- The lowest monthly SD (0.5 h/day) and lowest annual mean SD (2.5 h/day) are observed in Tshela.
- The provincial weighted SD maximum is 5.1 h/day (March), and the minimum is 3.0 h/day (September).
- PV planning in Kongo Central must be territory-specific due to strong local climatic contrasts.
- High-potential zones can support large-scale PV deployment, while low-SD areas require hybrid and storage-optimized solutions.

3.2.1.8. Province of Maniema

Data analysis was carried for the city of Kindu and the territories of Kasongo, Kibombo, Lubutu, Pangi and Punia. Table 3.8 presents monthly averages SD for selected locations in Maniema.

Table 3.8: Weighted MASD for Maniema

Latitude (°)	4°27'S	3°54'S	2°57'00"S	0°44'S	3°11'00"S	1°28'S	Averages
Longitude (°)	26°39'E	25°55'E	25°57'00"E	26°35'E	26°38'00"E	26°27'E	
Area (Km²)	17,000	24,953	101	16,055	14,542	19,805	
Sites	Kasongo	Kibombo	Kindu	Lubutu	Pangi	Punia	
January	5.2	5.3	5.5	6.0	5.5	5.9	5.6

Latitude (°)	4°27'S	3°54'S	2°57'00"S	0°44'S	3°11'00"S	1°28'S	Averages
Longitude (°)	26°39'E	25°55'E	25°57'00"E	26°35'E	26°38'00"E	26°27'E	
Area (Km²)	17,000	24,953	101	16,055	14,542	19,805	
Sites	Kasongo	Kibombo	Kindu	Lubutu	Pangi	Punia	
February	5.3	5.3	5.5	5.9	5.6	5.9	5.6
March	5.0	5.0	5.0	5.5	5.0	5.3	5.2
April	5.0	4.8	4.5	5.0	4.7	4.7	4.8
May	5.7	5.0	4.5	4.7	4.8	4.5	4.9
June	7.1	6.4	5.6	5.2	5.9	5.0	5.9
July	7.4	7.1	6.4	5.6	6.8	5.7	6.5
August	6.7	6.2	5.7	5.0	6.0	5.0	5.8
September	5.7	5.4	5.2	4.7	5.2	4.7	5.2
October	5.0	5.0	4.9	4.5	4.7	4.5	4.8
November	4.5	4.7	4.7	4.7	4.7	4.6	4.6
December	4.5	4.7	4.7	5.2	4.8	5.1	4.9
Anual average	5.6	5.4	5.2	5.2	5.3	5.1	5.3

Moderate SD values with limited spatial variability indicate stable solar conditions. Peak SD occurs in June–July, with minima in November. Figure 3.10 illustrates the temporal evolution of SD in Maniema.

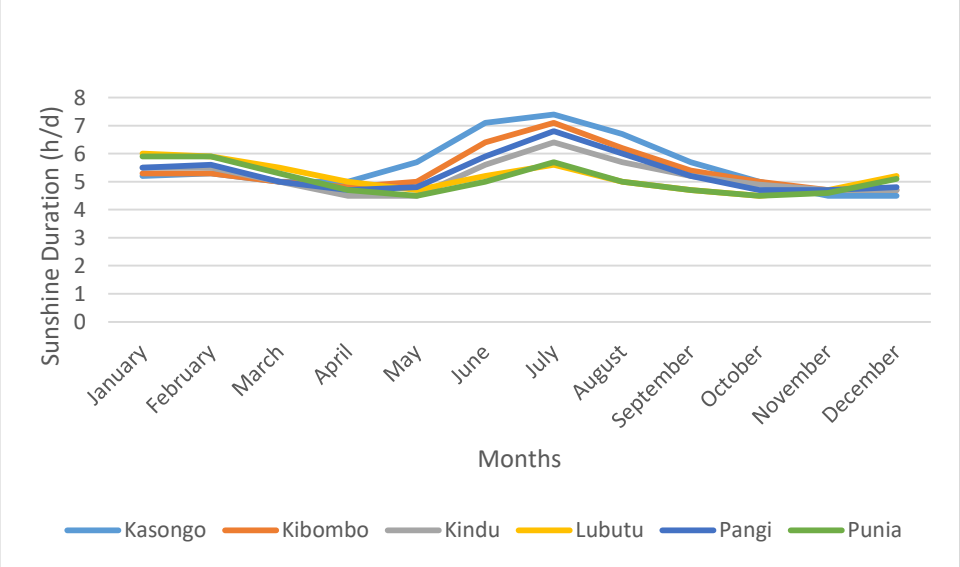

Figure 3.10: Tempotal Trend of monthly SD for Maniema

Figure 3.10 outlines smooth seasonal cycles, suggesting minimal local disturbances. The stability supports reliable predictive modeling for PV systems.

Analysis of the Observed Characteristics

The province of Maniema presents an annual weighted SD of 5.3 h/day. At first glance, this value may appear moderate when considered alone. However, Maniema belongs, together with Katanga, to the Very High Potential Area (sction 3.1.2.3) of SI in the DRC, characterized by an average annual GHI of approximately 6.5 kWh/m²/day.

This apparent contrast between a moderate SD (5.3 h/day) and a very high irradiation level (≈ 6.5 kWh/m²/day) is scientifically coherent. In equatorial continental climates such as Maniema the solar elevation angles are high throughout the year, the extraterrestrial solar input is strong, while diffuse irradiation contributes significantly under partially cloudy conditions. Therefore, even when SD is not extremely high in terms of hours, the energy intensity per hour of sunshine remains elevated, explaining the classification of Maniema within the very high irradiation zone.

Unlike coastal western provinces, Maniema benefits from its inland continental positioning, the reduced maritime moisture influence, a strong dry-season atmospheric transparency, and the high solar zenith angles near the equator. These factors jointly enhance annual irradiation levels.

Implications for Photovoltaic (PV) System Planning

Belonging to the Very High Potential Area (≈ 6.5 kWh/m²/day) significantly strengthens Maniema's strategic value for solar development.

Despite an SD of 5.3 h/day, the high irradiation intensity implies: elevated PV module output per installed kWp, favorable performance ratios, Competitive LCOE. Maniema can therefore sustain: utility-scale PV plants, hybrid PV–hydro systems (given regional hydrological resources), rural mini-grids, off-grid electrification programs.

Since June corresponds to maximum SD and atmospheric clarity, then performance testing and benchmarking should use June as peak reference. Also, Grid injection studies should

consider June for maximum feed-in scenarios. Conversely, November should be used for conservative yield modeling in off-grid systems.

Because seasonal variation remains moderate thus, battery storage sizing can remain optimized rather than oversized,hybridization needs are strategic rather than mandatory, and system reliability remains high even during lower SD months.

Based on provincial weighted data, Kasongo (5.6 h/day) emerges as a strong candidate for large-scale PV installations. While Punia (5.1 h/day) remains fully viable but may require marginal array oversizing for identical annual output.

3.2.1.1.6 Synthesis for Maniema

Maniema Province, together with Katanga, belongs to the Very High Solar Irradiation Zone of the DRC (≈ 6.5 kWh/m²/day). Although the annual weighted SD is 5.3 h/day, the high irradiation intensity compensates for moderate sunshine hours, ensuring strong photovoltaic performance. Key characteristics of this province include:

— Maximum monthly SD of 7.4 h/day in June (Kasongo),
— Minimum monthly SD of 4.5 h/day around November,
— Highest annual mean SD of 5.6 h/day (Kasongo),
— Lowest annual mean SD of 5.1 h/day (Punia),
— Provincial weighted SD range between 4.6 and 5.9 h/day.

The seasonal maximum in June and minimum in November confirm a clear ITCZ-driven climatic modulation.

Overall, Maniema offers structurally strong and strategically attractive conditions for PV development, combining high irradiation intensity, moderate seasonal variation, spatial homogeneity, and favorable long-term energy predictability.

3.2.1.9. Nord Kivu

Data analysis was carried out for the city of Goma and the territories of Beni, Butembo, Goma, Lubero, Masisi, Rutshuru and Walikale. The findings are described in the Table 3.9.

Table 3.9: Weigted MASD for Nord Kivu

Latitude (°)	0°07'40"S	1°41'36"S	0°09'S	1°24'S	1°11'S	1°25'S	Weighted averages (h/d)
Longitude (°)	29°17'15"	13°31"E	29°14'E	28°48'E	29°27'E	28°02'E	
Aire (Km²)	190	900	18,096	4,734	5,289	23,475	
City/Town	Butembo	Goma	Lubero	Masisi	Rutshuru	Walikale	
January	6.4	6.3	5.5	5.9	7.1	7.2	6.5
February	6.6	6.3	5.9	5.9	7.1	7.1	6.5
March	5.7	5.9	4.8	5.2	6.6	6.5	5.8
April	5.3	5.9	4.6	5.3	6.5	6.2	5.6
May	5.4	6.1	5.0	5.6	6.5	5.9	5.6
June	5.6	6.8	5.3	6.1	7.0	6.1	5.9
July	5.5	7.3	5.4	6.5	7.4	6.5	6.2
August	5.1	7.1	5.0	5.7	7.1	5.9	5.7
September	5.0	6.6	4.8	4.6	6.7	5.3	5.2
October	4.8	5.9	4.6	4.1	6.3	5.3	5.1
November	5.0	5.6	4.3	4.4	6.1	5.9	5.2
December	5.7	5.9	4.8	5.3	6.5	6.6	5.9
Anual average (h/d)	5.5	6.3	5.0	5.4	6.7	6.2	5.8

Source: Compiled from [14].

Table 3.10 highlights moderate SD values (~5.8 h/d) with an atypical seasonal peak in January–February highlight regional climatic peculiarities, while Figure .3.11 illustrates its the temporal trend of MASD.

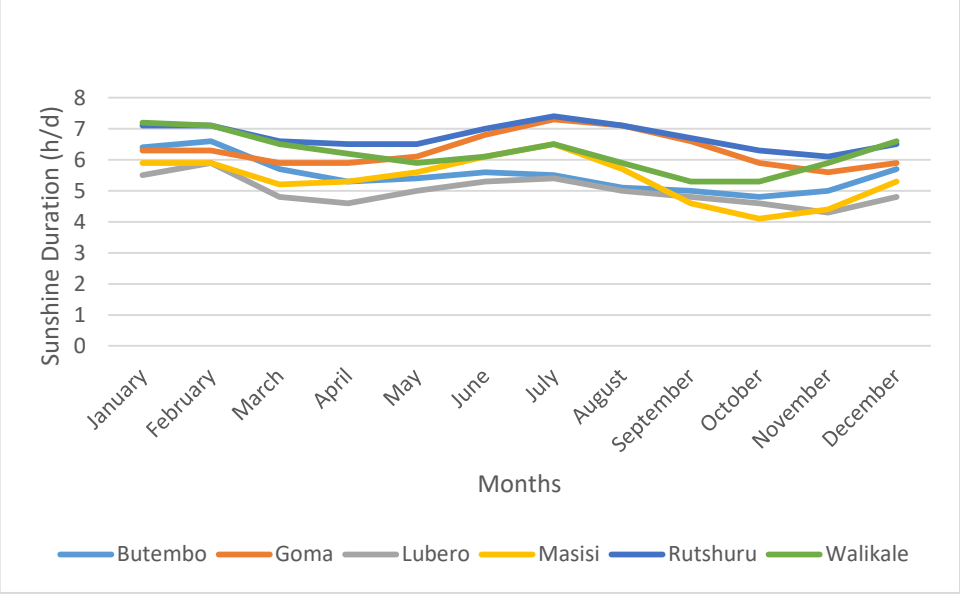

Figure 3.11: Tempotal Trend of monthly SD for Nord Kivu

The shifted seasonal pattern outlined in figure 3.11 can be explained by high-altitude and volcanic influences, indicating that province-specific PV modeling approaches are necessary, as standard tropical assumptions may not apply.

Analysis of the Observed Characteristics

Nord Kivu presents an annual weighted SD of 5.8 h/day, which is slightly higher than several equatorial western provinces. This aligns with its classification within the “High Solar Potential Area” of the DRC. Although Nord Kivu does not reach the “Very High Potential Area” category (such as Katanga or Maniema in terms of irradiation), it benefits from elevated terrain (high-altitude plateaus), reduced atmospheric density at higher elevations, lower optical air mass, enhanced solar transmissivity.

The difference between the highest annual mean SD: 6.8 h/day (Rutshuru) and the lowest annual mean SD: 5.0 h/day (Lubero) indicates a 1.8 h/day dispersion, which is more pronounced than in Maniema. This variability can scientifically be explained by topographic contrasts, orographic cloud formation, localized microclimates, volcanic highlands influencing atmospheric circulation. Such heterogeneity requires territory-specific solar assessment before large-scale installations.

Nord Kivu’s classification within the High Solar Potential Area offers strong strategic opportunities with its weighted SD of 5.8 h/day. Thus, PV systems can achieve a good annual capacity factors, reliable production profiles, competitive LCOE compared to thermal alternatives. While its elevated terrain provides higher module efficiency due to cooler temperatures, reduced performance losses, and improved long-term yield stability [67].

This is particularly advantageous for utility-scale PV. Because the minimum SD occurs in October, system sizing should account for lower production during this month, integrate adequate storage for off-grid systems and consider hybridization in isolated zones.

3.2.1.1.7 Synthesis of Nord Kivu

Nord Kivu, located within the High Solar Potential Area of the DRC, exhibits:

- Annual weighted SD of 5.8 h/day,
- Maximum monthly SD of 7.4 h/day (Rutshuru),
- Minimum monthly SD of 4.1 h/day (Masisi),
- Highest annual mean SD of 6.8 h/day (Rutshuru),
- Lowest annual mean SD of 5.0 h/day (Lubero),
- Provincial SD variation between 6.5 and 5.3 h/day.

Its high-altitude equatorial positioning can explain its strong solar resource despite seasonal cloud dynamics. Overall, Nord Kivu presents solid technical and economic conditions for photovoltaic deployment, with particular advantages linked to elevation-driven efficiency gains and strong annual irradiation levels.

3.2.1.10. Province Orientale

Former Province Orientale was the largest province in the DRC. To facilitate the analysis of its SD, this province was categorized into its four former Districts: Bas-Uele, Haut Uele, Ituri and Tshopo. The MASD values for former Province-Orientale districts are summarized in Table 3.10. Details on the SD of distrcts are provided in Appendix E.

Table 3.10: Weighted MASD for Province-Orientale

	Bas-Uele	Haut Uele	Ituri	Tshopo	Tshuapa
January	7,3	7,5	7,1	6,4	6,2
February	7,0	7,3	7,0	6,3	5,9
March	6,4	6,7	6,1	5,7	5,6
April	5,6	6,0	5,6	5,0	4,9
May	5,1	5,3	5,3	4,6	5,0
June	5,2	5,1	5,1	4,8	6,1
July	5,3	5,3	5,1	5,0	6,5
August	4,9	5,1	4,9	4,7	5,7
September	4,6	4,8	4,7	4,6	5,4
October	4,0	4,2	4,5	4,4	5,1
November	4,8	5,5	4,9	4,3	4,8
December	6,5	6,9	6,2	5,3	5,2
Averages	5,6	5,8	5,5	5,1	5,5

Analysis of the Observed Facts

Province Orientale belongs to the zone classified as Medium Solar Potential Area, with solar irradiation ranging from 4.5 to 6 kWh/m²/day. However, its weighted annual average SD of 5.5 h/day indicates that this province benefits from relatively moderate SD throughout the year. This Province exhibits a structured spatial variability as folloows:

— Haut-Uele (5.8 h/day) appears as the most sun-exposed district, suggesting relatively stable atmospheric transparency and less persistent cloud cover.

— Tshopo (5.1 h/day) remains the least sun-exposed district, likely due to stronger convective activity and higher humidity influence.

Figure 3.12 presents the temporal trend of this province as follows:.

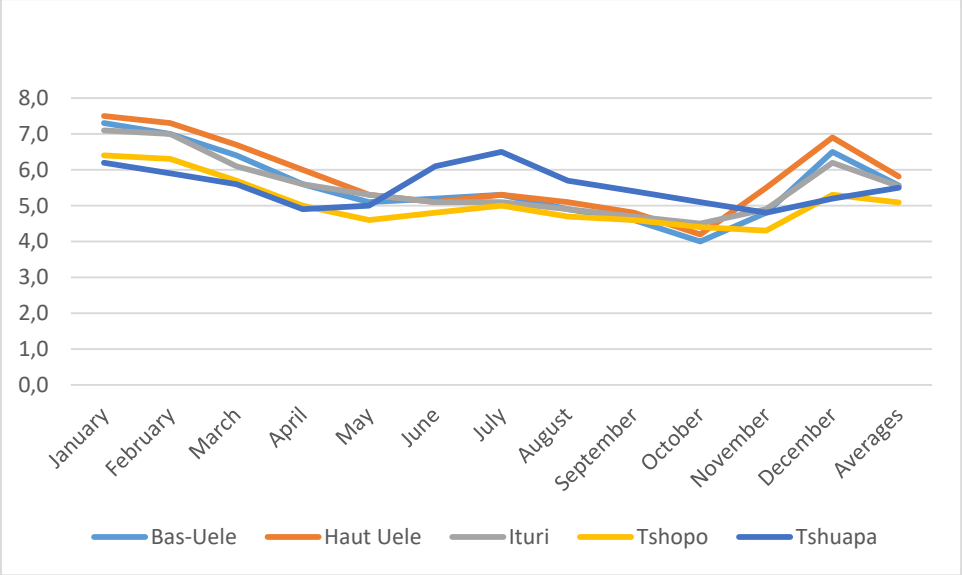

Figure 3.12: Tempotal Trend of MASD (in h/day) for Province-Orientale

The Figure 3.12 exhibits a seasonal distribution, which follows a coherent equatorial pattern:

— This seasonal January (followed by February) records the highest SD, corresponding to a relatively drier atmospheric window.

— October records the lowest SD, generally associated with increased cloud formation and rainfall intensity.

This behavior can be explained by the strong influence of atmospheric convection and cloud dynamics on SD variability.

Although Province Orientale and Equateur Province are located almost at the same latitudes, they do not present identical annual SD nor identical solar irradiation levels. Four scientific factors can explain this difference:

i. Cloud Cover Persistence
    a. Equateur Province is deeply embedded within the central Congo Basin forest ecosystem, where high atmospheric moisture and dense cloud cover persist throughout the year. This reduces effective solar irradiation transmission.

ii. Convective Rainfall Intensity
    a. The frequency and intensity of convective systems differ between the two provinces. Even small regional differences in atmospheric circulation can significantly affect solar radiation reception.

iii. Land Cover and Surface Energy Balance
    a. Province Orientale includes transitional zones between dense forest and more open areas, which influence local albedo and microclimatic behavior. These differences impact solar energy absorption and atmospheric transparency.

iv. Difference Between SD and Solar Irradiation
    a. Sunshine Duration (h/day) measures time, whereas solar irradiation (kWh/m²/day) measures energy.

A province may experience long sunshine hours but with reduced intensity due to atmospheric scattering, humidity, and aerosols. This explains why Province Orientale, remains within the Medium Solar Potential classification. Thus, latitude alone does not determine solar potential. Atmospheric physics and regional climatic dynamics play a decisive role.

From a planning perspective, Province Orientale presents strong but carefully structured opportunities for PV deployment, such are.

(i) Favorable Conditions for Decentralized Systems

With 5.5 h/day annual weighted SD, the province is suitable for: stand-alone PV systems, rural mini-grids, institutional electrification (health centers, schools), agricultural productive-use systems.

(ii) Seasonal Optimization Requirement

Since October presents the lowest SD, system sizing must account for slight oversizing of PV arrays, adequate battery storage capacity, optimized tilt angle to maximize dry-season production.

(iii) District-Based Planning Strategy

— Haut-Uele (5.8 h/day): highly favorable for large PV farms and commercial solar installations.
— Tshopo (5.1 h/day): requires reinforced storage strategy and potentially hybridization with other sources.

(iv) Medium Solar Potential Optimization Strategy

In a Medium Solar Potential Area, high-efficiency modules are recommended, performance ratio optimization becomes critical, and proper maintenance to reduce soiling losses is essential.

3.2.1.1.8 Summary

A direct comparison between Province Orientale and Équateur Province, both located within the equatorial belt, reveals a non-negligible divergence in sunshine duration (SD) despite their similar latitudinal positioning. While Équateur records a slightly higher weighted SD (~6.0 h/day), Province Orientale exhibits lower values (~5.4 h/day), with a broader intra-provincial variability (5.1–5.8 h/day). This contrast cannot be attributed to solar geometry, which remains nearly identical, but rather reflects differences in regional atmospheric regimes. Province Orientale is more strongly influenced by persistent convective systems, higher cloud cover frequency, and moisture recycling processes, leading to reduced atmospheric transmissivity. In contrast, Équateur—although also humid—appears to benefit from relatively more stable cloud dynamics or shorter cloud persistence durations.

This comparison provides compelling evidence of spatial non-stationarity within the equatorial climate zone itself, demonstrating that even minimal geographic displacement can induce measurable differences in solar resource availability. From a modeling standpoint, this result strongly supports the need for region-specific calibration of SD–GSI relationships, as

assuming homogeneity within the equatorial band would introduce systematic bias in solar resource assessment and, consequently, in photovoltaic (PV) system design and energy yield predictions.

3.2.1.11. Sud Kivu

In Sud Kivu, data analysis was conducted for the city of Bukavu and the territories of Fizi, Kabare, Kalehe, Mwenga, Shabunda, Uvira and Walungu. Table 3.11 presents the monthly Sunshine Duration (SD) across selected territories of Sud Kivu, providing a detailed spatial and temporal characterization of solar availability within the province.

Table 3.11: Monthly SD for Sud Kivu

Latitude (°)	2°30'55"S	4°18'S	2°30'S	2°07'S	3°03'S	2°42'S	2°38’S	3°26'S
Longitude (°)	28°50'42^{E}	28°57'E	28°48'57"E	28°55'E	28°26'E	27°21'E	28°40’E	29°08'E
Aire (Km²)	60	15,788	1,960	5,125	11,172	25,116	1,800	3,148
City	Bukavu	Fizi	Kabare	Kalehe	Mwenga	Shabunda	Walungu	Uvira
January	5.5	7.6	6.5	7.3	6.3	5.8	5.5	7.7
February	6.0	7.7	6.5	7.4	6.7	5.6	6.0	7.7
March	5.9	7.4	5.9	7.2	6.5	5.3	5.9	7.4
April	5.8	6.8	5.8	7.0	6.7	6.5	5.8	6.5
May	6.3	7.4	5.9	7.0	7.0	5.3	6.3	6.6
June	6.9	7.7	6.1	7.4	7.0	6.9	6.9	7.6
July	7.3	7.8	6.4	7.7	7.1	6.8	7.3	7.8
August	7.2	7.9	5.9	7.7	6.7	6.2	7.2	7.9
September	6.8	7.9	5.3	7.5	5.9	5.4	6.8	7.8
October	5.9	7.7	4.9	7.1	5.3	5.0	5.9	7.4
November	5.3	7.4	5.3	7.0	5.6	5.0	5.3	7.2
December	5.3	7.4	6.1	7.1	5.9	5.1	5.3	74
Anual average	6.2	7.6	5.9	7.3	6.4	5.7	6.2	7.4

Source: Compiled from [14].

The dataset reveals a marked intra-provincial heterogeneity, with annual averages ranging from 5.7 h/day (Shabunda) to 7.6 h/day (Fizi). This dispersion highlights the strong

influence of local geographic controls, particularly topography, proximity to Lake Tanganyika, and forest cover.

From a temporal perspective, the monthly values suggest a well-defined seasonal structure, yet with attenuated variability compared to purely continental climates. The relatively elevated SD values observed in several territories indicate that, despite its classification within a lower irradiation zone, Sud Kivu maintains a non-negligible solar resource in terms of sunshine duration.

This confirms that SD alone is insufficient to fully characterize solar energy potential, reinforcing the need to integrate additional atmospheric variables in irradiance modeling.

Figure 3.13 illustrates the temporal evolution of monthly SD across the selected territories of Sud Kivu, highlighting seasonal dynamics and inter-territorial variability.

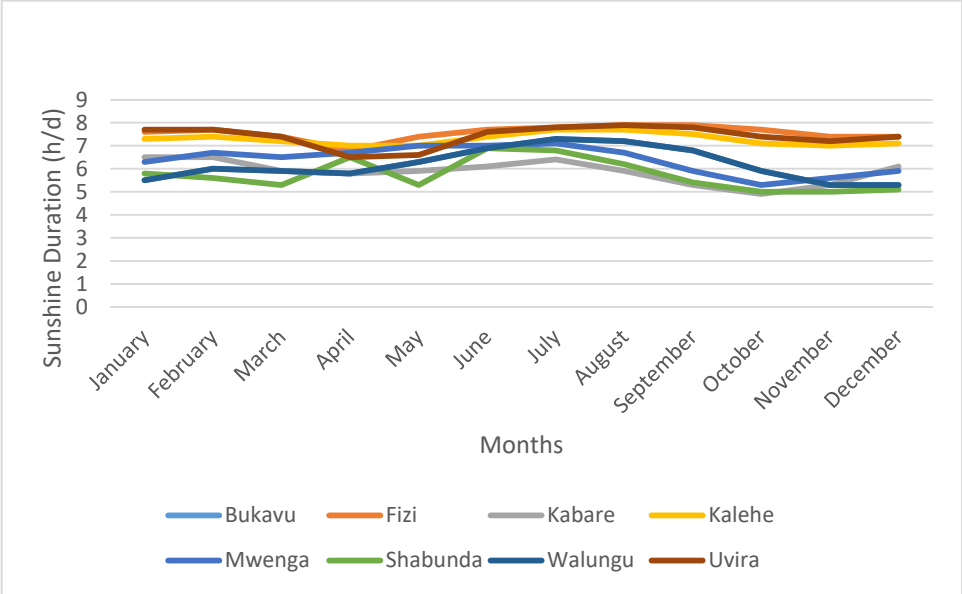

Figure 3.13: Temporal Trend of monthly SD for Sud Kivu

The figure 3.13 clearly emphasizes a coherent seasonal cycle dominated by atmospheric dynamics, with a systematic peak during the dry season (June–August) and a minimum during the onset of the rainy season (October–November).

Beyond this general pattern, the divergence between curves reveals the role of mesoscale climatic effects, including orographic lifting, localized convection, and lake-induced atmospheric stabilization. In particular, territories such as Fizi and Uvira exhibit persistently

higher SD, suggesting reduced cloud persistence and enhanced atmospheric transparency, while inland forested areas such as Shabunda display dampened SD profiles due to high humidity and convective cloud development.

Importantly, the moderate seasonal amplitude (~1.3 h/day) indicates a relatively stable solar regime, which is advantageous for PV system predictability, even though irradiance levels may remain constrained by cloud optical properties.

The statistical indicators confirm a moderately high but structurally constrained SD regime, with a provincial weighted average of 6.5 h/day. The relatively narrow gap between maximum (7.2 h/day) and minimum (5.9 h/day) weighted SD values suggests limited intra-annual variability, reinforcing the notion of a stable yet climate-regulated solar regime.

However, the coexistence of relatively high SD values with low SI levels points to a decoupling between SD and effective solar energy yield, primarily driven by cloud optical thickness, atmospheric moisture content, and scattering processes. This highlights a critical implication for the study: Accurate solar irradiance modeling in Sud Kivu cannot rely solely on SD, but must incorporate climatic parameters such as humidity, temperature, and rainfall, which directly affect atmospheric transmissivity.

Overall, Sud Kivu exemplifies a climatically complex solar regime where relatively favorable SD coexists with reduced irradiance efficiency, underscoring the necessity of multi-variable modeling approaches for reliable PV resource assessment.

3.2.1.1.1.2. Comparison with Nord Kivu

Sud Kivu and Nord Kivu share a similar equatorial-altitude climatic regime. However, Nord Kivu is classified within the High Solar Potential Area, with annual irradiation between 6 and 6.5 kWh/m²/day, almost double that of Sud Kivu. The difference can be explained by:

1. *Volcanic and Atmospheric Conditions*

Nord Kivu benefits from:

— More frequent clear-sky windows
— Lower persistent cloud layers in certain zones

— Different atmospheric circulation influenced by the Rift Valley structure

2. Cloud Persistence Differences

Sud Kivu experiences:

— Stronger lake–mountain convection
— Higher annual humidity
— Greater cumulative cloud cover

Thus, even if SD values appear comparable in duration, the quality and intensity of SI differ significantly.

This confirms that: SD alone does not fully determine solar potential; but, irradiance intensity and atmospheric transmissivity are decisive factors.

3.2.1.1.9 Photovoltaic Development Opportunities in Sud Kivu

Despite being classified as a Low Solar Potential Area, Sud Kivu still presents significant opportunities for PV deployment.

Given the dispersed rural population and limited grid coverage, technics such are solar home systems, community mini-grids; hybrid solar-diesel systems can be viable and economically justified. The peak SD during the dry season (June–August) coincides with reduced hydroelectric output in some micro-hydro plants [68] and increased agricultural processing demand. Thus, PV can complement hydro resources effectively.

Urban zones with stable SD around 6–7 h/day are suitable for commercial rooftop PV, institutional solarization (universities, hospitals) or public lighting systems. Compared to Nord Kivu, which is more suitable for higher-yield grid-scale installations, Sud Kivu's comparative advantage lies in distributed generation rural electrification, hybridization strategies

3.3 Analysis of Sunshine Duration

3.3.1 Provinces Sunshine Duration

Table 3.12 provides a synthetic overview of the spatial distribution of SD across both the former and the newly established provinces of the DRC. It enables a comparative assessment of solar resource variability at different administrative scales.

Table 3.12: Provinces' SD

Provinces (Former)	Weighted SD (h/day)	Districts /New Provinces	Weighted SD (h/day)
Bandundu	6.2	Kwilu	6.1
		Kwango	6.4
		Mai-Ndombe	6.2
Equateur	5.9	Équateur	6.0
		Mongala	5.7
		Nord-Ubangi	6.1
		Sud-Ubangi	6.0
		Tshuapa	5.5
Kasaï-Occidental	5.6	Kasaï-Central	5.9
		Kasaï	5.5
Kasaï-Oriental	5.9	Kasaï-Oriental	5.6
		Lomami	6.4
		Sankuru	5.6
Katanga	6.8	Haut-Katanga	6.8
		Haut-Lomami	6.6
		Lualaba	6.8
		Tanganyika	6.8
Kinshasa	4.5	Kinshasa	4.5
Kongo-Central	4.2	Kongo-Central	4.2
Maniema	5.3	Maniema	5.3
Nord Kivu	5.8	Nord-Kivu	5.8
Province-Orientale	5.4	Bas-Uele	5.6
		Haut-Uele	5.8
		Ituri	5.5
		Tshopo	5.1
		Tshuapa	5.5
Sud Kivu	6.5	Sud-Kivu	6.5

Table 3.12 reveals a marked spatial heterogeneity of SD across the country, with values ranging from 4.2 h/day to 6.8 h/day, indicating significant regional contrasts in solar resource

availability. This contrast can be primarily explained by the interaction between large-scale atmospheric circulation and regional climatic regimes. This is particularly pronounced in regions located within or near the equatorial belt , such as Équateur, which are subject to persistent convective activity and high cloud cover driven by the recurrent passage of the ITCZ, reducing effective SD. In contrast, southeastern regions, particularly the former Katanga, experience more stable atmospheric conditions, characterized by reduced cloud persistence and longer clear-sky periods, leading to higher SD values.

Additionally, local factors such as altitude, land cover, and moisture availability further modulate this pattern by influencing cloud formation and atmospheric transparency. As a result, the observed spatial variability reflects a coupled climate–surface control, where both macro-scale circulation and meso-scale environmental conditions jointly determine the distribution of solar resources.

Figure 3.14 presents a heat map visualization of the spatial distribution of sunshine duration (SD), highlighting regional variability and intensity patterns across the study area.

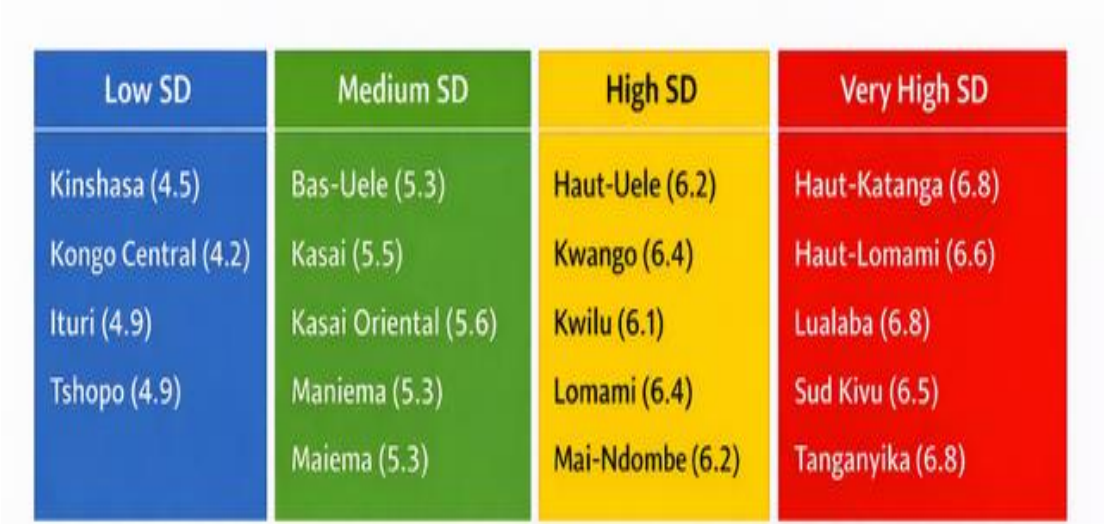

Figure 3.14: Provincial-level Heat Map of Weighted Daily SD across the DRC

The latitudinal analysis of SD across the RDC reveals that solar resource variability cannot be explained by solar geometry alone. Provinces located at comparable latitudes exhibit substantial differences in SD, with equatorial regions such as Équateur (~6.0 h/day) and Province Orientale (~5.1–5.8 h/day) showing clear divergence, while low-latitude western provinces (Kinshasa: 4.5 h/day; Kongo Central: 4.2 h/day) contrast sharply with southeastern

regions (Haut-Katanga: 6.8 h/day; Haut-Lomami: 6.6 h/day). These discrepancies highlight the dominant role of longitudinal atmospheric gradients, moisture advection, and cloud dynamics, which override latitudinal control. Consequently, SD in the DRC must be interpreted as a climate-driven rather than geometry-driven variable, providing strong justification for spatially explicit SD–GSI modeling frameworks.

3.3.2 Synthetic Scientific Analysis of the Spatial Distribution of SD in the DRC

The heat map summarizes provincial SD patterns, complementing the monthly tables and figures. Provinces such as Katanga (Haut-Katanga, Lualaba, Tanganyika), and Sud-Kivu fall in the **Very High** (red) category, confirming their prime solar potential for both decentralized and grid-connected PV systems. Kwango (in the former province of Bandundu), Lomami (in the former province of Kasaï-Oriental), and Haut-Uele (in the former Province-Orientale) appear in the **High** (yellow) category, still favorable for PV deployment. Central and northern provinces, including Équateur, Nord-Ubangi, and Tshopo, lie in the **Medium** or **Low** (green and blue) zones, reflecting moderate to low SD.

3.3.2.1. Spatial Distribution Insights

A synthetic analysis of provincial SD reveals that spatial variability is not governed solely by latitude. Instead, atmospheric and climatic controls, particularly cloud cover dynamics, play a dominant role. Seasonal migration of the ITCZ modulates rainfall and cloud formation, shaping effective SD patterns across the country. This explains why southern and southeastern provinces experience the highest SD, while central equatorial and coastal provinces are less sun-exposed.

Interpretation by Heat Map Zones:

The Heat Map Zones can be interpreted as follows:

— Low SD (blue): Provinces like Kongo Central, Kinshasa, and Maniema experience reduced SD due to oceanic influence, or dense equatorial forests, and persistent cloud cover. These areas are less favorable for solar PV deployment.

— Medium SD (green): Central and northern provinces, including Équateur, Nord-Ubangi, Tshopo, Bas-Uele, and Ituri, exhibit moderate SD. Seasonal dry periods improve sunshine hours, but equatorial humidity and cloud formation limit annual totals.

— High SD (yellow): Provinces such as Kwango, Lomami, and Haut-Uele enjoy favorable SD with fewer annual clouds, suitable for efficient PV systems. Elevation in eastern areas also enhances solar exposure.
— Very High SD (red): Haut-Katanga, Lualaba, Tanganyika, and Sud-Kivu record the highest SD nationally. These provinces benefit from continental climatic influence, longer dry seasons, making them the priority zones for solar energy development.

This heat map provides a strategic, visually integrated summary of provincial solar potential, complementing all previous tables and figures, and enabling immediate identification of priority areas for PV deployment.

Interpretation of Extreme MASD Areas

The classification discussed above was based on SD magnitudes. The present analysis shifts the focus from absolute values to the timing of provincial extreme MASD (maximum and minimum), providing deeper insight into the seasonal dynamics governing solar availability. The results indicate that MASD divides the DRC into four distinct climatic–radiative regimes:

(i) Area 1 (Max in July, Min in November):

This regime reflects provinces dominated by a pronounced mid-year dry season, during which reduced cloud cover leads to peak solar availability. The sharp decline toward November corresponds to the onset of convective rainfall and increased atmospheric opacity. This pattern is characteristic of continental tropical climates, where SD variability is strongly controlled by seasonal cloud dissipation rather than astronomical factors.

(ii) Area 2 (Max in January–February, Min in October):

This area corresponds to equatorial bimodal rainfall regimes, where two rainy seasons structure the annual cycle. The SD maxima observed at the beginning of the year coincide with relatively clearer atmospheric conditions between rainfall peaks, while the October minimum aligns with intensified cloud formation. This indicates a cloud-modulated radiative regime, typical of equatorial environments.

(iii)Area 3 (Max in March, Min in August–September):

Provinces in this zone are influenced by Atlantic maritime dynamics, which alter the seasonal distribution of cloud cover. The early-year maximum suggests a transient period of reduced marine cloud intrusion, while the late dry-season minimum reflects persistent low-level cloudiness and humidity. This regime highlights the role of ocean–atmosphere interactions in modulating SD.

(iv) Area 4 (Katanga: Max in September, Min in March):

This regime is indicative of a southern tropical climate with a delayed seasonal cycle, where the dry season peaks toward the end of the austral winter. The high SD in September results from minimal cloud cover and enhanced atmospheric transparency, whereas the March minimum corresponds to peak rainy season conditions. This area exhibits the strongest seasonal contrast in SD.

(v) Synthesis and Implications for Solar Energy Modelling

The absence of a uniform national pattern demonstrates that SD variability in the DRC is fundamentally controlled by regional climatic regimes rather than by simple latitudinal gradients. The temporal distribution of MASD extremes reveals that cloud cover dynamics, driven by the seasonal migration of the ITCZ, continentality, and maritime influence, constitute the primary regulator of effective solar availability.

From a solar energy perspective, this zonation has direct implications for photovoltaic system planning and optimization. Provinces within Area 1 and Area 4, characterized by well-defined dry seasons and high seasonal peaks of SD, are particularly suitable for both grid-connected and decentralized PV systems, as they offer predictable periods of high solar yield. In contrast, Areas 2 and 3 require adaptive system design, accounting for intra-annual variability and cloud-induced intermittency.

Furthermore, this MASD-based classification provides a critical foundation for the modelling of SI across the provinces of the DRC, which constitutes the main objective of this study. By incorporating not only the magnitude but also the seasonal timing of SD extremes, the proposed approach enables a more accurate representation of solar resource variability, thereby improving the reliability of irradiance estimation models and their applicability for energy planning at both provincial and national scales.

3.4 SUMMARY OF CHAPTER 3

This chapter has examined the national distribution of solar resources in the DRC through two complementary indicators:

(i) Annual mean daily SI (kWh/m²/day),
(ii) Annual mean daily SD (h/day).

The analysis of SI allowed the identification of four solar potential zones: low, medium, high, and very high. The highest irradiation levels are mainly concentrated in the Southeast (Katanga) and parts of the East, while comparatively lower values are observed in western coastal provinces. The subsequent analysis of SD confirmed a structured but not identical spatial distribution. The DRC can be divided into three SD zones, with values ranging from 4.2 h/day in Kongo Central to 6.8 h/d in Katanga.

A comparative East–West analysis at similar latitudes reveals a consistent longitudinal gradient, with eastern and southeastern provinces generally recording higher SD than western provinces. This pattern suggests that maritime influence, continentality, altitude, and cloud dynamics play a critical role in modulating effective SD. Furthermore, the absence of a theoretical June minimum in most provinces indicates that cloud cover associated with seasonal ITCZ migration exerts a stronger control on SD than astronomical day length alone.

Overall, the combined analysis of irradiation and sunshine duration demonstrates that the most favorable zones for solar energy development are located in the Southeast and parts of the Eastern highlands, whereas western coastal and central basin regions present comparatively lower, though still significant, solar potential. These results provide a scientifically grounded framework for regional solar energy planning and constitute a solid basis for the subsequent modeling and simulation analyses developed in the following chapters.

3.5 Physical and Methodological Justification for the Combined Use of Solar Irradiation and Sunshine Duration

While the joint use of SI (kWh/m²/day) and SD(h/day) is introduced in the methodological framework, its full relevance emerges at the interpretation stage, where both indicators provide complementary insights into the solar resource

This joint use in this study is methodologically justified by the complementary physical nature of these two indicators. SI represents the total amount of radiant energy received per unit surface over a given period. It directly determines the theoretical energy yield of photovoltaic (PV) systems and constitutes the primary design parameter for solar power assessment. SD, by contrast, measures the effective number of hours during which direct solar radiation exceeds a defined threshold (typically 120 W/m² for Campbell–Stokes instruments). Although SD does not quantify energy intensity, it reflects atmospheric transparency, cloud persistence, and seasonal sky conditions.

Using irradiation alone may lead to incomplete interpretation because two regions with similar annual irradiation values may exhibit different temporal distributions of sunshine. Conversely, SD alone does not capture variations in solar intensity during clear-sky conditions.

The combined analysis therefore allows:verification of coherence between energy magnitude (irradiation) and atmospheric clarity (SD), identification of regions where high irradiation may be associated with shorter but more intense radiation periods, permits better understanding of seasonal variability, which is crucial for PV sizing, storage requirements, and grid integration.

Thus, the integrated use of irradiation and Sunshine Duration enhances both the physical interpretation of the solar resource and the reliability of energy system planning conclusions. This combined approach also provides a robust foundation for subsequent irradiance modeling, where SD serves as a key explanatory variable for capturing atmospheric modulation of solar radiation.

CHAPTER 4: SPATIAL AND CLIMATIC FACTORS INFLUENCING SUNSHINE IN THE DEMOCRATIC REPUBLIC OF CONGO

While Chapter 3 analysed the spatial distribution and zonal structure of SD across the DRC from a territorial and energy-resource perspective, the present chapter investigates the underlying geographic and climatic mechanisms responsible for the observed patterns. The objective is not merely to describe how SD is distributed across the country, but to identify the principal spatial gradients and atmospheric processes that govern its variability.

SD over a territory of continental scale such as the DRC is supposed to be influenced by a combination of geographic position, altitude contrasts, continentality effects, large-scale atmospheric circulation, rainfall regimes, and cloud persistence dynamics. Understanding these drivers is essential for interpreting regional disparities in solar resource availability and for ensuring the statistical consistency of subsequent irradiance modelling.

Although numerous international studies have established relationships between SD and meteorological variables such as temperature, humidity, and precipitation over long-term temporal scales [69, 70, 71, 72, 73], these investigations predominantly focus on time-series variability. In contrast, the present research adopts a spatial analytical framework. Long-term averaged SD values are assumed to characterise the prevailing climatic regime of each province and are therefore analysed in relation to geographic and climatic gradients across the national territory.

Particular emphasis is placed on longitudinal variation, relative humidity and rainfall processes. In a country marked by equatorial rainforest, extensive basin topography, and high-elevation eastern plateaus, such factors may produce differentiated SD regimes. These regional climatic contrasts may, in turn, influence the stability and transferability of a unified national relationship between GSI and SD.

The central question addressed in this chapter is whether SD behaves as a spatially homogeneous predictor across the DRC or whether certain regions exhibit statistically significant deviations from the general trend. Identifying such heterogeneity is critical for assessing the robustness of the GSI–SD regression models developed in Chapter 5 and for

determining whether differentiated modelling scenarios may be required in climatically complex areas.

To quantify these relationships, Pearson's correlation coefficient and associated confidence intervals are employed to evaluate the strength and significance of associations between SD and selected spatial variable, particularly longitude. The statistical findings are interpreted within a climatological framework integrating atmospheric circulation patterns, cloud persistence mechanisms, and orographic influences.

By clarifying the dominant geographic and meteorological determinants of SD, this chapter establishes the explanatory and methodological foundation necessary for the formulation, validation, and interpretation of the solar irradiance prediction models presented in Chapter 5. It therefore represents a critical step in ensuring the physical coherence and statistical reliability of photovoltaic resource assessment across the DRC.

4.1 Spatial variables

Data analysis focuses on how SD varies with site longitude across the DRC. The objective is to evaluate whether a longitudinal gradient exists at a macro-spatial scale.

For each province, one site with complete and reliable SD records was selected, and its SD and longitude were recorded. The selection criterion was strictly based on data completeness and measurement reliability in order to avoid missing-data bias and ensure statistical consistency. Since one qualified station was retained for each province, this procedure does not introduce systematic spatial bias and preserves the geographic representativeness of the dataset at the provincial scale.

The monthly average SD for the province is substituted by the SD from the nearest selected city, ensuring that the substitution error does not exceed 3%. This small deviation indicates a strong agreement between Provincial Monthly Averages (PMA) and Site Monthly Averages (SMA). In solar climatology studies, discrepancies below 5% are generally considered acceptable and do not indicate systematic bias. In practical terms, a 3% deviation corresponds to less than 0.2 hours per day (approximately 10 minutes), which remains within the expected natural variability range under tropical atmospheric conditions. Therefore, this

substitution does not significantly affect the statistical analysis nor the estimation of correlation coefficients.

Although the number of spatial observations is limited to the eleven provincial units, each value represents a long-term climatological average, thereby integrating substantial temporal information and ensuring statistical stability at macro-territorial scale. Longitudes are converted from degrees, minutes, and seconds to decimal degrees to ensure uniformity in statistical computation.

Given the large west–east spatial extension of the DRC and the transition from Atlantic-influenced western regions to elevated eastern plateaus, longitude is considered a relevant spatial variable for detecting potential geographic gradients. The purpose of this section is not to model intra-provincial microclimatic variability but to examine large-scale spatial patterns. At this macro-spatial level, one representative and reliable station per province is sufficient to capture broad longitudinal trends. To quantify the strength and direction of the relationship between SD and longitude, Pearson's correlation coefficient is employed. Confidence intervals are computed to assess the statistical reliability of the estimated correlation. This approach ensures that any observed spatial relationship is evaluated not only in terms of magnitude but also in terms of statistical significance.

Overall, the adopted methodology provides a coherent and statistically defensible framework for analysing the spatial structure of SD across the national territory. Table 4.1 lists the eleven former provinces of the DRC and the corresponding sites (city) selected for analysis, while Table 4.2 compares the Provincial Monthly Average SD (PMA) with the Site Monthly Average SD (SMA).

Table 4.1: Mapping of Provinces to Representative Observation Sites

Province	Former Bandudu	Fomer Equateur	Former Kasaï-Occid.	Form Kasaï Or.	Former Katanga	Kinshasa prov.
City	3Maisons	Gbadolite city	Kananga city	Mbuji Mayi city	Lubumbashi city	Kinshasa province
Province	Kongo-Central	Maniema province	Nord-Kivu	Former Prov. Orientale	Sud Kivu	
City	Boma city	Kindu city	Sake city	Aba city	Uvira city	

Adapted from [69]

Table 4.2:Results for PMA and SMA

	PMA	SMA
January	6.0	6.2
Februay	6.0	6.1
March	5.7	5.8
April	5.4	5.5
May	5.5	5.5
June	6.0	6.0
July	6.3	6.2
August	5.7	5.8
September	5.3	5.3
October	5.0	5.2
November	5.1	5.4
December	5.5	5.7
Yearly Mean	5.6	5.7

Adapted from [69]

The results presented in Table 4.2 indicate a strong consistency between the Provinces Monthly Averages (PMA) and the Site Monthly Averages (SMA), with only marginal deviations observed throughout the year. The differences remain systematically small across all months, leading to a negligible discrepancy in the annual mean (5.6 h/day for PMA against 5.7 h/day for SMA).

From an analytical perspective, this close agreement suggests that the selected site effectively captures the dominant atmospheric and climatic conditions governing SD at the provincial scale. The absence of systematic bias between PMA and SMA further indicates that local variability within the province does not significantly distort the monthly SD signal when aggregated at the annual scale. Consequently, SMA can be considered a statistically reliable proxy for PMA in subsequent spatial analyses for this study.

4.1.1 Pearson's Correlation Coefficient And Confidence Interval

Pearson's correlation coefficient is employed to analyze the relationship between SD and the longitude of the selected sites. This coefficient measures the strength and direction of the linear association between two quantitative variables. Its value ranges from –1 to +1. A positive value indicates a positive linear correlation, whereas a negative value indicates a negative linear correlation. The absolute value |r| ranges from 0 to 1 and reflects the strength of the association. A coefficient close to ±1 denotes a strong linear relationship, whereas a coefficient approaching 0 indicates a weak linear association. A value of 0 implies no linear correlation between the variables [80].

In the present spatial framework, the two variables are defined as follows:

— X represents the longitude of the selected sites, expressed in decimal degrees (°).
— Y represents the corresponding long-term mean SD recorded at each site.

Each observation therefore corresponds to one province–site pair. This design ensures territorial representativeness while preserving statistical independence between observations at national scale. Given the provincial scale of aggregation and the use of long-term climatological means, small-scale spatial autocorrelation effects are assumed to be limited and do not compromise the validity of the national-scale correlation analysis.

The Pearson correlation coefficient r between the two variables X and Y is defined by Equation (4.1) [82]. The magnitude and statistical significance of r will determine whether SD exhibits a sufficiently structured longitudinal gradient to justify its subsequent use as a stable explanatory variable in the irradiance regression modelling developed in Chapter 5.

$$r = \frac{\sum_{i=1}^{n}(X_i - \bar{X}).(Y_i - \bar{Y})}{\sqrt{\sum_{i=1}^{n}(X_i - \bar{X})^2 * \sum_{i=1}^{n}(Y_i - \bar{Y})^2}} \quad (4.1)$$

The confidence interval is obtained using some steps as in [70]:

4.1.1.1. Slope and trend of correlation

The least squares method was employed to determine the slope of the relationship between SD and longitude for each month. The slope highlights the months during which SD

varies most rapidly with longitude. This helps to explore why this phenomenon occurs in a given month and to explain the tendency of the least squares line obtained. The relationship of the least squares line is expressed as follows:

$$Y = aX + b \tag{4.2}$$

Where X is the independent variable and Y the dependent variable, a is the slope of the line, and b is the intercept. The coefficients a and b are obtained using relationships described as in [71].

The coefficient a represents the slope of the line. A large value of a indicates a substantial change in SD per degree of longitude. As longitude increases from the western to the eastern DRC, a large positive value of a implies a significant increase in SD per degree of longitude, whereas a small positive value of a indicates only a slight increase in SD across the same longitudinal span.

4.1.1.2.Results

(i) Pearson correlation coefficient

To examine the spatial distribution of sunshine duration (SD) across the Democratic Republic of Congo (DRC), the Pearson correlation coefficient was calculated between the monthly SD values and the corresponding longitude of each observation site. The analysis covers the twelve months from January to December. The objective is to determine whether a longitudinal gradient exists in the spatial variability of sunshine duration over the national territory.

The results show a positive relationship between SD and site longitude throughout the year. In other words, sunshine duration tends to increase progressively from the western part of the country toward the eastern regions. This pattern appears consistently across most months, although its intensity varies slightly over the year.

The confidence interval at the 95% level was also calculated for each monthly correlation coefficient. The results indicate that the correlation remains relatively strong during most months, with values ranging from 0.55 to 0.76. A slightly weaker relationship is observed during February and March, where the coefficients are 0.49 and 0.44, respectively. These values

still indicate a moderate positive relationship, suggesting that longitude remains a relevant spatial indicator of sunshine duration even during these months.

Table 4.3 reports the longitudinal coordinates associated with the selected provincial sites used to investigate the spatial dependence of sunshine duration across the DRC.

Table 4.3: Provinces and corresponding Longitudes

Prov.	Band.	Eq .	Kas. Oc	Kas. or	Kat.	Kin.	Kong.c	Man.	N.Kiv.	Pr.or.	S.Kiv.
Long. (°)	17.39	20.91	22.42	23.59	27.47	15.32	13.06	25.95	29.04	30.23	29.14

The longitudinal distribution exhibits a wide spatial span (~13°E to ~30°E), providing a robust gradient for assessing east–west atmospheric variability. This range is sufficiently large to capture variations in synoptic circulation patterns, moisture advection, and cloud formation regimes. Consequently, longitude can be treated as a proxy variable for large-scale climatic transitions, particularly between Atlantic-influenced western regions (Kongo-Central and Kinshasa) and more continental or rift-influenced eastern zones (Katanga and Sud Kivu).

Table 4.4 presents the monthly SD values across the selected provincial sites, forming the empirical basis for subsequent spatial correlation analysis.

Table 4.4: Adapted Provinces MASD

Prov.	Band.	Eq .	Kas.oc	Kas.or.	Kat.	Kin.	Kong.c	Man.	N.Kiv.	Pr.or	S.Kiv.
January	6.1	7.7	5.9	6.2	6.0	5.0	4.2	5.5	5.5	8.0	7.7
February	6.1	7.4	5.7	6.4	5.9	4.9	4.2	5.5	5.6	7.9	7.7
March	5.8	7.1	5.3	6.0	5.4	5.2	4.5	5.0	4.8	7.6	7.4
April	5.1	6.5	4.7	6.0	5.9	5.0	4.1	4.5	4.9	7.1	6.5
May	5.2	6.2	5.0	6.9	7.4	4.4	2.6	4.5	5.5	6.7	6.6
June	6.9	6.3	6.5	7.6	7.6	3.8	1.6	5.6	5.9	6.6	7.6
July	7.4	6.2	6.9	7.7	7.7	3.8	1.5	6.4	6.5	6.7	7.8
August	6.8	5.6	6.1	7.1	7.9	3.2	0.8	5.7	6.2	6.4	7.9
September	5.7	5.4	5.6	5.6	8.1	3.5	0.5	5.2	5.3	5.9	7.8
October	5.1	5.2	5.3	5.1	8.1	4.4	1.7	4.9	4.4	5.8	7.4
November	5.1	5.8	5.0	5.2	7.2	4.9	3.8	4.7	4.1	6.8	7.2
December	5.4	7.1	5.2	5.7	6.0	5.0	4.1	4.7	4.9	7.7	7.4

Source : Reproduced from [69]

The dataset reveals a structured spatio-temporal organization of SD rather than random dispersion. The persistence of higher SD values in eastern provinces compared to western ones suggests a systematic longitudinal gradient, likely driven by differential cloud cover regimes and atmospheric transparency. Moreover, the seasonal coherence across provinces indicates that large-scale climatic forcing dominates over purely local effects, thereby justifying the use of simplified spatial predictors such as longitude in first-order modeling approaches.

The monthly SD values reveal a structured spatio-temporal organization of SD rather than random dispersion. The persistence of higher SD values in eastern provinces compared to western ones suggests a systematic longitudinal gradient, likely driven by differential cloud cover regimes and atmospheric transparency. Moreover, the seasonal coherence across provinces indicates that large-scale climatic forcing dominates over purely local effects, thereby justifying the use of simplified spatial predictors such as longitude in first-order modeling approaches.

In table 4.5, the “national average” column provides national monthly averages of SD, obtained by taking the weighted monthly averages of all DRC provinces. The “territorial average” column provides monthly average of eleven sites chosen from whole eleven provinces of DRC. For each province, the longitude of corresponding site was employed. The error occurred by this substitution does not exceed 7%.

In order to verify whether the selected observation sites adequately represent the spatial conditions of the country, national averages of SD were compared with territorial averages calculated from the eleven selected locations. Table 4.5 compares national weighted averages of SD with territorial averages derived from representative provincial sites.

Table 4.5: National MASD vs Territorial MASD

Months	National Averages (h/day)	Territorial averages(h/day)	Relative error (%)
January	6.0	6.2	3%
February	6.0	6.1	2%
March	5.7	5.8	2%
April	5.4	5.5	2%
May	5.5	5.5	1%
June	6.0	6.0	0%
July	6.3	6.2	1%
August	5.7	5.8	2%
September	5.3	5.3	1%
October	5.0	5.2	-4%
November	5.1	5.4	7%
December	5.5	5.7	5%
Annual Average	5.6	5.7	3%

The low relative error (generally ≤3%) indicates that the selected sites provide a statistically representative sampling of national SD variability. The isolated deviation observed in November (7%) can be attributed to increased atmospheric instability during the transition to the rainy season, where localized convective activity introduces higher spatial variability. From a statistical standpoint, this level of discrepancy remains within acceptable bounds for geophysical datasets characterized by high natural variability.

The observed discrepancy (≤7%) falls within the standard representativeness error range reported in climatological and solar radiation studies, particularly in regions characterized by strong convective variability [20, 72].

The monthly Pearson correlation coefficients, together with their 95% confidence intervals, are presented in Table 4.6 to assess the statistical robustness of the relationship between longitude and SD.

Table 4.6: Pearson correlation coefficient
Between SD and Longitude across the Year

Months	r	Borne inf. CI	Borne sup. CI
January	0.59	-0.01	0.88
February	0.49	-0.16	0.84
March	0.44	-0.22	0.82
April	0.55	-0.07	0.87

Months	r	Borne inf. CI	Borne sup. CI
May	0.72	0.21	0.92
June	0.69	0.16	0.91
July	0.71	0.20	0.92
August	0.76	0.29	0.93
September	0.76	0.29	0.93
October	0.68	0.14	0.91
November	0.57	-0.04	0.87
December	0.55	-0.07	0.87

Reproduced from [69]

The results reveal a temporally heterogeneous but structurally consistent relationship between longitude and SD. While moderate correlations persist throughout the year, the widening of confidence intervals during February–March indicates increased atmospheric stochasticity, likely associated with enhanced convective activity and cloud variability. Conversely, the strengthening and statistical stabilization of correlations from May to September suggest a more spatially organized radiative regime, where longitudinal gradients become a dominant control factor. This seasonal modulation highlights that longitude acts as a secondary but non-negligible proxy for SD, whose explanatory power is conditional upon atmospheric stability. Such behavior is particularly relevant for SD-based irradiance modeling, as it implies that spatial predictors gain reliability under reduced cloud-driven variability.

(ii) Slope and trend of correlation

To quantify the longitudinal variation of SD, the least squares method was applied in order to estimate the slope of the linear relationship between SD and longitude. The slope represents the rate at which SD changes for each degree of longitude across the national territory. Table 4.7 presents the monthly slopes derived from the linear regression between SD and longitude, quantifying the spatial gradient of SD across the national territory.

Table 4.7: Monthly slopes

Months	Slope (h/d/°)
January	0.12
February	0.12
March	0.08
April	0.09
May	0.17
June	0.22
July	0.23

Months	Slope (h/d/°)
August	0.27
September	0.26
October	0.19
November	0.11
December	0.11

The consistently positive slopes confirm the existence of a persistent west-east radiative gradient, reflecting large-scale atmospheric circulation patterns and regional differences in cloud cover regimes. The marked amplification of slope values between May and September indicates a seasonal reinforcement of spatial contrast, likely driven by reduced convective and enhanced eastern atmospheric transparency. From a modeling perspective, this non-stationary gradient suggests that the sensitivity of SD to longitude is not constant but seasonally modulated. This has direct implications for regression-based SI estimation, as it justifies the inclusion of season-dependent spatial coefficients in SD–SI transfer functions to improve predictive accuracy.

Figures 4.1 to 4.13 illustrate the monthly linear variation between SD and longitude, highlighting the seasonal evolution of spatial gradients across the study domain.

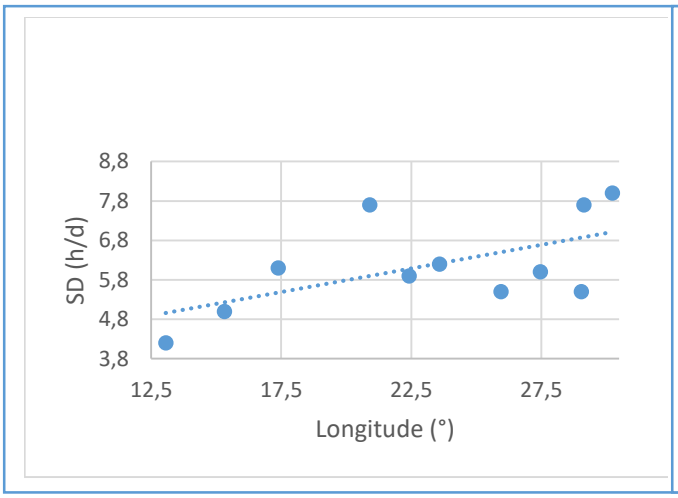

Figure 4.1 SD variation from longitude on January

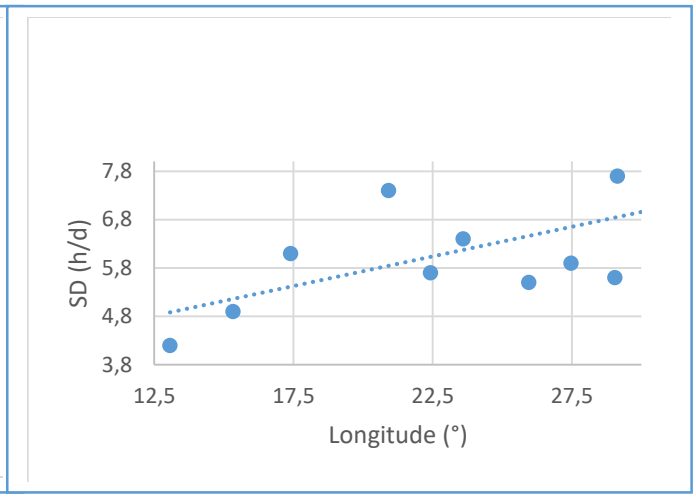

Figure 4.2 SD variation from longitude on February

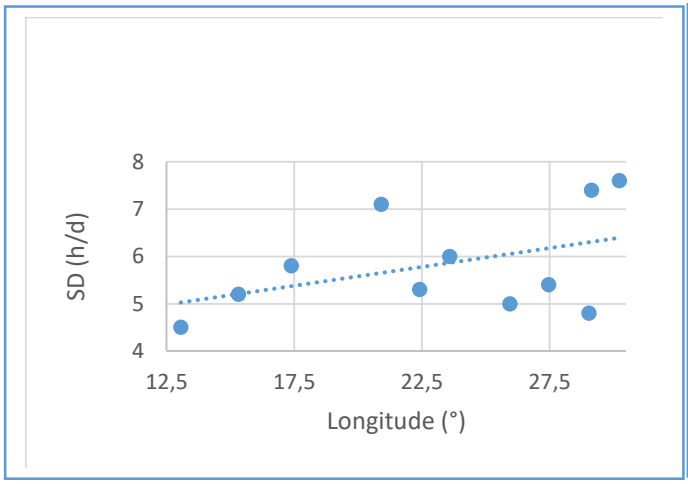

Figure 4.3 SD variation from longitude on March

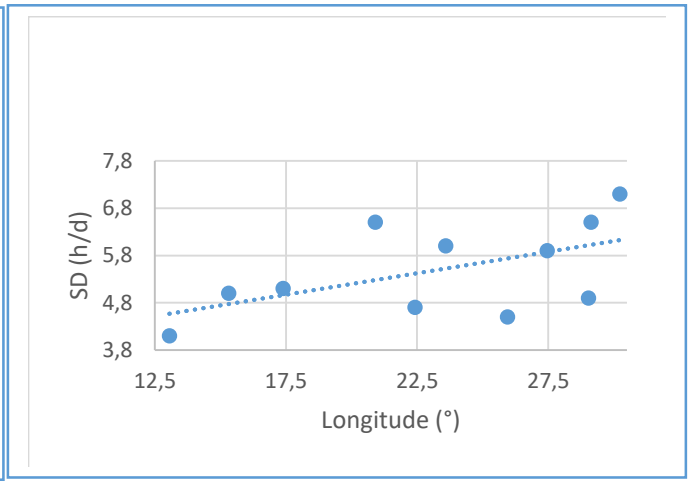

Figure4.5 SD variation from longitude on April

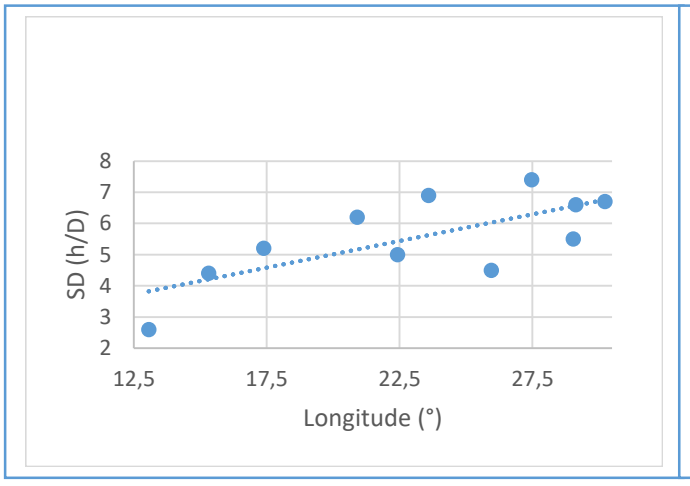

Figure 4.6 SD variation from longitude on May

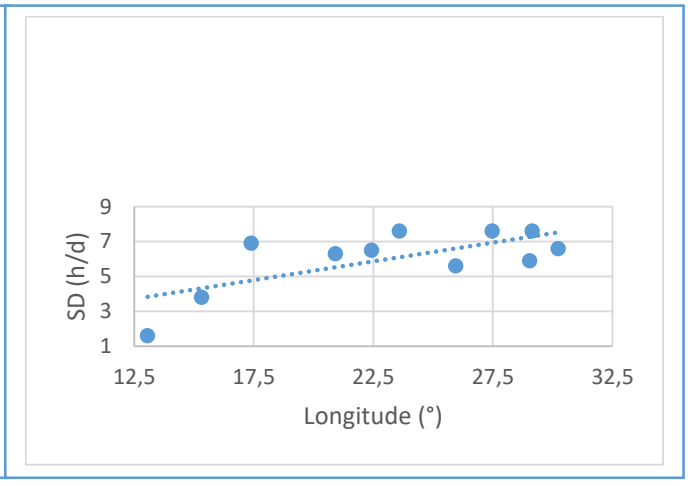

Figure 4.7 SD variation from longitude on June

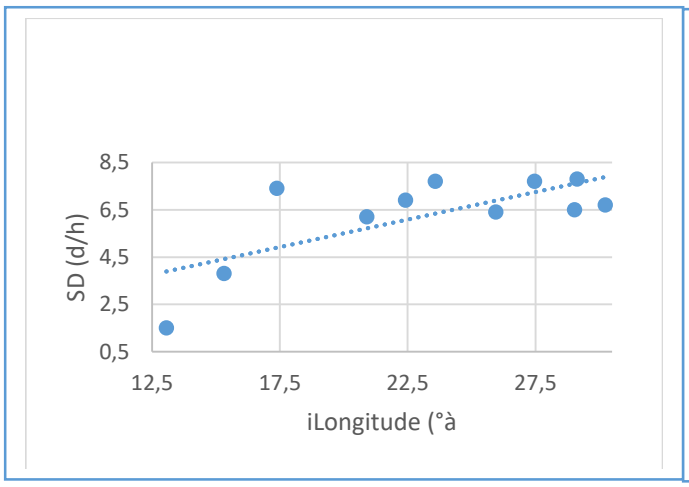

Figure 4.8 SD variation from longitude July

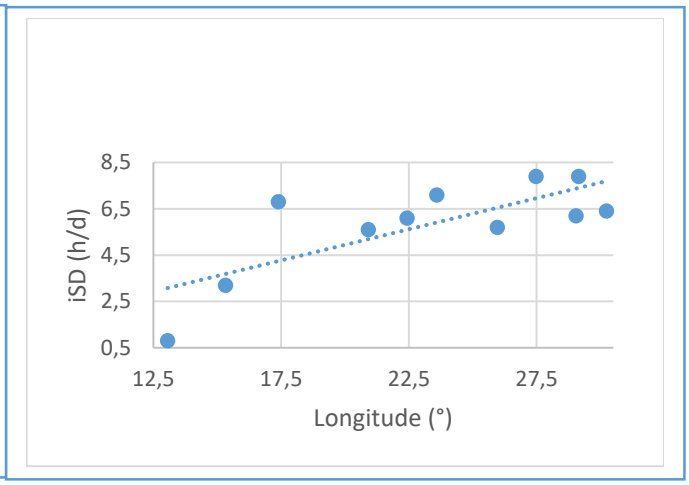

Figure 4.9 SD variation from longitude on August

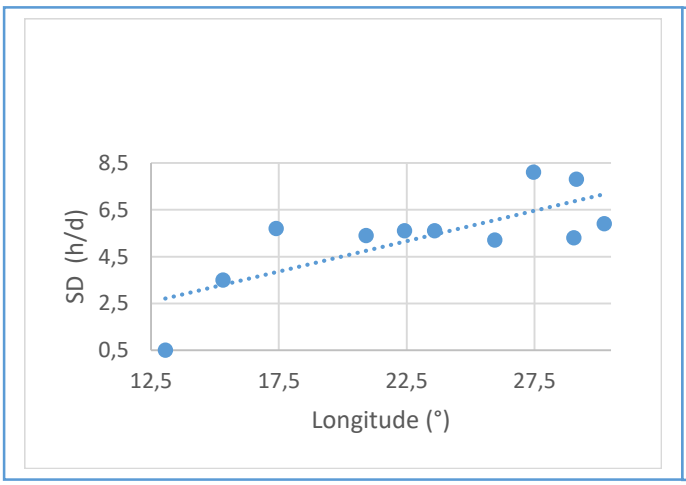

Figure 4.10 SD variation from longitude September

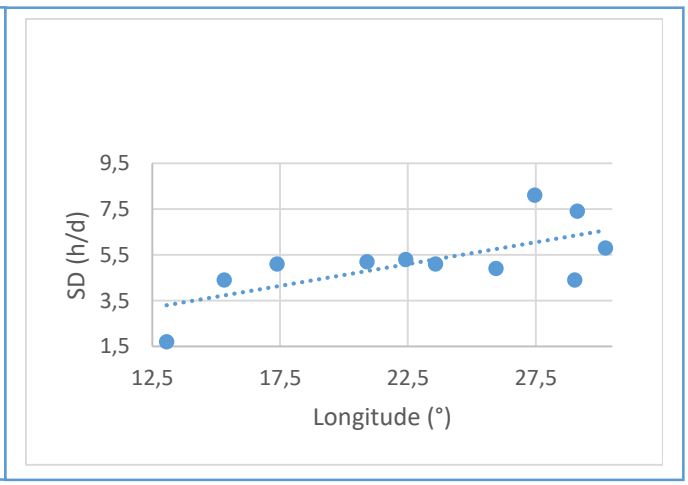

Figure 4.11 SD variation from longitude on October

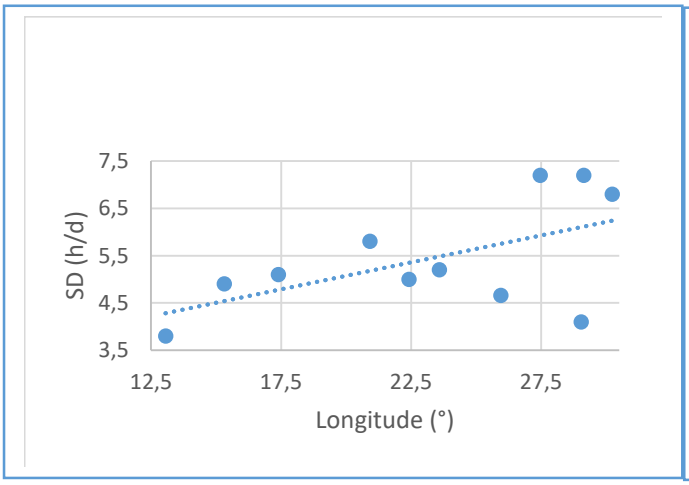

Figure 4.12 SD variation from longitude on November

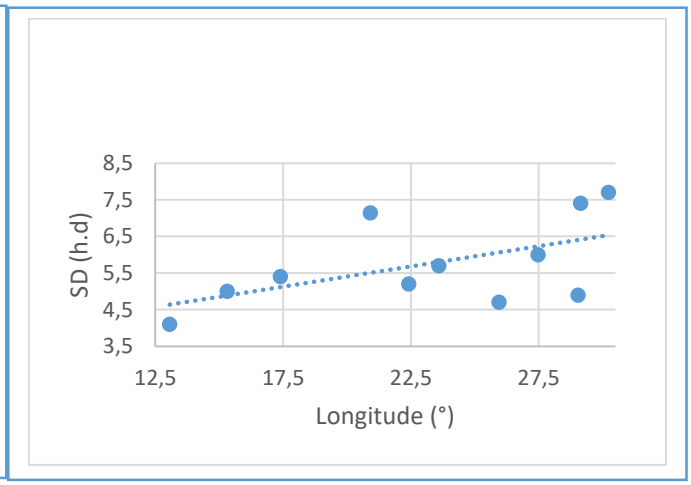

Figure 4.13 SD variation from longitude on December

The graphical representation confirms the progressive structuring of the SD–longitude relationship over the annual cycle. During the early months (January–March), the dispersion of data points reflects weak spatial organization, consistent with lower correlation coefficients and reduced slope magnitudes. As the year progresses toward the dry season (May–September), the alignment of observations along a clearer positive linear trend indicates a strengthening of the longitudinal control on SD, with reduced variance and improved linearity. This transition reflects a shift from convection-dominated to radiation-dominated atmospheric conditions.

4.1.1.3. Discussion

Seasonal atmospheric conditions may also contribute to the variations observed in the statistical indicators. The central basin is generally characterized by high humidity and frequent cloud cover, which can reduce the effective SD [87, 88]. In contrast, several eastern regions experience periods with reduced cloud cover during certain parts of the year when the effective SD is increased [80, 89].This seasonal contrast appears in the statistical results. Between May and October, both the correlation coefficients and the regression slopes become larger, indicating that the spatial gradient in SD becomes more visible during this period. During months with more frequent cloud cover, the spatial differences in SD become less pronounced, which may explain the lower correlations observed during some months.

The positive correlation observed between longitude and SD is consistent with the spatial distribution of atmospheric conditions across the DRC. The positive slope obtained in the regression model indicates a gradual increase in SD from western provinces toward the eastern part of the country. Ths statistical behaviour suggests that the regression captures a real climatic gradient reflecting the transition from humid Atlantic-influenced environements to more continental atmospheric conditions further inland.

Moving eastward, the terrain gradually rises toward a series of plateaus and mountainous regions associated with the western branch of the East African Rift system[85,86],. These areas include elevated regions such as the Uélé plateaus, the Kasaï uplands, and the Rwenzori Mountains, which reach 5,109 m, as well as the Virunga volcanic chain, including Nyiragongo (3,470 m).

Taken together, these observations suggest that the distribution of SD across the DRC reflects the combined influence of terrain structure, seasonal atmospheric conditions, and regional climatic variability.

The spatial patterns identified in this analysis are not only of climatological interest but also provide useful insights for energy planning. In particular, understanding how SD varies across the territory can help inform strategies for solar energy development.

4.1.1.4. Implications for photovoltaic system planning across the DRC

The spatial gradient in SD identified in this analysis has practical implications for the deployment and optimization of PV energy systems across the DRC..

The positive relationship between SD and longitude observed indicates that eastern provinces generally benefit from slightly longer SD particularly during the mid-year period when the correlation is strongest. This suggests that eastern provinces may offer slightly higher photovoltaic productivity potential, especially for large-scale solar installations operating during the dry season.

However, the relatively moderate slopes obtained from the regression analysis indicate that the increase in SD from west provinces to east provinces remains progressive rather than abrupt. This means solar resources are broadly available across most provinces of the country, even in western and central provinces where SD is slightly lower.

For national energy planning, this finding implies that photovoltaic development should not be geographically restricted to a limited area. Instead, PV deployment strategies should consider the entire national territory, while integrating the longitudinal gradient as one of several decision-making criteria.

In addition to SD, other factors such as local electricity demand, grid infrastructure, land availability, accessibility, and regional climate variability must be considered in order to identify the most suitable locations for solar power development.

Thus, by combining spatial solar resource assessment with infrastructure and demand considerations, it could be possible to design a balanced photovoltaic expansion strategy capable of supporting energy access across both western and eastern provinces of the DRC.

4.2 Climatic Variables

The climatic parameters considered in this analysis include monthly maximum temperature (MAXT) expressed in degrees Celsius, monthly minimum temperature (MINT) expressed in degrees Celsius, relative humidity (HUM) expressed in %, and rainfall (RNF) expressed in mm. The selection of maximum temperature, minimum temperature, relative humidity, and rainfall reflects a deliberate focus on variables that are both physically meaningful and operationally accessible at large spatial scales [73]. These parameters collectively capture the key processes influencing solar radiation transfer through the atmosphere, including moisture content, cloud formation, and convective activity.

While other variables such as altitude, cloud cover fraction, aerosol optical depth, or atmospheric pressure could provide additional explanatory power, their integration often requires higher-resolution datasets or introduces additional sources of uncertainty, particularly in data-sparse regions. The present choice therefore reflects a trade-off between physical completeness and modeling robustness.

Importantly, this study does not exclude the relevance of these additional variables. Rather, it establishes a baseline modeling framework upon which future research can build. Subsequent studies could extend this approach by incorporating more advanced atmospheric descriptors and comparing their contribution to predictive performance against the parsimonious structure adopted here. Such comparative analyses would be particularly valuable for refining SD–SI transfer functions and improving the physical interpretability of solar resource models.

From a modeling standpoint, the selected variables ensure a balance between physical interpretability, statistical stability, and scalability, thereby making them well-suited for integration into SD-driven SI models and subsequent PV performance simulations.

4.2.1 Correlation between sunshine duration and climatic variables

To evaluate the statistical relationships between monthly SD and the selected climatic variables, the Pearson correlation coefficient was calculated for each month from January to December. This procedure permits to determine both the direction and the strength of the linear association between SD and each atmospheric parameter.

For each correlation coefficient obtained, the 95% confidence interval was also estimated in order to provide a statistical indication of the reliability of the calculated values. Table 4.8 provides a comprehensive monthly dataset of SD and key climatic variables (temperature, humidity, and rainfall) across representative locations of the DRC, forming the empirical basis for subsequent correlation and modeling analyses.

Table 4.8: DRC Climativ Variables

		Band	Eq.	K .oc	K .or	Kat.	Kin.	K.cent.	Man.	N. Kivu	Pr.Or.	S. Kiv
Months	Variables	Value	Value	Value	Value	Value	Value	Value	Value	Value	Value	Value
JANUARY	SD (h/d)	6.1	7.7	5.9	6.2	6	5	4.2	5.5	5.5	8	7.7
	MAXT (° C)	30.4	30.5	29,8	29.8	29.9	29.4	29.7	29.2	23.4	33.1	22.7
	MINT (°C)	23,1	22.8	21.6	20.8	21.8	22.5	23.3	22	17.1	21.6	15.9
	Humidity (%)	82	47	85	81	84	83	86	86	78	35	71
	RNF (mm)	137	147	154	149	149	126	178	153	196	18	138
FEBRUARY	SD	6.1	7.4	5.7	6.4	5.9	4.9	4.2	5.5	5.6	7.9	7.7
	MAXT (° C)	31	30.8	30,1	30.7	30.4	30	30.1	29.9	24	33.9	23.3
	MINT (°C)	23.4	23	21.9	21.1	22.1	22.8	23.7	22.3	17.4	22.5	16.1
	Humidity (%)	82	55	85	80	83	82	86	85	78	37	68
	RNF (mm)	135	146	143	137	143	110	151	143	196	29	92
MARCH	SD	5.8	7.1	5.3	6	5.4	5.2	4.5	5	4.8	7.6	7.4
	MAXT (° C)	31.1	23	30	30.5	30.1	30.4	30.4	26.9	23.6	31.8	22.9
	MINT (°C)	23.5	30.4	21.8	21.1	22.1	23	23.9	22.3	17	21.7	16.2
	Humidity (%)	84	69	86	81	82	81	86	87	84	58	69
	RNF (mm)	152	166	159	186	167	118	154	168	317	102	84
APRIL	SD	5.1	6.5	4.7	6	5.9	5	4.1	4.5	4.9	7.1	6.5
	MAXT (° C)	30.3	29.8	29.4	30.5	29.6	29.8	29.9	29	23.1	29.6	22.2
	MINT (°C)	23.3	23	21.8	21.1	22	22.9	23.8	22.4	16.7	20.8	15.9
	Humidity (%)	86	79	88	81	70	84	87	89	85	74	71
	RNF (mm)	172	165	157	148	172	146	189	170	292	212	110
MAY	SD	5.2	6.2	5	6.9	7.4	4.4	2.6	4.5	5.5	6.7	6.6
	MAXT (° C)	30.8	30.2	29.6	31.8	30	29.7	29.1	29.1	23.2	28.2	22.3
	MINT (°C)	23.4	22.9	21.8	20.7	22	22.5	23	22.3	16.9	20	15.5
	Humidity (%)	83	80	87	69	52	82	86	88	82	81	68
	RNF (mm)	111	99	115	40	100	83	33	118	182	219	55

		Band	Eq.	K .oc	K .or	Kat.	Kin.	K.cent.	Man.	N. Kivu	Pr.Or.	S. Kiv
Months	Variables	Value	Value	Value	Value	Value	Value	Value	Value	Value	Value	Value
JUNE	SD	6.9	6.3	6.5	7.6	7.6	3.8	1.6	5.6	5.9	6.6	7.6
	MAXT (° C)	31.9	31.2	30.3	32.9	31.4	29.8	27.6	29.7	23.3	27.1	21.8
	MINT (°C)	23	22.3	21.2	19	21.1	20.7	20.3	21.8	17	19.2	14.9
	Humidity (%)	69	81	78	50	47	73	81	81	76	83	65
	RNF (mm)	28	27	44	7	25	6	9	45	96	179	13
JULY	SD	7.4	6.2	6.9	7.7	7.7	3.8	1.5	6.4	6.5	6.7	7.8
	MAXT (° C)	32.7	32.2	31	33.6	32.6	30	27	30.7	23.8	26.8	21.8
	MINT (°C)	22.9	22.2	21.1	19	21.1	19.8	18.7	21.6	17.1	18.7	14.6
	Humidity (%)	58	82	71	41	43	67	78	73	69	83	62
	RNF (mm)	15	21	43	3	18	1	7	37	54	200	3
AUGUST	SD	6.8	5.6	6.1	7.1	7.9	3.2	0.8	5.7	6.2	6.4	7.9
	MAXT (° C)	32.6	31.6	30	32.9	31.7	30.2	26.7	30.2	23.9	27.1	22.6
	MINT (°C)	23.2	22.6	21.3	20.5	21.8	20.3	19.1	21.8	17.2	18.7	15.1
	Humidity (%)	66	84	81	55	36	65	78	79	71	83	58
	RNF (mm)	49	69	118	33	69	7	13	81	108	22.6	4
SEPTEMBER	SD	5.7	5.4	5.6	5.6	8.1	3.5	0.5	5.2	5.3	5.9	7.8
	MAXT (° C)	31.9	30.7	29.6	30.9	30.5	31.3	27.9	29.4	23.5	27.6	23.6
	MINT (°C)	23.1	22.4	21.2	20.8	21.6	21.7	20.6	21.7	17	18.8	15.9
	Humidity (%)	78	84	86	75	31	66	79	84	79	82	56
	RNF (mm)	107	135	177	119	141	20	21	145	233	219	7
OCTOBER	SD	5.1	5.2	5.3	5.1	8.1	4.4	1.7	4.9	4.4	5.8	7.4
	MAXT (° C)	30.3	29.9	29.4	29.8	29.7	30.4	29.4	28.9	22.9	27.6	23.2
	MINT (°C)	22.8	22.4	21.3	20.7	21.6	22.5	22.4	21.7	16.7	19.5	16
	Humidity (%)	84	84	86	82	38	75	79	87	85	82	60
	RNF (mm)	186	196	206	170	192	120	64	218	384	158	29
	SD	5.1	5.8	5	5.2	7.2	4.9	3.8	4,7	4.1	6.8	7.2
	MAXT (° C)	29.7	29.9	29.1	29.4	29.1	29	29.9	28.4	22.6	30.8	22.4
	MINT (°C)	22.8	22.4	21.3	20,6	21.5	22.3	23.3	21.7	16.4	20.3	15.8
	Humidity (%)	85	79	87	83	67	84	84	88	86	73	67
NOVEMBER	RNF (mm)	192	192	193	191	197	192	161	215	399	158	60
	SD	5.4	7.1	5.2	5.7	6	5	4.1	4.7	4.9	7.7	7.4
	MAXT (° C)	29.6	29.7	29.1	29.2	29.2	28.8	29.4	28.3	22.8	30.8	22.2
DECEMBER	MINT (°C)	22.9	22.6	21,4	20.7	21.7	22.3	23.2	21.8	16.7	20.3	15.8
	Humidity (%)	85	65	87	83	81	85	67	89	82	51	71
	RNF (mm)	185	177	179	179	178	166	194	199	259	32	158

Reproduced from [69]

The structure of the dataset in the Table 4.7 reveals that SD variability is not governed by a single dominant atmospheric parameter but rather emerges from a coupled thermodynamic–radiative regime. The apparent anti-phase behavior between SD and both

HUM and RNF suggests that cloud optical depth and persistence act as first-order modulators of solar availability. Conversely, the weaker and less consistent association with temperature indicates that thermal variables operate more as indirect indicators of atmospheric state than as direct controls on radiative transmission.

This multi-variable interaction highlights a key modeling implication: SD should not be interpreted as a purely geometric or astronomical variable, but as an emergent proxy of atmospheric transmissivity. As such, its integration into SI modeling frameworks is physically justified, particularly in regions where cloud dynamics dominate radiative attenuation. The dataset therefore supports the use of SD as an intermediate state variable linking large-scale atmospheric conditions to surface solar energy availability.

4.3.1.1. Monthly Maximum Temperature (MAXT)

The Pearson correlation coefficient between SD and MAXT [73] was calculated for each month of the year. The associated confidence intervals were also determined in order to evaluate the statistical consistency of the relationships observed.

The results indicate that the statistical relationship between SD and MAXT remains weak during most months of the year. A very weak positive correlation is observed in January and February, with coefficients of 0.04 and 0.28 respectively at the 95% confidence level. Similar weak positive relationships appear again during June, July, and August.

During the remaining months, the correlation becomes slightly negative, with coefficients ranging approximately from −0.04 to −0.23, as shown in Table 4.9.

Table 4.9: Pearson correlation coefficient
Between SD and MAXT across the Year

Months	r	Lower Bound CI	Upper Bound CI
January	0.04	-0.57	0.63
February	0.28	-0.38	0.76
March	-0.23	-0.73	0.43
April	-0.11	-0.57	0.52
May	-0.08	-0.65	0.55
June	0.09	-0.54	0.66

Months	r	Lower Bound CI	Upper Bound CI
July	0.15	-0.50	0.69
August	0.08	-0.55	0.65
September	-0.11	-0.67	0.53
October	-0.21	-0.72	0.45
November	-0.05	-0.63	0.57
December	-0.04	-0.63	0.57

Reproduced from [69]

From a physical standpoint, these results suggest that MAXT is not a primary determinant of SD variability at the spatial scale considered. Surface temperature responds partly to incoming solar radiation, but it is also influenced by surface heat exchanges, atmospheric mixing, and regional circulation processes. Consequently, variations in maximum temperature do not systematically translate into proportional changes in SD.

4.3.1.2. Monthly Minimum Temperature (MINT)

The Pearson correlation coefficient between SD and MINT was also calculated for each month of the year, together with the associated confidence intervals. The results indicate that the SD–MINT relationship is predominantly negative throughout the annual cycle. Only March and July display weak positive correlations (0.07 and 0.03 respectively at the 95% confidence level). For all other months, the correlations remain negative. The smallest negative value (−0.02) occurs in August, whereas the strongest negative value (−0.39) is observed in May, as indicated in Table 4.10.

Table 4.10: Pearson Correlation Coefficients between SD and MINT

Months	r	Lower Bound CI	Upper Bound CI
January	-0.30	-0.76	0.36
February	-0.33	-0.78	0.34
March	0.07	-0.56	0.64
April	-0.04	-0.62	0.58
May	-0.39	-0.80	0.27
June	-0.18	-0.70	0.47
July	0.03	-0.58	0.62
August	-0.02	-0.61	0.59
September	-0.23	-0.73	0.43
October	-0.34	-0.78	0.33

November	-0.28	-0.75	0.38
December	-0.35	-0.79	0.31

Reproduced from [69]

Minimum temperature largely reflects nocturnal radiative balance and the thermal inertia of the lower atmosphere. Nights characterized by higher humidity or persistent cloud layers tend to maintain higher minimum temperatures while simultaneously reducing the amount of direct SI reaching the surface during the following day. This mechanism explains why the statistical association between MINT and SD tends to be weakly negative in most months.

4.3.1.3. Relative Humidity (HUM)

The Pearson correlation coefficient between SD and HUM) was calculated for each month of the year, together with the associated confidence intervals.

The results reveal a moderate negative correlation between June and September, with coefficients ranging from −0.45 to −0.53 at the 95% confidence level. During the remaining months, the relationship becomes strongly negative, with values ranging approximately between −0.65 and −0.92, as presented in Table 4.11.

Tableau 4.11: Correlation between SD and humidity

Months	r	Lower Bound CI	Upper Bound CI
January	-0.81	-0.95	-0.41
February	-0.76	-0.93	-0.28
March	-0.92	-0.98	-0.72
April	-0.84	-0.96	-0.47
May	-0.74	-0.93	-0.24
June	-0.53	-0.86	0.1
July	-0.49	-0.84	0.16
August	-0.45	-0.83	0.2
September	-0.49	-0.84	0.15
October	-0.66	-0.9	-0.1
November	-0.92	-0.98	-0.71
December	-0.65	-0.9	-0.08

Reproduced from [69]

The results could be explained by this fact: HUM is closely linked to the moisture content of the lower troposphere and therefore to the likelihood of cloud formation and atmospheric opacity [74], [75]. When humidity increases, the probability of cloud development and aerosol condensation also increases, which reduces the duration of direct solar radiation reaching the ground. The consistently negative correlation observed between SD and humidity therefore reflects the fundamental role played by moisture-controlled cloud processes in regulating sunshine duration.

4.3.1.4. Rainfall (RNF)

The Pearson correlation coefficient between SD and RNF was calculated for each month of the year, together with the associated confidence interval.

The results show a weak positive correlation between May and September, with coefficients ranging from 0.14 to 0.32 at the 95% confidence level. In contrast, strong negative correlations appear during January, March, November, and December, with coefficients ranging from −0.53 to −0.68. A weak negative correlation is observed in April and October, whereas February exhibits a moderate negative correlation. Figure 4.14 illustrates the distribution of relative monthly rainfall, providing a visual framework to identify seasonal variations and pluviometric transition periods within the study area.

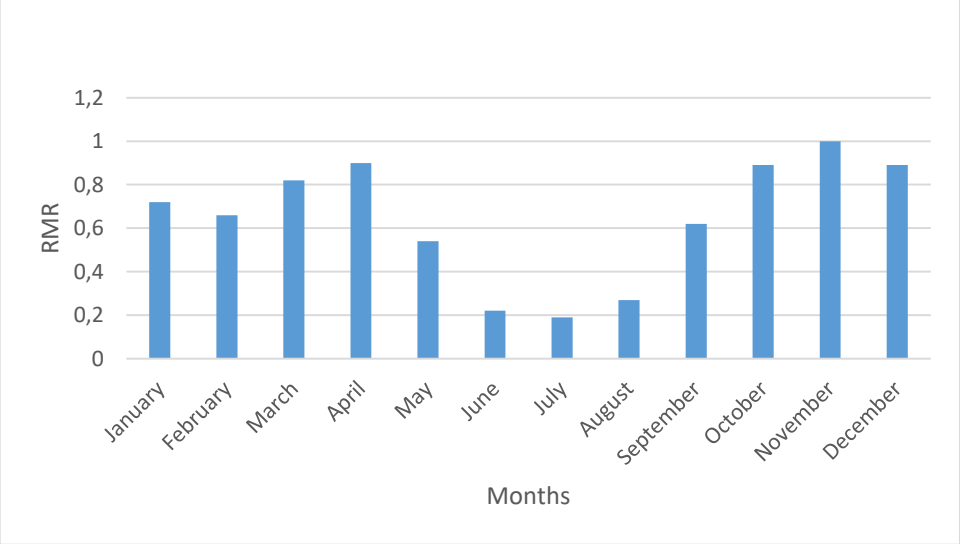

Figure 4.14 Relative Monthly Rainfall

The examination of Figure 4.14 reveals a pronounced cyclicity, suggesting that the local hydrological regime is directly influenced by the mechanisms of the Intertropical Convergence Zone (ITCZ). Beyond mere fluctuations in precipitation depth, the observed seasonal asymmetry indicates a differentiated water recharge dynamic. This configuration implies that solar radiation (SD) prediction models must rigorously account for these seasonal shifts, as the cloud cover associated with peak rainfall represents a critical attenuation factor for direct irradiance. Table 4.12 exhibits the correlation coefficients between SD and the Rainfall for all months of the year.

Table 4.12: Correlation between SD and the Rainfall

Months	r	Lower Bound CI	Upper Bound CI
January	-0.6	-0.88	-0.01
February	-0.46	-0.83	0.19
March	-0.53	-0.86	0.1
April	-0.19	-0.71	0.46
May	0.24	-0.42	0.73
June	0.16	-0.48	0.69
July	0.14	-0.5	0.68
August	0.28	-0.38	0.75
September	0.32	-0.35	0.77
October	-0.02	-0.61	0.59
November	-0.55	-0.86	0.07
December	-0.68	-0.91	-0.13

Rainfall reflects the presence of organized convective or stratiform cloud systems, which directly modulate the penetration of solar radiation through the atmosphere. During months characterized by intense precipitation activity, extended cloud cover tends to reduce SD, producing negative correlations between rainfall and SD. During relatively drier periods, precipitation events may remain localized or short-lived, allowing sunshine duration to remain relatively high despite moderate rainfall amounts.

4.3.1.5. Discussion

The observed between SD and MAXT, MINT, humidity, and rainfall The statistical correlations identified between SD and the climatic variables considered in this analysis reflect the radiative and thermodynamic processes governing the lower tropical atmosphere over the DRC and align with findings from other studies [86], [88], [71], [87].

Among the variables examined, HUM exhibits the most consistent influence on SD. From a climate-physics perspective, this result is expected because atmospheric moisture directly controls cloud nucleation, cloud optical thickness, and atmospheric transmissivity. As humidity increases, the probability of cloud formation rises, leading to a reduction in the duration of direct solar radiation reaching the surface.

RNF represents the macroscopic expression of these moisture-driven processes. Periods characterized by strong convective activity and persistent cloud systems tend to coincide with reduced SD, explaining the negative correlations observed during several months of the year. During transitional or comparatively drier periods, RNF events may occur without maintaining long-lasting cloud cover, which explains the weaker or occasionally positive correlations observed between RNF and SD.

Temperature variables, by contrast, appear to exert a secondary influence on SD variability. MAXT and MINT mainly reflect the resulting thermal state of the atmosphere and the land surface, which depends on multiple energy-balance mechanisms including radiation, latent heat flux, and atmospheric mixing. For this reason, their statistical association with SD remains relatively weak.

A comparison between RNF distribution and SD across provinces also reveals that spatial differences in SD across the DRC cannot be fully explained by precipitation totals alone.. For instance, although Nord Kivu records one of the highest annual rainfall totals, it does not systematically display the lowest SD values. Conversely, Kongo Central and Kinshasa, where rainfall amounts are comparatively moderate, present relatively low SD values. This apparent inconsistency indicates that SD is influenced not only by RNF intensity but also by regional atmospheric circulation, cloud persistence, and local geographical conditions such as topography and proximity to maritime air masses.

From an energy resource perspective, these climatic interactions are particularly relevant because SD represents an important proxy indicator of SI availability. Understanding the atmospheric mechanisms controlling SD therefore provides useful information for assessing the spatial and seasonal variability of solar energy potential across the DRC.

4.3 Summary

The analysis conducted in this chapter highlights several correlation between SD and the principal climatic variables across the DRC. The results reveal a strong negative correlation between SD and HUM, indicating that increased atmospheric moisture is generally associated with shorter SD. This behaviour reflects the effect of cloud formation processes that limit the transmission of solar radiation through the atmosphere.

The correlation between SD and RNF varies according to the seasonal rainfall regime. A weak positive correlation appears from May to September, whereas negative correlations dominate during the remaining months, when precipitation activity and cloud cover are more frequent.

The correlation between SD and MAXT remains generally weak throughout the year. Slight positive correlations are observed in January, June, and August, while weak positive correlations occur in February and July. In contrast, very weak negative correlations appear in November and December, with weak negative correlations also observed in September and October.

Similarly, the relationship between SD and MINT is predominantly negative over most of the year. Only March and July show weak positive correlations. The weakest negative correlation occurs in August, whereas the strongest negative value (−0.35) is recorded in December. Thus, these results indicate that SD variability across the DRC is primarily governed by atmospheric moisture and precipitation dynamics, whereas temperature variables play a more limited role. Combined with the spatial patterns identified earlier, the findings also indicate that SD tends to increase progressively from the western regions toward the eastern part of the country, reflecting the combined influence of climatic and geographical factors.

CHAPTER 5: STATISTICAL MODELING AND VALIDATION OF THE SD-GSI RELATIONSHIP

Chapter 2 reviewed the principal theoretical and empirical models commonly used to estimate global solar irradiation on both horizontal and inclined surfaces. The mathematical formulations of these models were presented in detail in Eqs. (2.1–2.33) and apply to global solar irradiation on horizontal surface. Chapter 4 examined the spatial and climatic factors controlling sunshine duration across the DRC and analyzed their relationship with the variability of solar irradiation.

Building upon these foundations, the present chapter investigates the relationship between SD and GSI across the provinces of the DRC. The objective is to establish reliable predictive models capable of estimating SI in regions where direct measurements remain unavailable.

From a radiative transfer perspective, the GSI reaching the Earth's surface is determined by the combined effects of extraterrestrial solar radiation and atmospheric attenuation processes. As solar radiation travels through the atmosphere, it undergoes scattering by molecules and aerosols, absorption by atmospheric gases, and extinction by cloud droplets. These processes collectively determine the fraction of incoming solar radiation that ultimately reaches the surface.

A convenient dimensionless measure of this atmospheric attenuation is the clearness index K_T, defined as the ratio of global solar radiation at the surface to extraterrestrial solar radiation at the top of the atmosphere. This parameter encapsulates the integrated effects of atmospheric transmissivity, including cloud cover, aerosol loading, and water vapor absorption.

In equatorial regions such as the Congo Basin, seasonal variability in extraterrestrial radiation is relatively weak due to the near-equatorial solar geometry. Consequently, variations in surface solar radiation are largely controlled by atmospheric processes, particularly cloud formation associated with tropical convection.

The DRC lies within the equatorial belt strongly influenced by the ITCZ. The seasonal migration of the ITCZ governs the regional distribution of convective cloud systems, rainfall

patterns, and atmospheric humidity. These processes strongly modulate solar radiation transmission through the atmosphere and therefore play a central role in determining the spatial distribution of solar energy resources across the country.

Given the limited availability of ground-based pyranometer measurements across the national territory, empirical models linking SD to SI provide an effective approach for estimating solar energy potential. Such models have been widely applied in tropical regions where SD observations are more readily available than direct irradiation measurements [76] [77].

This chapter calibrates five local statistical models—linear, quadratic, cubic, logarithmic, and exponential—to predict solar irradiation across the eleven former DRC provinces from weighted daily sunshine, assessing performance under two scenarios (with and without North and South Kivu) using R^2, NMAE, NMBE, NRMSE, and Nash–Sutcliffe efficiency, providing a concise, province-specific evaluation of model accuracy.

5.1 Modeling Framework: From Spatial Variability of SD to SD–GSI Formulations

The spatial analysis conducted in Chapter 4 demonstrates that SD exhibits a pronounced longitudinal gradient across the DRC, primarily controlled by variations in atmospheric moisture, including relative humidity and rainfall. This spatial structure suggests that the relationship between SD and GSI cannot be assumed to be spatially uniform.

To account for this variability, the SD–GSI relationship is formulated using normalized variables of the form:

$$\frac{\bar{H}}{\bar{H}_0} = f\left(\frac{\bar{S}}{\bar{S}_0}\right) \tag{5.1}$$

where $\frac{\bar{H}}{\bar{H}_0}$ denotes the clearness index and $\frac{\bar{S}}{\bar{S}_0}$represents normalized SD.

In this chapter, five functional models are established in order to capture different levels of atmospheric complexity as described in Equatns 2.2-2.10:

Given the spatial variability identified in Chapter 4, the coefficients of these models are not assumed to be constant at the national scale but are expected to depend on regional atmospheric conditions:

$$a, b, c, d = f(\theta, HUM, RNF) \tag{5.2}$$

where θ is longitude.

This framework provides the basis for the province-level calibration of SD–GSI models, enabling the evaluation of their performance under contrasted climatic regimes across the country.

5.2 Data Analysis

5.2.1 Sunshine Duration Dataset

As previously described in Section 1.6, the SD data used in this study were obtained from the ECMWF climate database for the period 1999–2019. Satellite-derived SD estimates provide a valuable alternative to ground observations in regions where meteorological monitoring networks are sparse. However, satellite retrieval algorithms infer SD indirectly from cloud detection schemes and radiative measurements at the top of the atmosphere. In tropical regions characterized by deep convective cloud systems [57], these algorithms may slightly overestimate effective surface SD because they do not fully resolve the vertical structure and optical thickness of cloud systems [78].

Convective clouds typical of equatorial climates often exhibit large cloud optical depths, which significantly reduce the direct component of solar radiation reaching the surface. Multiple scattering processes within these clouds increase the diffuse radiation fraction while reducing the duration of direct sunshine observed at the surface.

To account for this systematic discrepancy, a correction factor of 0.75 was applied to the satellite-derived SD values. This correction can be interpreted physically as an adjustment for the attenuation of direct beam radiation caused by convective cloud systems and high atmospheric humidity typical of the Congo Basin. Similar correction magnitudes have been reported in tropical radiation studies where satellite sunshine estimates were compared with ground observations [79]. The corrected dataset therefore represents the effective SD

contributing to surface SI, which is the quantity most relevant for photovoltaic energy applications.

5.2.2 Modeling

The empirical solar radiation models evaluated in this chapter correspond to the formulations introduced in Chapter 2–. These include the linear Ångström–Prescott model(Eq. (2.2)), polynomial extensions :quadratic and cubic formulation (Eqs. (2.6 and 2.7)), logarithmic and exponential formulations (Eqs. (2.8-2.10)).

These models describe the relationship between the clearness index (Eq. 2.26) and the sunshine fraction and therefore provide a simplified representation of atmospheric transmissivity as a function of cloud cover variability.

Table 5.1 presents the mean GSI on horizontal surfaces across the provinces of the DRC:

Table 5.1: Annual averages GSI across DRC provinces

Provinces	**Average (Kwh/m²/d)**
Bandundu	5.75
Equateur	5.25
Kasaï-occidental	4.77
Kasaï-Oriental	5.21
Katanga	6.50
Kinshasa	4.50
Kongo central	4.10
Maniema	6.35
Nord Kivu	4.75
Province Orientale	4.96
Sud Kivu	3.68

Reproduced from [80]

The apparent availability of provincial-scale SI data provided by the Table 5.1. should not be interpreted as evidence of data sufficiency. Rather, it highlights a critical scale mismatch: in a country as vast and climatically heterogeneous as the DRC, provincial averages mask substantial intra-regional variability. Reliance on such aggregated values may therefore lead to significant bias in PV system sizing, through overestimation or underestimation of the actual resource. This apparent contradiction is not a limitation, but the very motivation of this study,

which seeks to restore spatial representativeness through normalized SD–GSI modeling. The SD data for the DRC are presented in table 5.2 .

Table 5.2 : Weighted MASD across DRC provinces

Provinces	SD (h/d)
Bandundu	6.2
Equateur	5.9
Kasaï-Occidental	5.6
KasaÏ-Oriental	5.9
Katanga	6.8
Kinshasa	4.4
Kongo central	4.2
Maniema	5.3
Nord Kivu	5.8
Province	5.4
Sud Kivu	6.5

Source: Reproduced from [80]

The table highlights the spatial gradient of SD across DRC provinces, with generally higher values in the south eastern regions, consistent with the longitudinal trends disccussed in Chapter 4 (See Section 4.1), while table 5.3 presents the AASD and the corresponding GSI for the provinces of the DRC.

Table 5.3: Annual Averages SD and corresponding GSI

Provinces	**SD (h/d)**	**Average (Kwh/m²/d)**
Bandundu	6.2	5.75
Equateur	5.9	5.25
Kasaï-occidental	5.6	4.77
Kasaï-Oriental	5.9	5.21
Katanga	6.8	6.50
Kinshasa	4.4	4.50
Kongo central	4.2	4.10
Maniema	5.3	6.35
Nord Kivu	5.8	4.75
Prov. Orientale	5.4	4.96
Sud Kivu	6.5	3.68

Source: Reproduced from [80]

Overall, the data presented in the table 5.3 empirically confirm the general relationship between the weighted annual average of SD and the corresponding annual averages of GSI across the eleven provinces of the DRC in their former administrative configuration. Nevertheless, an apparent inconsistency emerges: despite relatively high SD values, Sud Kivu records lower GSI levels than western provinces such as Kinshasa and Kongo Central, which exhibit some of the lowest SD values in the country. This apparent discrepancy is consistent with the regional climatic mechanisms discussed in Chapter 4, Section 4.2.

5.1.2.1. Scenario 1: Nord and Sud Kivu excluded

Table 5.4 presents the polynomial models for the scenario 1, where the provinces of Nord and Sud Kivu are excluded.

Table 5.4: GSI-SD polynomial models

Model	Linear model		Quadratic model			Cubic model				
Relationship	$\frac{\bar{H}}{\bar{H}_0} = a + b\frac{\bar{S}}{\bar{S}_0}$		$\frac{\bar{H}}{\bar{H}_0} = a + b\frac{\bar{S}}{\bar{S}_0} + c\left(\frac{\bar{S}}{\bar{S}_0}\right)^2$			$\frac{\bar{H}}{\bar{H}_0} = a + b\frac{\bar{S}}{\bar{S}_0} + c\left(\frac{\bar{S}}{\bar{S}_0}\right)^2 + d\left(\frac{\bar{S}}{\bar{S}_0}\right)^3$				
R^2	0.79		0.88			0.93				
NS	0.94		0.97			0.97				
Nomalized MAE	6.05%		3.92%			3.97				
Normalized MBE	4.06%		0.09%			0.84				
Normalized RSME	7.94%		5.07%			0.26				
Model coefficients	a	b	c	a	b	c	a	b	c	d
Coefficient Confidences bounds	95%	95%	-	95%	95%	95%	95%	95%	95%	95%
Grand Bandundu	0.12	0.63	-	1.34	-1.68	1.06	1.07	-3.10	4.15	-1.12
Grand Equateur	0.13	0.63	-	1.35	-1.70	1.07	1.10	-3.18	4.26	-1.15
Kasaï-occidental	0.12	0.63	-	1.34	-1.68	1.06	1.06	-3.07	4.11	-1.11
Kasaï-Oriental	012	0.63	-	1.34	-1.68	1.06	1.06	-3.06	4.10	-1.10
Katanga	0.12	0.63	-	1.34	-1.67	1.06	1.04	-3.01	4.03	-1.08
Kinshasa	0.12	0.63	-	1.34	-1.68	1.06	1.07	-3.09	4.13	-1.11
Kongo central	0.12	0.63	-	1.34	-1.68	1.06	1.06	-3.07	4.11	-1.11
Maniema	0.12	0.63	-	1.34	-1.68	1.06	1.08	-3.11	4.16	-1.12
Province Orientale	0.13	0.63	-	1.35	-1.69	1.07	1.10	-3.17	4.25	-1.14

Source : Reproduced from [80]

The results presented in Table 5.4 indicate that the predictive performance of the polynomial models improves with increasing model order. The cubic model provides the highest explanatory power (R^2 = 0.93) and the lowest normalized RMSE (0.26), while the relatively small variation of the model coefficients across provinces suggests a spatially consistent SD–GSI relationship over most regions of the DRC.

Table 5.5 presents the logarithmic and exponential regression models established to describe the relationship between SD and GSI for the provinces of the DRC, excluding Nord and Sud Kivu.

Table 5.5 : GSI-SD Logarithmic and Exponential models

Models	Logarithmic		Exponential		
Relationship	$\frac{\bar{H}}{\bar{H}_0} = a + blog\left(\frac{\bar{S}}{\bar{S}_0}\right)$		$\frac{\bar{H}}{\bar{H}_0} = a + be^{\left(\frac{\bar{S}}{\bar{S}_0}\right)}$		
R^2	0.74		0.80		
NS	0.92		0.94		
Nomalized MAE	5.46%		0.05%		
Normalized MBE	0.15%		-0.09%		
Normalized RSME	7.08%		6.06%		
Model coefficients	a	b	a	b	c
Coefficient Confidences bounds	95%	95%	95%	95%	-
Bandundu	0.75	1.47	0	0.35	-
Equateur	0.76	1.48	0	0.35	-
Kasaï-occidental	0.75	1.46	0	0.35	-
Kasaï-Oriental	0.75	1.46	0	0.34	-
Katanga	0.75	1.46	0	0.34	-
Kinshasa	0.75	1.46	0	0.35	-
Kongo central	0.75	1.46	0	0.35	-
Maniema	0.75	1.47	0	0.35	-
Province Orientale	0.76	1.48	0	0.35	-

Source : Reproduced from [80]

An important observation emerging from Table 5.5 is the remarkable stability of the regression coefficients across provinces for the logarithmic and the exponential models. Their parameters exhibit very limited variation between regions, suggesting that the statistical relationship between SD and GSI remains spatially consistent across most parts of the DRC. This stability indicates that the derived models may be applicable at a broader national scale.

To further illustrate the behaviour of the proposed models, the regression relationships derived from the SD–GSI dataset are presented graphically in the following figures. The empirical relationships between SD and GSI obtained from the statistical models are illustrated in Figures 5.1(a–e), which present the regression curves corresponding to the five tested models (linear, quadratic, cubic, logarithmic, and exponential).

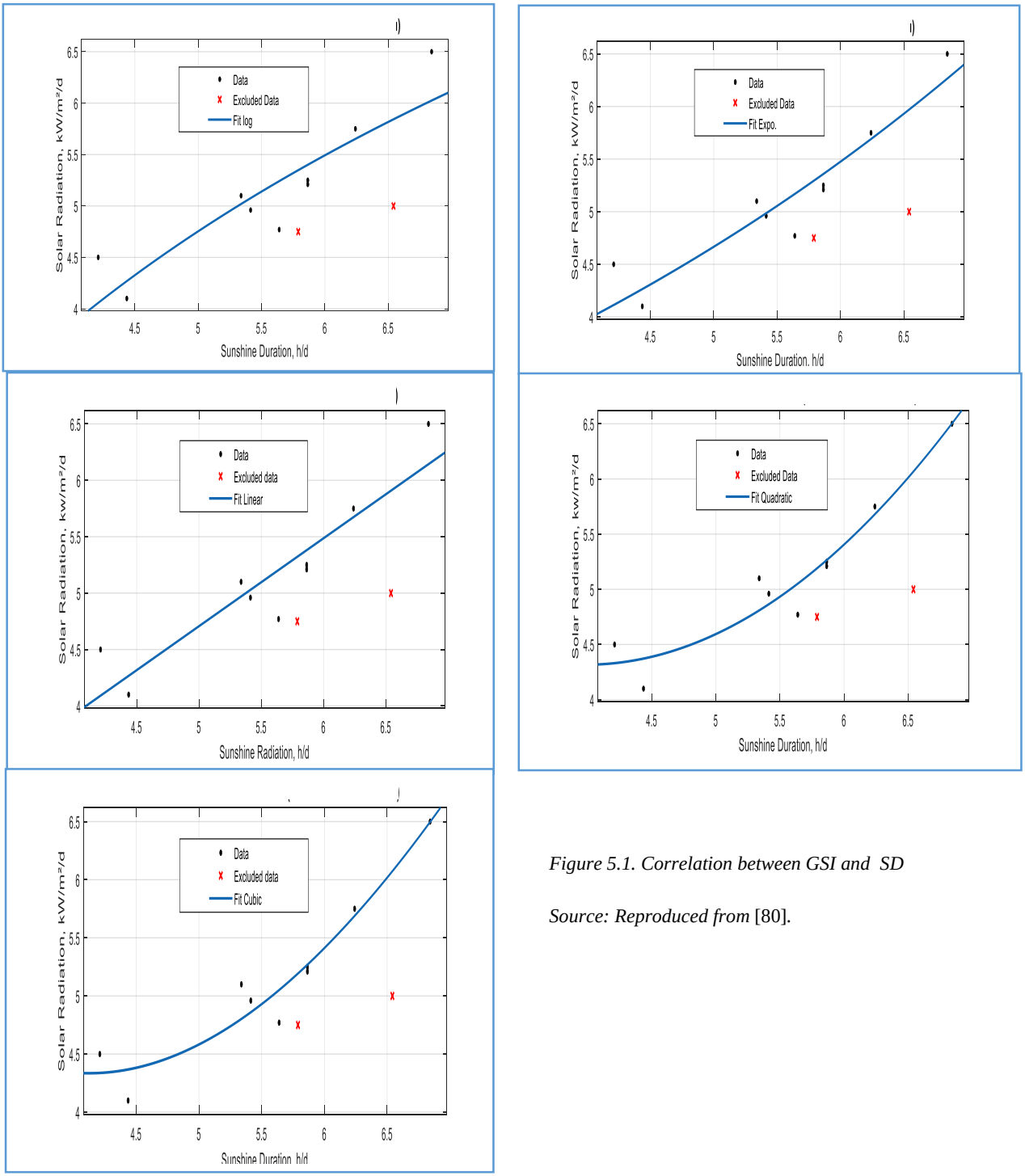

Figure 5.1. Correlation between GSI and SD

Source: Reproduced from [80].

As shown in Figures 5.1(a–e), the polynomial models, particularly the cubic formulation, provide a closer fit to the observed data points, indicating their greater ability to capture the nonlinear behaviour of the SD–GSI relationship across the studied provinces.

5.1.2.2. Scenario 2: Nord and Sud Kivu included

Table 5.6 presents the polynomial models for the scenario 2, where the provinces of Nord and Sud Kivu are included.

Table 5.6: GSI-SD polynomial models

Models	Linear			Quadratic			Cubic			
Relationship form	$\frac{\bar{H}}{\bar{H}_0} = a + b\frac{\bar{S}}{\bar{S}_0}$			$\frac{\bar{H}}{\bar{H}_0} = a + b\frac{\bar{S}}{\bar{S}_0} + c\left(\frac{\bar{S}}{\bar{S}_0}\right)^2$			$\frac{\bar{H}}{\bar{H}_0} = a + b\frac{\bar{S}}{\bar{S}_0} + c\left(\frac{\bar{S}}{\bar{S}_0}\right)^2 + d\left(\frac{\bar{S}}{\bar{S}_0}\right)^3$			
R^2	0.64			0.70			0.71			
NS	0.87			0.90			0.70			
Nomalized MAE	6.30%			6.18%			12.28%			
Normalized MBE	0.51%			0.46%			6.40%			
Normalized RSME	7.55%			7.10%			6 .94%			
Model coefficients	*a*	*b*	*c*	*a*	*b*	*c*	*a*	*b*	*c*	*d*
Coefficient Confidences bounds	95%	95%	-	95%	95%	95%	95%	95%	95%	95%
Grand Bandundu	0.23	0.60	-	1.27	-1.69	1.07	-3.03	17.65	-29.27	16.60
Grand Equateur	0.23	0.60	-	1.28	-1.69	1.06	-3.11	18.10	-30.02	17.03
Kasaï-occidental	0.23	0.60	-	1.26	-1.69	1.07	-3.00	17.48	-28.98	16.44
Kasaï-Oriental	0.23	0.60	-	1.26	-1.69	1.07	-2.99	17.42	-28.88	16.38
Grand Katanga	0.23	0.59	-	1.26	-1.68	1.06	-2.94	17.12	-28.38	16.10
Kinshasa	0.23	0.60	-	1.27	-1.69	1.08	-3.02	17.56	-29.12	16.52
Kongo central	0.23	0.60	-	1.26	-1.69	1.07	-3.00	17.44	-28.93	16.41
Maniema	0.23	0.60	-	1.27	-1.69	1.07	-3.04	17.69	-29.33	16.64
Nord Kivu	0.23	0.60		1.28	-1.69	1.06	-3.10	18.04	-29.92	16.97
Province Orientale	0.23	0.60		1.27	-1.69	1.06	-3.08	17.93	-29.73	16.87
Sud Kivu	0.23	0.60		1.27	-1.70	1.07	-3.16	18.36	-30.45	17.27

Source: Reproduced from [80]

The results presented in Table 5.6 show that the inclusion of Nord and Sud Kivu significantly reduces the explanatory power of the regression models, as reflected by the lower coefficients of determination (R^2 = 0.64–0.71). This decline suggests that the SD–GSI relationship becomes less consistent when these provinces are considered, likely due to the distinct meteorological and topographic conditions of the eastern highland region.

Table 5.7 presents the logarithmic and exponential regression models established to describe the relationship between SD and GSI for the provinces of the DRC, including Nord and Sud Kivu.

Table 5.7: Exponential and Logarithmic models

Model	Logarithmic model			Expoential model		
Relationship form	$\frac{\bar{H}}{\bar{H}_0} = a + b\log\left(\frac{\bar{S}}{\bar{S}_0}\right)$			$\frac{\bar{H}}{\bar{H}_0} = a + be^{\left(\frac{\bar{S}}{\bar{S}_0}\right)}$		
R^2	0.61			0.66		
NS	0.85			0.87		
Nomalized MAE	6.37%			0.14%		
Normalized MBE	0.54%			0.25%		
Normalized RSME	7.81%			7.33%		
Model coefficients	a	b	c	a	b	c
Coefficient Confidences bounds	95%	95%	95%	95%	-	[i]
Bandundu	0	0.38	-	0.81	1.22	-
Equateur	0	0.38	-	0.81	1.23	-
Kasaï-occidental	0	0.37	-	0.81	1.22	-
Kasaï-Oriental	0	0.37	-	0.81	1.21	-
Katanga	0	0.37	-	0.80	1.21	-
Kinshasa	0	0.37	-	0.81	1.22	-
Kongo central	0	0.37	-	0.81	1.21	-
Maniema	0	0.38	-	0.81	1.22	-
Nord Kivu	0	0.38	-	0.81	1.23	-
Province Orientale	0	0.38	-	0.81	1.22	-
Sud Kivu	0	0.38	-	0.81	1.22	-

Source: Reproduced from [80]

As shown in Table 5.7, the logarithmic and exponential models exhibit relatively modest predictive performance when all provinces are included, with R^2 values not exceeding 0.66. This outcome further indicates that the nonlinear SD–GSI relationship becomes more difficult to capture statistically when the particular climatic conditions of Nord and Sud Kivu are incorporated into the dataset.

The corresponding regression relationships obtained when Nord and Sud Kivu are included in the dataset are presented in Figures 5.2(a–e), which illustrate the statistical behaviour of the five models under the full national dataset.

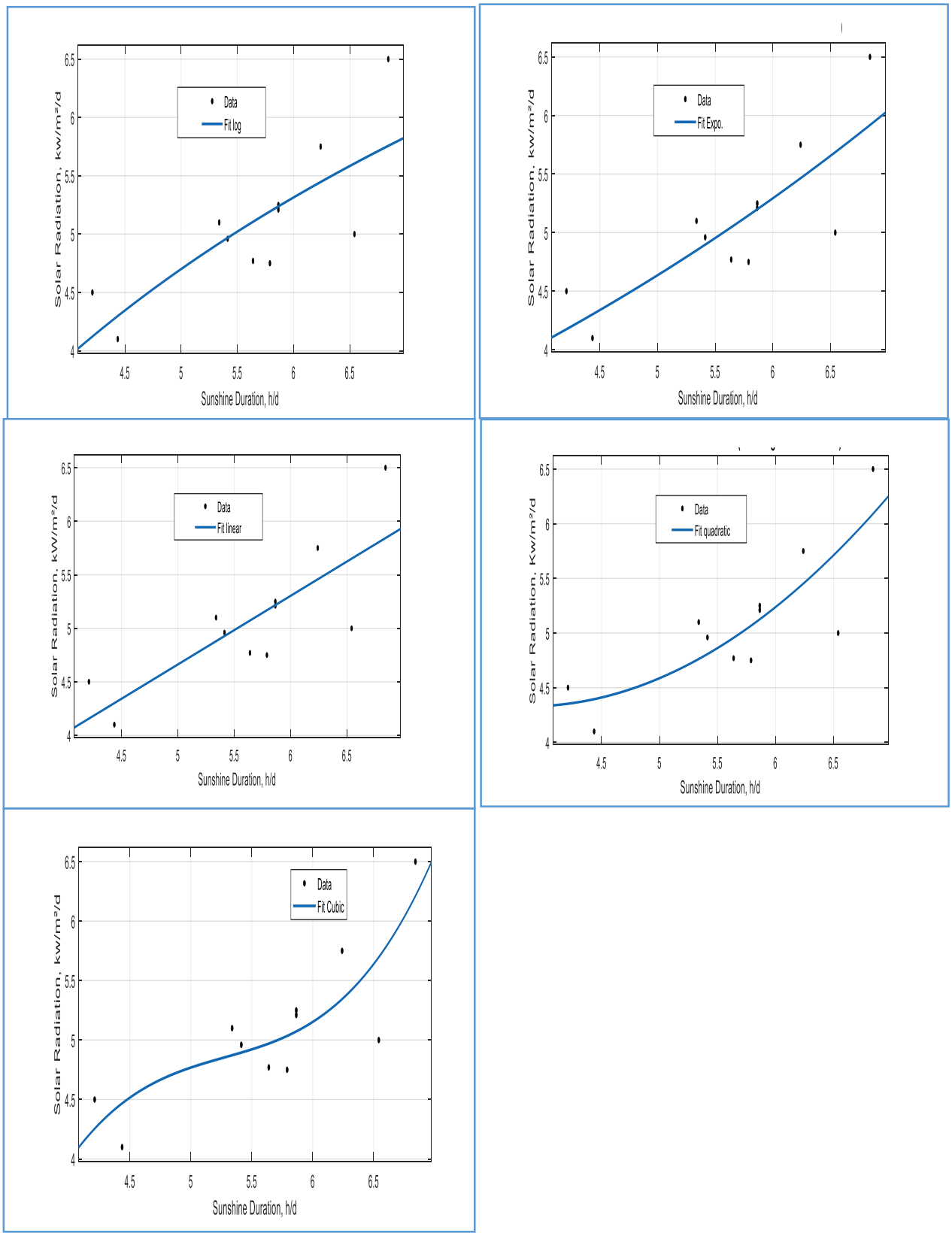

Figure 5.2. Correlation between GSI and SD.

Source: Reproduced from [80]

Compared with the previous case, the dispersion of the data points appears more pronounced, reflecting the reduced strength of the SD–GSI relationship when the particular climatic conditions of North and South Kivu are taken into account.

5.3 Model Validation

In this study, model validation is performed using a combination of complementary criteria that capture different aspects of model performance, including explanatory power, predictive accuracy, and systematic bias.

5.3.1 Explanatory power and predictive accuracy

1. Coefficient of determination (R^2):

The coefficient of determination, R^2, quantifies the fraction of variance in the dependent variable (GSI) that is explained by the independent variable (SD). A higher R^2 indicates that the model captures more of the observed variability in SI, reflecting strong explanatory capability. In this study, R^2 is considered acceptable if it exceeds 0.7, a threshold commonly adopted in solar resource modeling studies to ensure meaningful predictive strength, particularly when working with spatially heterogeneous datasets.

2. Nash–Sutcliffe efficiency (NS):

The Nash–Sutcliffe efficiency coefficient (NS) [22], also called the model acceptability index, evaluates the overall predictive skill of a model relative to the observed mean. Values of NS approaching 1 indicate high model reliability, while NS values below 0 suggest that the model performs worse than the mean of the observed data. In this work, models are considered robust if NS falls within the range of 0.7–1.0 [81].which guarantees that the model sufficiently captures the temporal and spatial dynamics of GSI across the provinces . The NS is defined as in [22].

5.3.2 Normalized error metrics:

To complement R^2 and NS, three normalized error metrics or Non-dimensional (ND) versions of these metrics are employed: NDMAE, NDMBE and NDRSME, expressed as a percentage and defined as in [21].

5.3.3 Integration of complementary criteria:

By evaluating models simultaneously using R^2, NS, NMAE, NMBE, and NRMSE, a multidimensional assessment of performance is achieved. This ensures that a model is not selected solely based on its fit to the data (high R^2) while neglecting systematic errors or deviations (bias and normalized errors). In this Chapter, only models that satisfy all criteria simultaneously are retained for further analysis, ensuring both statistical robustness and physical plausibility.

5.3.4 Justification in the context of the DRC:

Given the scarcity of direct SI measurements across the DRC, and the reliance on SD as a proxy, rigorous validation is essential. The combination of these metrics provides a comprehensive assessment, accounting for both the nonlinearity of the SD–GSI relationship and the spatial heterogeneity of solar resources across provinces. This multi-criteria approach strengthens the credibility of the derived statistical models, facilitating their application for PV system planning and solar energy assessments across diverse climatic zones.

In summary, the validation framework adopted in this study ensures that the developed models are not only statistically significant but also operationally reliable, providing a sound basis for both theoretical insights and practical applications in solar energy deployment in the DRC

5.3.5 Analysis of Coefficient of Determination (R^2)

Scenario 1: Nord and Sud Kivu excluded

Table 5.8 presents the coefficients of determination (R^2) for the five statistical models (linear, quadratic, cubic, logarithmic, and exponential) obtained when the provinces of Nord

Kivu and Sud Kivu are excluded. These values quantify the proportion of variance in annual mean GSI that is explained by the annual mean daily SD for each model.

Table 5.8: Coefficients of Determination (R^2)of the Evaluation Models

Models	Linear	Quadratic	Cubic	Logarithmic	Exponential
R^2	0.79	0.88	0.93	0.74	0.80

Source : Compiled and processed by the author.

Excluding Nord and Sud Kivu reveals that the polynomial models—particularly the cubic formulation—capture the SD–GSI relationship with the highest fidelity. Specifically, the quadratic and cubic models explain 88% and 93% of the observed variance, respectively, indicating their superior ability to represent the underlying nonlinear dynamics of solar radiation across the DRC provinces. In contrast, the logarithmic model exhibits the lowest explanatory power ($R^2 = 0.74$), suggesting a limited capacity to capture complex spatial patterns when these two climatically distinct provinces are omitted.

Scenario 2: Nord and Sud Kivu included

Table 5.9 reports the coefficients of determination for the same set of models, this time including the Nord and Sud Kivu provinces. The inclusion of these regions, characterized by distinct meteorological regimes, allows for assessment of model robustness across the full diversity of climatic conditions within the DRC.

Table 5.9: Coefficients of Determination (R^2)of the Evaluation Models

Models	Linear	Quadratic	Cubic	Logarithmic	Exponential
$\boldsymbol{R^2}$	0.64	0.70	0.71	0.66	0.61

Source : Compiled and processed by the author.

When Nord and Sud Kivu are incorporated, the explanatory power of all models declines due to the increased climatic heterogeneity. Only the quadratic ($R^2 = 0.70$) and cubic ($R^2 = 0.71$) models maintain moderate predictive capability, capturing approximately 70% of the variance between SD and GSI. The linear, logarithmic, and exponential models fall below the 70% threshold, indicating inadequate representation of the complex SD–GSI relationship across the full national territory. This contrast highlights the sensitivity of simpler models to regional

climatic anomalies and reinforces the necessity of higher-order polynomial formulations for robust solar radiation estimation in diverse tropical contexts.

5.3.6 Analysis of Nash-Sutcliffe Efficiency Values

5.2.6.1. Scenario 1: Nord and Sud Kivu excluded

Table 5.10 reports the NS efficiency values for the five statistical models (linear, quadratic, cubic, logarithmic, and exponential) obtained when the provinces of Nord and Sud Kivu are excluded. NS quantifies the predictive power of each model, with values approaching 1 indicating superior performance and values below 0.7 considered insufficient for reliable predictions.

Table 5.10 : Performance Assessment of Models Using Nash-Sutcliffe Efficiency

Models	Linear	Quadratic	Cubic	Logarithmic	Exponential
NS value	0.94	0.97	0.97	0.74	0.80

Source : Compiled and processed by the author.

All models satisfy the NS acceptance threshold of 0.7, confirming their overall adequacy. Notably, the cubic and quadratic models exhibit NS values near 1, demonstrating their superior capacity to capture the nonlinear relationship between SD and GSI. Although the logarithmic model meets the minimum criterion, its lower NS value reflects a reduced predictive robustness compared to the polynomial formulations. These results indicate that higher-order models are more appropriate for precise solar radiation estimation when the climatically unique Nord and Sud Kivu provinces are excluded.

5.2.6.2. Scenario 2: Nord and Sud Kivu included

Table 5.11 presents the NS values obtained for the same set of models when all provinces of the DRC are included. The inclusion of Nord and Sud Kivu introduces increased climatic heterogeneity, allowing an assessment of model robustness across the entire national territory.

Table 5.11: Model NS values

Models	Linear	Quadratic	Cubic	Logarithmic	Exponential
NS	0.87	0.89	0.70	0.85	0.87

Source : Compiled and processed by the author.

All models remain above the 0.7 acceptance threshold, confirming general robustness. However, the cubic model now exhibits the lowest NS value, while the quadratic model maintains the highest efficiency. This suggests that although polynomial models generally perform well, climatic and topographic variability in the eastern highlands (Nord and Sud Kivu) reduces the effectiveness of higher-order models. Consequently, quadratic formulations may offer a more stable and reliable approach for solar radiation prediction under full national conditions.

5.3.7 Statistical Performance Assessment

5.2.7.1. Scenario 1: Nord and Sud Kivu excluded

Table 5.12 summarizes the normalized statistical error metrics (NMAE, NMBE, and NRMSE) obtained for the five regression models when Nord and Sud Kivu provinces are excluded.

Table 5.12: Normalized Performnce Metrics

Models	Linear	Quadratic	Cubic	Logarithmic	Exponential
Nomalized MAE	6.05%	3.92%	3.97	5.46%	0.05%
Normalized MBE	4.06%	0.09%	0.84	0.15%	-0.09%
Normalized RSME	7.94%	5.07%	0.26	7.08%	6.06%

The relatively low error values (all below 10%) confirm the robustness of the models under this scenario, with the quadratic and cubic formulations providing the lowest prediction errors and therefore the most reliable estimation of GSI from SD.

5.2.7.2. Scenario 2: Nord and Sud Kivu included

Table 5.13 presents the normalized statistical errors of the regression models obtained when all provinces of the DRC, including Nord and Sud Kivu, are incorporated into the analysis.

Table 5.13: Normalized Performnce Metrics

Models	Linear	Quadratic	Cubic	Logarithmic	Exponential
Nomalized MAE	6.30%	6.18%	12.28%	5.46%	0.05%
Normalized MBE	0.51%	0.46%	6,40%	0.15%	-0.09%
Normalized RSME	7.55%	7.10%	6 ,94%	7.08%	6.06%

The increase in prediction errors—particularly the higher NMAE observed for the cubic model—reflects the influence of regional climatic anomalies in eastern DRC, which introduce greater uncertainty in the empirical SD–GSI relationship.

5.4 Discussion of Model Performance and Implications

5.4.1 Performance Across Scenarios

The statistical analysis performed in this chapter highlights several important characteristics of the relationship between SD and GSI across the DRC.

First, the results demonstrate that polynomial models—particularly the quadratic and cubic formulations—provide the most accurate representation of the SD–GSI relationship. These models consistently exhibit higher coefficients of determination (R^2), higher Nash–Sutcliffe efficiency values, and lower statistical errors compared to the linear, logarithmic, and exponential models. This finding confirms that the relationship between SD and GSI in tropical environments is inherently nonlinear.

Second, the comparative analysis between the two scenarios clearly reveals the influence of regional climatic conditions on model performance. When Nord and Sud Kivu provinces are excluded, the models explain up to 93% of the variance in SI, indicating a very strong statistical relationship between SD and GSI across most provinces of the country.

However, when these provinces are included, the explanatory power of the models decreases significantly.

This reduction in predictive performance can be attributed to the particular climatic and geographical conditions of the eastern highlands of the DRC. Nord and Sud Kivu are characterized by high altitudes, complex topography, frequent cloud formation, and strong convective atmospheric processes associated with the Great Rift Valley system. These conditions modify the relationship between SD and GSI by increasing atmospheric attenuation and cloud variability.

Consequently, the empirical SD–GSI relationship becomes less stable in these regions than in the central and western parts of the country.

5.4.2 Implications for National PV System Planning

These results have direct implications for solar energy planning in the DRC:

- The robust correlation between SD and GSI across most provinces enables reliable estimation of solar potential in regions lacking direct irradiance measurements.
- Quadratic models provide a balance between predictive accuracy and stability, making them suitable for large-scale PV resource assessment.
- The observed reduction in predictive performance in Nord and Sud Kivu emphasizes the need for localized calibration or hybrid models when designing PV systems in highland or climatically complex regions.
- Accurate regional modeling of SI is crucial for optimally sizing PV installations, forecasting energy generation, and informing national energy policy and investment decisions.

5.5 Synthesis: Spatial Non-Stationarity of the SD–GSI Relationship

The results obtained in this chapter demonstrate that the relationship between SD and GSI, expressed through normalized formulations is inherently spatially non-stationary across the DRC. The calibration of the five models reveals significant variability in the coefficients a, b, c, d between provinces. This variability is consistent with the spatial patterns identified in Chapter 4, where longitudinal gradients and moisture-related atmospheric processes were

shown to control SD distribution. In particular, regions such as Nord and Sud Kivu exhibit distinct model responses, reflecting complex atmospheric dynamics and high cloud variability. Their inclusion in a unified calibration systematically degrades model performance, thereby providing empirical evidence of structural heterogeneity in the SD–GSI relationship.

These findings indicate that the coefficients of empirical SD–GSI models cannot be treated as universal constants, but must be interpreted as location-dependent parameters governed by regional climatic conditions.

From a modeling perspective, this confirms the necessity of:adopting province-specific calibrations, and selecting functional forms capable of capturing non-linear atmospheric effects.

Also, from an application standpoint, the results highlight that neglecting spatial variability may lead to biased solar resource estimation, with direct implications for PV system sizing, energy yield prediction, and regional energy planning.

5.6 Summary

This chapter comprehensively evaluated the statistical relationships between annual mean daily sunshine duration (SD) and global solar irradiation (GSI) across the provinces of the DRC. Key findings include:

— High model fidelity in most provinces: Polynomial models, especially quadratic and cubic, consistently achieved $R^2 \geq 0.88$ and NS ≥ 0.97 when Nord and Sud Kivu were excluded.
— Impact of climatic heterogeneity: Including the eastern highlands reduced model performance, with R^2 values decreasing to 0.70–0.71 and NS ranging from 0.70–0.89, highlighting the influence of topography and microclimate on solar irradiation variability.
— Statistical validation: Normalized errors (NMAE, NMBE, NRMSE) remained within acceptable thresholds for all validated models, confirming their reliability for solar radiation estimation.
— Practical implications: Quadratic models provide a robust, nationally applicable tool for PV system planning, while highland provinces may require additional calibration.

Conclusion: The comparative analysis conducted in this chapter demonstrates that the SD–GSI relationship is fundamentally robust across most provinces. However, the inclusion of Nord and Sud Kivu reveals the significant impact of specific climatic and topographic conditions on model performance, reinforcing the need for context-specific adjustments in solar resource planning and PV system optimization across the DRC.

5.7 Comparison with Other Tropical Regions

Empirical sunshine-based solar radiation models have been widely applied across tropical regions including Africa, Southeast Asia, and Latin America. Studies conducted in West Africa have reported similar relationships between sunshine duration and clearness index under humid tropical conditions [82, 83], Comparable results have also been obtained in Southeast Asia, where monsoon-driven cloud systems produce radiative regimes similar to those observed in equatorial Africa [32, 84].

In Latin America, particularly within the Amazon Basin, the relationship between sunshine duration and solar radiation exhibits similar characteristics due to comparable atmospheric moisture conditions and convective cloud dynamics [85].

These comparisons suggest that the empirical relationships identified in this study are consistent with broader patterns observed in tropical climates worldwide.

GENERAL CONCLUSION AND PERSPECTIVES

6.1 Problem

Reliable solar radiation data remain scarce in the DRC, which significantly constrains evidence-based PV planning and energy policy development. The limited number of radiometric stations across the country makes direct measurement of GSI difficult, while the strong spatial variability in cloud cover, atmospheric humidity, and topography further complicates solar resource assessment.

Under these conditions, SD represents one of the most consistently recorded meteorological variables and therefore offers a valuable proxy for estimating GSI. The present research was motivated by the need to develop robust and transferable empirical models capable of estimating GSI from SD data across the heterogeneous climatic environments of the DRC.

6.2 Method

To address this challenge, empirical regression models linking SD to GSI were developed using long-term ground observations and satellite-derived datasets. Satellite-based SD values were corrected using an empirical adjustment factor in order to account for atmospheric attenuation and local cloudiness. Five regression formulations were systematically evaluated: linear, quadratic, cubic, logarithmic, and exponential models.

In order to obtain spatially representative values of SD at the provincial level, a hierarchical area-weighted aggregation method was implemented, allowing territorial and district-level data to be combined into provincial averages.

Two modelling scenarios were analysed to evaluate the influence of regional climatic heterogeneity:

— Scenario 1: exclusion of Nord Kivu and Sud Kivu provinces, whose mountainous topography and particular climatic conditions may influence the SD–GSI relationship.
— Scenario 2: inclusion of all provinces, allowing a full national assessment of solar resource variability.

Model performance was evaluated using multiple complementary statistical indicators, including the coefficient of determination (R^2), the Nash–Sutcliffe efficiency coefficient (NS) and normalized error metrics (NMAE, NMBE, and NRMSE), ensuring both predictive accuracy and statistical robustness.

6.3 Results

The results demonstrate that SD constitutes a reliable predictor of GSI across most provinces of the DRC. Among the tested models, the quadratic and cubic regressions consistently provided the highest predictive performance, effectively capturing the nonlinear nature of the SD–GSI relationship.

In the first modelling scenario, excluding Nord Kivu and Sud Kivu, the models achieved strong statistical performance, with coefficients of determination reaching approximately 93% for the cubic model, indicating a strong relationship between SD and GSI under relatively homogeneous climatic conditions.

When the two eastern provinces were included in the analysis, the statistical performance of the models slightly decreased, reflecting the influence of the complex topography and convective cloud systems characteristic of the eastern highlands. Nevertheless, the quadratic and cubic models maintained acceptable predictive skill, confirming the robustness of the SD–GSI relationship at the national scale.

A particularly notable finding of this research is the solar paradox observed in Sud Kivu, where relatively high SD does not translate into proportionally high GSI. This phenomenon highlights the strong influence of local atmospheric dynamics and mountainous terrain on solar radiation availability.

The spatial analysis further revealed clear regional variations in solar resources. Based on the annual average SD, three broad solar potential zones can be distinguished within the DRC. The Katanga region exhibits the highest solar potential, with approximately 2717 hours of sunshine per year, whereas Kongo Central shows the lowest value, with approximately 1783 hours. Despite these variations, all provinces demonstrate sufficient solar resources to support photovoltaic energy development.

6.4 Interpretation

The results confirm that SD can serve as a reliable proxy for estimating GSI in tropical environments characterized by limited observational infrastructure. The remarkable stability of the regression coefficients across most provinces indicates that the SD–GSI relationship is relatively robust and transferable within the Congolese climatic context.

However, the comparison between the two modelling scenarios demonstrates that regional climatic heterogeneity plays a significant role in modulating this relationship. The lower model performance observed when including Nord Kivu and Sud Kivu suggests that mountainous regions with strong convective activity may deviate from the generalized SD–GSI behaviour observed elsewhere in the country.

The Sud Kivu paradox therefore illustrates the importance of integrating local topographic and atmospheric factors when interpreting sunshine-based solar resource estimates.

6.5 Impact

Beyond its scientific contributions, this research provides practical tools for solar energy planning in the Democratic Republic of Congo. The developed empirical models allow reliable estimation of solar radiation using sunshine duration data that are more widely available than direct radiometric measurements.

These results can support engineers, policymakers, and investors in identifying favourable locations for photovoltaic system deployment and optimizing system design. The modelling framework proposed in this thesis also provides a scalable methodological approach that may be applied in other tropical countries facing similar data limitations.

By highlighting spatial heterogeneities in solar potential and identifying climatic anomalies such as the Sud Kivu paradox, this work contributes to more realistic and data-driven strategies for renewable energy development.

6.6 Future Directions

Future research should focus on improving the predictive accuracy of solar radiation models by incorporating additional atmospheric variables such as cloud cover, humidity, aerosol concentration, and precipitation. Expanding the meteorological observation network across the country would also significantly enhance the spatial resolution of solar resource assessments.

Furthermore, advanced modelling approaches, including machine learning techniques and hybrid statistical–physical models, could be explored to better capture complex nonlinear interactions between meteorological variables.

Integrating climatic, geographic, and socio-economic factors into solar energy planning models will ultimately enable high-resolution forecasting and support the sustainable expansion of photovoltaic energy systems throughout the Democratic Republic of Congo.

6.7 Closing Statement

Although the Democratic Republic of Congo enjoys abundant sunshine, unlocking its full solar potential requires robust empirical modelling capable of capturing both the large-scale climatic patterns and the subtle local effects of topography and atmospheric dynamics, thereby providing a scientific foundation for a sustainable and resilient solar energy future.

References

[1] World Bank, Acces to electricity (% the population), 2022.

[2] World Bank, “World Development Indicators,” [Online]. Available: https://databank.worldbank.org/Population-growth-rate-DRC/id/8a4029ee. [Accessed 2 November 2025].

[3] Angström A., “Solar and Terrestrial radiation,” *Quartely Journal of the Royal Meteorological Society,* vol. 50, no. 210, pp. 121-125, 1924.

[4] J. Prescott, “Evaporation from a Water Surface in Relation to Solar Radiation,” *Transactions of the Royal Society of South Australia,* vol. 64, pp. 114-118, 1940.

[5] H. Ögelman, A. Ecevit and E. Tasdemiroğlu, “A new method for estimating solar radiation from bright sunshine data,” *Solar Energy,* vol. 33, no. 6, pp. 619-625, 1984.

[6] M. El-Metwally, “Sunshine and global solar radiation estimation at different sites in Egypt,” *Journal of Atmospheric and Solar-Terrestrial Physics,* vol. 67, no. 14, pp. 1331-1342, 2005.

[7] A. Mefti, M. Bouroubi, M.Y. and A. Khellaf, “Analyse Critique du Modèle de l’Atlas Solaire de l’Algérie,” *Rev. Energ. Ren.,* vol. 2, no. 1999, pp. 69-85, 1999.

[8] Capderou M., *Atlas Solaire De L'Algérie,* vol. 1&2, Alger: Office des publications universitaires, 1988.

[9] M. Salmi , H. Bouzgou and L. Laissaoui , “Estimation de l'irradiation solaire globale dans la ville de M'sila (Algérie),” in *1ère Conférence Maghrébine sur les Matériaux et l’énergie*, Tunisia, 2010.

[10] T. David and K. Jackson. , “Comparison Between Linear and Quadratic Models For Estiming Solar Radiation Data in Yola, Adamawa State, Nigeria,” *International Journal of Research & Development (IJRD),* vol. 1, no. 5, pp. 1-8, 2016.

[11] e. a. Bernard B.T., “Empirical Relationships Between Global and Diffuse Radiation and Sunshine Duration in Chad: Polynomial Regression Approach,” *International Journal of Heat and Technology,* vol. 40, no. 1, pp. 121-129, 2022.

[12] R. Mbiaké , A. Wakata, E. Mfoumou and E. Ndjeuna, “The Relationship between Global Solar Radiation and Sunshine Durations in Cameroon,” *Open Journal of Air Pollution,* vol. 2018, no. 7, pp. , 107-119, 2018.

[13] Ministère de l'Environnement et ressources Hudrauliques, Atlas des énergies renouvelables de la RDC, 2014.

[14] European Centre for Medium-Range Weather Forecasts (ECMWF), “https://stringfixer.com/fr/ECMWF,” European Centre for Medium-Range Weather Forecasts (ECMWF), 16 June 2021. [Online]. Available: https://stringfixer.com/fr/ECMWF. [Accessed 16 june 2021].

[15] ANAPI, Agence Nationale pour la Promotion des Investissements, “Généralités sur la RDC/Ressources naturelles et profil géographique,” [Online]. Available: https://www.investindrc.cd/fr/Ressources-naturelles-et-profil-geographique. [Accessed 15 September 2021].

[16] S. Moriasi, J. Arnold and et al., “Model evaluation guidelines for systematic quantification of accuracy in watershed simulations,” *Transactions of ASABE,* vol. 50, no. 3, pp. 885-900, 2007.

[17] Cornillon P.A. and Matzner-Lober E., Régression: Théorie et aplications, Paris: Springer-Verlag, 2007, pp. 15-16, 33-44, 82-97.

[18] M. Schwarz, D. Folini, M. Hakuba and M. Wild, “From point to area Wordwide assessment of the representativeness of monthly surace solar radiationrecords,” *Journal of Geophysical Research: Atmosphere,* vol. 123, no. 10, pp. 5472-5493, 2018.

[19] Y. Huang and et al., “Representativeness errors of point-scale ground-based solar radiationmeasurements in the validation of remote sensing products,” *Remote Sensing of Environment,* vol. 181, pp. 146-161, 2016.

[20] R. Wang, E. Andrews and et al., “Spatial Representativeness error in the Ground-Level Observation Network for Black Carbon Radiation Absorption,” *Geophysical Reseaarch Letters,* vol. 45, no. 4, pp. 2106-2114, 2018.

[21] S. Zekai, Solar energy fundamentals and modeling techniques: atmosphere, environment, climate change and renewable energy, London: Springer-Verlag London Liited, 2008, pp. 47-98.

[22] Graie GT, *Critères & indicateurs d'auto-évaluation des modèles,* Graie, Ed., 2018, pp. 1-17.

[23] E. Efoto, “Les Correlations du rayonnement solaire en fonction de la fraction de la durée de l'insolation maximum à Kinshasa (Zaïre),” *Annales de la Faculté des sciences de l'Université de Kinshasa,* no. Numéro spécial 3, pp. 141-157, 1997.

[24] J. Fan,, L. Wu, , F. Zhang, , H. Cai, , W. Zeng, and X. Wang,, “Empirical and machine learning models for predicting daily global solar radiation from sunshine duration: A review and case study in China,” *Renewable and Sustainable Energy Reviews,* Vols. vol. 100,, pp. 186–212,, 2019..

[25] J. Almorox and C. Hontoria, “Global solar radiation stimation using sunshine duration in Spain,” *Energy Conversion and Management,* vol. 45, no. 9, pp. 1529-1535, 2004.

[26] M. Mayer and G. Gróf, “Extensive comparison of deterministic and machine learning solar irradiance forecasting methods,” *Applied Energy,* no. 283, , p. 116244, 2021..

[27] A. Archila-Busquets, and et al., “Global solar radiation estimation using sunshine duration in various climates: A review of the Angstrom-Prescott model coefficients,” *Renewable and Sustainable Energy Reviews,* vol. 158, p. 112111, 2022.

[28] C. Gueymard, “The sun’s total and spectral irradiance for solar energy applications and solar radiation models,” *Solar Energy,* vol. 76, pp. 423-453, 2004, 2024.

[29] J. Almorox, M. Bocco and E. Willington, “Estimation of daily global solar radiation from measured temperatures and sunshine hours in Argentina,” *Renewable Energy,* vol. 59, pp. 12-20, Nov. 2013..

[30] Z. Li, W. Wu, and X. Liu, “Global solar radiation estimation from sunshine duration in China: A review and case study,” *Renewable and Sustainable Energy Reviews,* vol. 115, p. 109357, Nov. 2019.

[31] J. A. Duffie and W. A. Beckman, Solar Engineering of Thermal Process, 4Th ed. ed., Hoboken, New Jerey(NJ): John Wiley & Sons, Inc., 2013.

[32] J. Yang, L. Zhao, Y. Wang and H. Li, “Review of empirical models for estimating global solar radiation using meteorological parameters,” *Renewable and Sustainable Energy Reviews,* vol. 81, pp. 854-871, 2018.

[33] S. Meenal and A. I. Selvakumar, “Assessment of SVM, empirical and ANN based solar radiation prediction models with most influencing meteorological parametrs,” *Renewable Energy,* vol. 121, pp. 324-343, 2018.

[34] A. Archila-Busquets, A. Ruiz-Arias and D. Pozo-Vázquez, “Global solar radiation estimation using sunshine duration in various climates: A review of the Angstrom-Prescott model coefficients,” *Renewable and Sustainable Energy Reviews,* vol. 158, p. 112111, Apr. 2022..

[35] O. Ajayi,, O. Ohijeagba, C. E. Mokwia and O. S. Ike, “Modelling and analysis of solar energy and sunshine duration of North-Eastern Nigeria,” *Renewable Energy,* vol. 68, pp. . 332-341,, Aug. 2014.

[36] C. A. Gueymard, “Direct and indirect uncertainties in the prediction of tilted irradiance for solar engineering applications,” *Solar Energy,* vol. 83, no. 3, pp. 432-444, 2009.

[37] M. J. Glover J., “The empirical relation between solar radiation and,” *Royal Meteorological Society,* vol. 84, no. 360, pp. 172-175, 1958.

[38] V. Bahel , H. Baksh and R. Srinivasan, “A correlation for estimation of global solar radiation,” *Energy,* vol. 12, no. 2, pp. 131-135, 1987.

[39] El-Metwally M., “Sunshine and global solar radiation estimation at different sites in Egypt,” *Journal of Atmospheric and Solar-Terrestrial Physics,* vol. 67, no. 14, pp. 1331-1342, 2005.

[40] D. B. Ampratwum and A. S. S. Dorvio, “Estimation pf solar radiation from the bumber of susnshine,” *Applied Energy,* vol. 63, no. 3, pp. 161-167, 1999.

[41] S. Pelland, J. Remund, J. Müller and B. Gschwind, “Photovoltaic and Solar Forecasting: State of the Art,” 2013.

[42] S. Hagemann, Stefan , C. Chen and et al, “Impact of a Statistical Bias Correction on the Projected Hydrological Changes Obtained from Three GCMs and Two Hydrology Models,” *Journal of Hydrometeorology,* vol. 12, no. 4, pp. 556-578, 2011.

[43] B. H. Liu and R. C. Jordan , “The long-Term Average Performance of Flat-Plate Solar Energy Collectors,” *Solar Energy,* vol. 7, no. 2, pp. 53-74, 1963.

[44] R. Perez , P. Ineichen . and R. Seals , “Modeling daylight availability and irradiance components from direct and global irradiance,” *Solar Energy,* vol. 44, no. 5, pp. 271-289, 1990.

[45] R. Perez , R. Seals and J. Michalsky, “All-weather model for sky luminance distributio-Preliminary configuration and validation,” *Solar Energy,* vol. 50, no. 3, pp. 235-245, 1993.

[46] R. Perez , R. Stewart and et al., “An anisotropic hourly diffuse radiation model for sloping surfaces descrption, performance validation,” *Solar Energy,* vol. 36, no. 6, pp. 481-497, 1986.

[47] R. Perez , R. Stewart , R. Seals and T. Guertin, “The Developmen and verification of the Perez Diffuse Radiation Model (SAND88-7030).,” Sandia National Lab. (SNL-NM), Albuquerque, NM (United States); State Univ. of New York, Albany (USA). Atmospheric Sciences Research Center, Albuquerque, 1988.

[48] B. Liu, , Y. Wu and J. Sun, “A review of models for estimating the diffuse fraction of daily solar radiation,” *Renewable Energy,* vol. 182, pp. 466-483,, Jan. 2022..

[49] S. Goni , H. A. Adannou , D. Diop , M. Darame and B. Tikri, “Long-Term Variation of Sunshine Duration and Their Inter-Action with Meteorogical Parameters over Chad, Central Africa,” *Natural Resources,* vol. 10, no. 3, pp. 47-58, 2019.

[50] Neske S., “About the relation between Sunshine Dration and cloudiness on the basis of data from Hamburg,” *Journal of Solar Energy,* vol. 2014, p. 306871, 2014.

[51] B. M. Bennett and G. A. Barton , “The enduring link between forest cover and rainfall: a historical perspective on science and policy discussions,” *Forest Ecosystems,* vol. 5, no. 5, 2018.

[52] A. Teuling, C. Taylor and et al, “Observational evidence for cloud cover enhancement over western European forests,” *Nature Communications,* vol. 8, no. 14065, 2017.

[53] Climats et voyages, “Climat - Republique Democratique Congo,” [Online]. Available: https://www.climatsetvoyages.com/climat/republique-democratique-congo. [Accessed 11 September 2021].

[54] Ministère d'Energie de la RDC, “Système d'information énergétique,” Kinshasa, 2010.

[55] D. Lusamba Yangindu, P. Luhumbu Luwembo and et al., “Etude de validation du backbone à fibre optique Kinshasa-Muanda,” *Annales de la faculté des sciences,* vol. 1, no. 1, pp. 1-8, 2014.

[56] F. Abdoula, “Calculating the variations of sunrise, sunset and day length times for Baghdad city.With comparison to different regions of the world in year 2019,” vol. 60, no. 12, p. 2732–2741, 2012.

[57] T. Fiolleau and R. Roca, “A database of deep convective systems derived from the intercalibrated meteorological geostationary satellite fleet and the TOOCAN algorithm (2012-2020),,” *Earth Syst. Sci. Data,* vol. 16, pp. 4021-4050, 2024.

[58] G. Weber,, “On the Seasonal Variation of Local Relationships Between Temperature, Temperature Range, Sunshine and Cloudiness,” *Theoretical and Applied climatology,* vol. 50, no. 1-2, pp. 15-22, 1994.

[59] K. Essa and S. Etman, “On the relation between cloud cover amount and sunshine duration,” *Meteorol Atmos Phys,* vol. 87, no. 4, p. 235–240, 2004.

[60] WMO, World Meteorological Organisation, “Commission des instruments et des méthodes d’observation - Seizième session:,” WMO, Saint-Petersbourg, 2014.

[61] Murthy V.R.K., “Crop Growth Modeling and Its Applications in Agricultural Meteorology,” 2011.

[62] L. Weiguang , M. Hou and J. Xin , “Low-cloud and sunshine duration in the low-latitude belt of South China for the period 1961–2005,” *Theoretical and Applied Climatology,* vol. 104, p. 473–478, 2011.

[63] D. Matuszko , R. Twardosz and Piotrowicz, “relationship betwen cloudiness, precipitation and temperature,” *Geographia Polonica,* vol. 77, no. 1, pp. 9-17, 2004.

[64] H. Wang , D. Liu , H. Lin , A. Monténégro and X. Zhu , “NDVI and vegetation phenology dynamics under the influence of sunshine duration on the Tibetan plateau,” *International Journal of Climatology,* vol. 35, no. 5, pp. 687-698, 2015.

[65] S. Nath , A. Middey, , S. Das and S. Chaudhuri, “Spatiotemporal trends in sunshine hours over India during three decades from 1988 to 2018,” *Scientific Reports (Nature),* vol. 15, no. n° 1, art. n° 432,, oct. 2025.

[66] T. Vo, L. Hu, L. Xue, and S. Chen,, “Trends in Cloud Covers across CONUS (1980–2020,” *J. Climate,* vol. 38, no. 19, pp. 5567-5584, oct. 2025.

[67] N. Faraj, V. Maruzzo, , I. Benesperi and N. Barbero, “Solar power at new heights: comparing photovoltaic performance across altitudes,” *Solar Energy,* vol. 305, p. 114256, feb. 2026.

[68] F. Kanyako, J. Lamontagne, E. Baker, S. Turner and Wild, “Seasonality and trade in hydro-heavy electricity markets: A case study with the West Africa Power Pool,” *Applied Energy,* vol. 329, no. 120214, 2023.

[69] D. Lusamba Yangindu, M. Sumbwanyambe, E. Phuku Phuati, J.-M. Tshitenge Mbuebue and M. Seke Vangu, “Correlation Between Sunshine Durationand Climatic Variables in the Democratic Republic of Congo,” in *2024 IEEE PES/IAS PowerAfrica Conference*, Johannesburg, 2024.

[70] Mathcracker, “Calculateur en ligne,” Mathcracker, 2023. [Online]. Available: https://mathcracker.com/fr/calculateur-intervalle-confiance-coefficient-correlation#results. [Accessed 23 january 2023].

[71] P. Cornillon and E. Matzner-Lober,, Regression. Théores et application, Paris: Springer-Verlag France, 2007, pp. 9-11.

[72] R. Urraca, A. M. Gracia-Amillo and et al., “Quality control of global solar radiation data with satellite-based products,” *Solar Energy,* vol. 158, pp. 49-62, 2017.

[73] M. T. Zateroglu, “Evaluating the Sunshine Duration Characteristics in Association with Other Climate variables,” *European Journal of Science and Technology,* vol. 29, pp. 200-207, 2021.

[74] Papachristopoulou, Kyriakoula; and et al., “Effects of clouds and aerosols on downwelling surface solar irradiance nowcasting and short-term forecasting,” *Atmospheric Measures Techniques,* vol. 17, no. 7, pp. 1851-1877, 2024.

[75] S. Zhang and X. Wang, “Influence of Clouds and Aerosols on Solar Irradiance and Application of Climate Indices in its Monthly Forecast over China,” *Atmosphere,* vol. 16, no. 730, june 2025.

[76] S. Qin, Z. Liu, R. Qiu, Y. Luo, J. Wu, B. Zhang, L. Wu and E. Agathokleous, “Short-termglobal solar radiationforecastingbased on an improved method for sunshine duration prediction and public weather forecasts,” *Appplied Energy,* vol. 343, no. S030626192300569X, 2023.

[77] Y. Gebreyohannes, M. Bayray and J. Lauwaert, “Comparative study of solar radiationestimation models based on sunshine durationand irradiancemeasurements in the Tigray Region, Ethiopian,” *Energy and ClimateModeling Exchange,* 2026.

[78] J. Sun, Y. Li, H. Hu, Q. Li, C. Ye, Y. Shi and Z. Chen, “Impact of cloud vertical structure pertubations on the retrieval of cloud optical thickness and effective radius from FY-4A/AGRI,” *Atmospheric Chemistry and Physics,* vol. 25, pp. 16347-16361, 2025.

[79] S. Kothe, U. Pfeifroth , R. Cremer and . J. a. Trentmann, “A Satellite-Based Sunshine Duration Climate Data Record for Europe and Africa,” *Remote Sensing,* 2018.

[80] D. Lusamba Yangindu, M. Sumbwanyambe, E. Phuku Phuati and J.-M. Tshitenge Mbuebue, “Modeling the Solar irradiance of Democratic Republic of Congo by Sunshine Duration,” *in Proceedings of the 2024 IEEE PES/IAS PowerAfrica Conference (PowerAfrica),* Oct. 2024.

[81] U. M. Monteith J., Principle of Environmental physics, Burlington: Academic Press, 2010.

[82] P. J. Asilevi, E. Quansah and a. et., “Modeling the spatial distribution of Global Solar Radiation (GSR) over Ghna using the Ängström-Prescott sushine duraion model,” *Scientific African,* vol. 4, no. e00094, pp. 1-12, 2019.

[83] A. A. Akpabio and S. E. Etuk, “Empirical relations for the determination of solar radiation in Ibadan, Nigeria,” *Solar Energy,* vol. 31, no. 1, pp. 87-94, 1983.

[84] Gueymard C., “Critical analysis and performance assessment of clear sky solar irradiance models using theoretical and measured data,” *Solar Energy,* vol. 51, no. 2, pp. 121-138, 1993.

[85] M. L. L. Gava, S. M. Costa and A. C. Porfirio, “Daily satellite-based sunshine duration estimates over Brazil:validation and intercomparison,” *Article,* vol. 16, no. 21, 2023.

[86] Earthscan, Planning and installing photovoltaic systems: a guide for installers, architects and engineers, vol. 2nd éd., Deutsche Gesellschaft fur Sonnenergie (DSG), 2012, pp. 5-12.

[87] P. Kenny, J. A. Olley and J. O. Lewis, “Whole-Sky Luminance Maps from Calibrated Digital Photography,” in *Eurosun 2006*, Glasgow, Scotland, 2006.

[88] ANAPI, Agence Nationale pour la Promotion des Investissements, “Energie,” 10 june 2020. [Online]. Available: https://www.investindrc.cd/fr/Energie. [Accessed 10 june 2020].

[89] UN Environment Programme - UNEP, “Les energies renouvelbles en RDC,” November 2011. [Online]. Available: https://postconflict.unep.ch/publications/UNEP_DRC_renewable_energy_FR.pdf. [Accessed 24 April 2019].

[90] SNEL, “Etat des lieux du secteur d'énernergie,” Commission Nationale d'Energie, Kinshasa,, 2005.

[91] PNUD, *Stratégie-cadre national Redd+ de la République démocratique du Congo,* Kinshasa, 2013.

[92] Yassine S., “Modélisation du rayonnement solaire sur quelques sites aglériens,” Dépôt Institutionnel de l'Université Ferhat ABBAS - Sétif 1, 16 April 2018. [Online]. Available: http://dspace.univ-setif.dz:8888/jspui/handle/123456789/1283. [Accessed 17 july 2021].

[93] Nyembo Kitungwa E., *Etat des lieux de l'offre et de la demande en énergie et cadre lgal et institutionnel,* Kinshasa,: Secrétariat Général à l"énergie,, 2011.

[94] Voyant C., *La simulation numérique: de la prévision solaire aux sciences du vivant,* Corse: Université de Corse Pascal Paoli, 2019, pp. 43-48.

[95] Merino L., *Modélisation du rayonnement solaire pour la simulation thermique en milieu urbain,* Compiègne: Université de Technologie de compiègne, 2013, pp. 5-40.

[96] Kandirmaz H.M. and Kaba K., “Estimation of Daily Sunshine Duration from Terra and Aqua,” *Advances in Meteorology,* vol. 2014, no. ID 613267, p. 9, 2014.

[97] Grenier D., *Electromagnétisme et transmission des ondes,* Laval: Univrsité de Laval, 2019.

[98] Abdoula F.M., “Calculating the variations of sunrise, sunset and day length times for Baghdad city.With comparison to different regions of the world in year 2019,” *Iraqi journal of sciences,* vol. 60, no. 12, pp. 2732-2741, 2019.

[99] Lecrenier P., “Les secrets du lac Kivu,” Université de Liège, 26 October 2012. [Online]. Available: https://www.reflexions.uliege.be/cms/e_340052/fr/les-secrets-du-lac-kivu. [Accessed 02 February 2022].

[100] Littelefair P., “A comparison of sky luminance models with measured data from Garston, United Kingdom,” *Solar Energy,* vol. 53, no. 4, pp. 315-322, 1994.

[101] Compagnon R., “Solar and daylight availability in the urban fabric,” *Energy and Buildings,* vol. 36, no. 4, pp. 321-328, 2004.

[102] Tregenza P.R., “Measured and calculated frequency distributions of daylight illuminance,” *Lighting Research and Technology,* vol. 19, no. 1, pp. 13-14, 1987.

[103] D. M. K. S. A. F. Khan M. T., “Online Knowledge-Based Model for Big Data Topic Extraction,” *Computational Intelligence and Neuroscience,* vol. 2016, no. ID 6081804, p. 10 pages, 2016.

[104] Angel JK., “Variation in United States Cloudiness and Sunshine Duration between 1950 and the Drought Year of 1988,” *Journal of climate,* vol. 3, no. 2, pp. 296-308, 1990.

[105] Matuszko D., “Influence of cloudiness on sunshine duration,” *International Journal of Climatology,* vol. 32, no. 2012, pp. 1527-1536, 3 june 2011.

[106] University of Liege, “correlation de Pearson,” University f Liege, [Online]. Available: http://www.biostat.ulg.ac.be/pages/Site_r/corr_pearson.html. [Accessed 14 january 2023].

[107] OpenStreetMap Foundation contributors, “Takedown procedure,” OpenStreetMap Foundation, ., 3 August 2022. [Online]. Available: https://wiki.osmfoundation.org/w/index.php?title=Takedown_procedure&oldid=9649. [Accessed 27 january 2023].

[108] L. Liu, C. Zhan, S. Hu and Y. Dong, “Vegetation change and its topographic effects in the karst mountainous areas of Guizhou and,” *Geographical Research,* vol. 37, no. 12, pp. 2433-2446, 2018.

[109] E. a. M. E. K.S., “On the Relation Between Cloud Cover Amount and Sunshine Duration,” *Meteorology and Atmospheric Physics,* vol. 87, no. 4, pp. 235-240, 2004.

[110] Matuszko D., “Influence of cloudiness on sunshine duration,” *International Journal of Climatology,* vol. 32, no. 10, pp. 1527-1536, 2012.

[111] Gueymard C., “Critical analysis and performance assessment of clear sky solar irradiance models using theoretical and measured data,,” *Énergie solaire,* vol. 51, no. 2, pp. 121-138, 1993.

[112] W. Schuepp, “Enregistrement séparés des composants du rayonnement solaire,” *Météo, Congo,* no. 8, 1952.

[113] Z. Bounoua and L. Ouazzani Chahidi, “Estimation of daily global solar radiation using empirical and machine-jearning methods. A case study of five Moroccan locations,” *Sustainable Materrials and Technologies,* vol. 28, no. e00261, 2021.

[114] D. Zhu, , Q. Yang, , K. KXiong, and H. Xiao, “Spatiotemporal Variations in Daytime and Night-Time Precipitation on the Yunnan–Guizhou Plateau from 1960 to 2017,” *Atmosphere,* vol. 13, no. 3, p. 445, 2022.

[115] D. Coster, , H. H. Schuepp and N. Van Elst N., “Le rayonnement sur les plans verticaux à Léopoldville, période 1953-1962,” *Inst.; Roy. Mét.,Mem. Acad. Roy. Sci. d'Outre-Mer Cl. Sc.Nat. et Med.,* vol. II, no. 1, 1954.

[116] S. Robaa,, “Evaluation of Sunshine Duration From Cloud Data in Egypt,” *Energy,* vol. 33, no. 5, pp. 785-795, 2008.

[117] J. J. Fan, , L. Wu, , F. Zhang, and e. al., “Empirical and machine learning models for predicting daily global solar radiation from sunshine duration: A review and case study in China,” *Renewable and Sustainable Energy Reviews,* Vols. 100,, pp. 186–212,, 2019.

[118] C. Paoli, C. Voyant, M. Muselli and M. Nivet, “Solar Radiation Forecasting Using Ad-Hoc Time Series Preprocessing and Neural Networks,” *Agroc. For. Meterol.,* vol. 33, pp. 109-128, 1984.

[119] C. Rigollier , O. Bauer and L. Wald , “On the sky model of the ESRA-European Radiation Atlas-with respect to the Heliosat method,” *Solar Energy,* vol. 68, no. 1, pp. 33-48, 2000.

[120] P. Moon and D. E. Spencer , “Illumination from non-uniform sky,” *Illuminating Engineering,* vol. 37, no. 10, pp. 707-726, 1942.

[121] L. Belila , A. Cesarano , F. Minichiello and Sibilio , “Videography for sky luminance distribution measurement,” *Lighting Research and Technology,* vol. 29, no. 1, pp. 40-46, 1997.

[122] Steven M.D. and Unsworth M.H., “The diffuse solar irradiance of slopes unde cloudless skies,” *Quartely Journal Royal Meteorological Society,* vol. 1979, no. 105, pp. 593-602, 1979.

[123] ECMWF, “Climate-data,” [Online]. Available: https://fr/climate-data.org. [Accessed 16 june 2021].

[124] J.-P. Descy, F. Darchambeau and M. Schmid , Lake Kivu: Limnology and biogeochemistry of a tropical great lake, Dordrecht: Springer, 2012, p. 190.

[125] J. A. Duffie and W. A. Beckman , Solar Engineering of ThermalProcesses, 2nd edition ed., Ne York: John Wiley & Sons, 1991.

[126] H. Harry Suehrcke , R. Bowden and K. Hollands, “Relationship between sunshine duration and solar radiation,” *Solar Energy,* vol. 92, pp. 160-171, 2013.

[127] C.-A. André and M.-L. Eric , Régression : Théorie et applications, France: Spring-Verlag, 2007, pp. 15-16,33-44,82-97.

[128] C. Paoli, C. Voyant, M. Muselli and M. Nivet, “Solar radiation forecasting using ad hoc tie series preprocessing and neural networks,” in *Conférence internationale sur l'informatique intelligente*, 2009.

[129] F. Hütz-Adams and G. Sarah, *Energie hydraulique des barrages d'Inga, grands potentiels pour le développement de la RDC et de l'Afrique,* Siegburg: Institut für Ökonomie und Ökumene, 2004.

[130] K. Bartoszek , D. Matuszko and J. Soroka , “Relationships between cloudiness, aerosol optical thickness, and sunshine,” *Atmospheric Research,* vol. 245, no. 105097, p. 13 pages, 2020.

[131] C. Tang, Y. Zung, Y. Wei, F. Zhao and X. Wu, “Spatiotemporal Characteristics and Influencing Factors of Sushine duration in Chna from 1970 to 2019,” *Atmosphere,* vol. 13, no. 2015, pp. 1-15, 2022.

[132] M. Mozafari,, Z. Hosseini, E. Fijani, and R. Eskandari,, “Effects of climate change and human activity on lake drying in Bakhtegan Basin, southwest Iran,” *Sustain. Water Resour. Manag,* vol. 8, no. 109, 2022.

[133] G. Gröger, T. H. Kolbe, A. Czerwinski and C. Nagel, “OpenGIS ® City Geography Markup,” *Encoding Standard (OGC 08-007r1),* vol. 243, 2008.

[134] L. Ikua and E. Hostaux , “Données du rayonnement solaire à Léopoldville, période 1953-1962,” *Inst. Roy. Mét.,* vol. Série A, no. 53, 1965.

[135] H. Ögelman , A. Ecevit and E. Tasdemiroğlu , “A new method for estimating solar radiation from bright sunshine data,” *Solar energy,* vol. 33, no. 6, pp. 619-625, 1984.

[136] ADPI-RDC, Agence de Développement et de Promotion du Projet Inga, *Grand Inga, Evolution,* Kinshasa, 2022, pp. 17-18.

APPENDIX A:

BANDUNDU-SPECIFIC SOLAR DATA RESULTS

Appendix A.1 Kwango District

Table A.1 presents the MASD for Kwango District, highlighting the seasonal variability between dry and rainy season.

Table A.1: Monthly averages SD for Kwango District (h/day)

Cities/Towns	Feshi	Kahemba	Kasongo-Lunda	Kenge	Popokabaka	Weighted Averages
January	6.5	6.5	6.2	6.4	6.5	6.4
February	6.5	6.5	6.4	6.5	6.5	6.5
March	6.2	6.0	6.0	6.4	6.5	6.2
April	5.7	5.9	4.9	5.6	5.3	5.5
May	6.5	7.4	6.5	5.9	6.0	6.5
June	7.6	7.7	7.7	7.3	7.3	7.6
July	7.8	7.9	7.9	7.7	7.7	7.8
August	7.3	7.6	7.6	7.1	7.3	7.4
September	5.9	6.3	6.8	6.5	6.5	6.4
October	5.1	5.3	5.6	5.6	5.8	5.5
November	5.1	5.0	5.2	5.6	5.7	5.3
December	5.9	5.9	5.6	5.9	6.0	5.8
Yearly average	6.3	6.5	6.4	6.4	6.4	6.4

Source: Compiled from [14].

Figure A.1 illustrates the temporal evolution of monthly SD across the Kwango District.

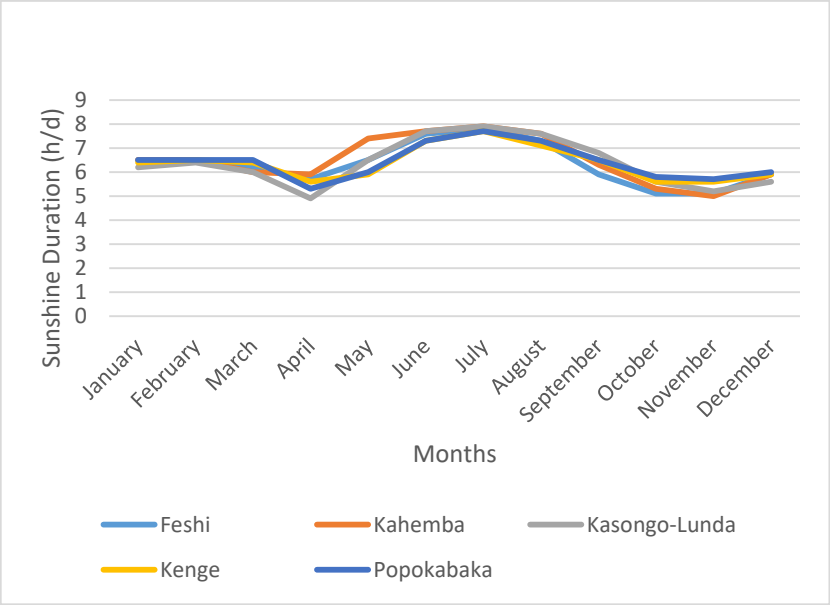

Figure A.1: *Temporel Trend of Monthly SD in the Kwango District*

The figure highlights the clear seasonal pattern of SD, characterized by a progressive increase toward a peak in July, followed by a decline toward the end of the year. The consistency of the curves across territories confirms the strong regional coherence of solar availability. Notably, the observed maximum during the dry season contrasts with purely astronomical expectations, emphasizing the dominant role of cloud cover in controlling SD variability.

Key Observations:

- The annual mean SD in Kwango is 6.4 h/day.
- Maximum SD occurs in July, peaking in all territories.
- Kahemba has the highest average SD (6.5 h/day), while Feshi has the lowest (6.3 h/day).
- The observed SD pattern contrasts with theoretical SD, which predicts minimum sunshine in June–August due to cloud cover.

Appendix A.2 Kwilu District

City and territories analyzed: Bandundu, Bagata, Bulungu, Gungu, Idiofa, Masi-Manimba. Table A.2 summarizes the monthly averages of SD for the main cities and territories of Kwilu District.

Table A.2: Monthly averages SD for District of Kwilu (h/day)

Cities/Towns	Bagata	Bandundu	Bulungu	Gungu	Idiofa	Masi-Manimba
January	6,2	6,2	6,2	6,6	6,2	6,5
February	6,2	6,2	6,2	6,6	6,3	6,4
March	5,9	6,1	5,9	6,3	5,9	6,2
April	5,2	5,3	5,3	5,7	5,6	5,6
May	5,3	5,5	5,4	6,4	5,9	5,6
June	7	6,9	7,1	7,5	7,1	7,2
July	7,4	7,2	7,5	7,7	7,5	7,7
August	6,8	6,8	6,9	7	6,7	7,1
September	6,2	6,3	5,9	5,8	5,6	6,2
October	5,5	5,7	5,2	5,3	5,1	5,4
November	5,3	5,6	5,2	5,5	5,3	5,5
December	5,6	5,6	5,6	6,2	5,7	5,9

Source: Compiled from [14]

The data reveal an annual mean SD of approximately 6.1 h/day, slightly lower than that of Kwango District. Seasonal fluctuations remain evident, with minimum values observed during the peak rainy months. The relatively small differences between localities indicate a spatially homogeneous distribution of sunshine duration within the district. The corresponding curves are shown in the figure A.2.

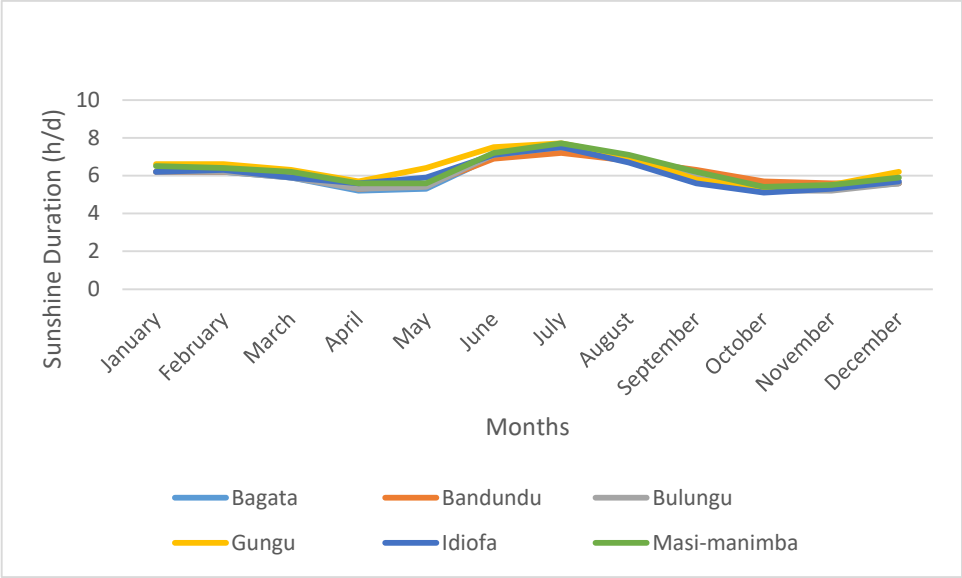

Figure A.2: Temporel Trend of Monthly SD in the Kwilu District

The graphical representation clearly emphasizes the seasonal dynamics of SD, with a pronounced peak in July and a marked during October–November. Compared to the tabular data, the figure better captures the smooth temporal transitions and confirms the dominant influence of seasonal cloud cover patterns over astronomical factors.

A. Analytical Observations

The annual mean SD in Kwilu District is approximately 6.1 h/day, which is slightly lower than that recorded in Kwango (6.4 h/day). Although the difference remains moderate, it reflects a real spatial variability linked to localized cloud cover patterns and rainfall distribution.

The maximum SD values are systematically observed in July, corresponding to the peak of the dry season. During this period, the reduction in atmospheric humidity and cloud density significantly enhances solar availability. In contrast, the lowest SD values occur mainly in October and November, which coincide with intensified rainfall and increased nebulosity.

At the territorial level, Gungu and Masi-Manimba present relatively higher SD values, while Bulungu and Idiofa tend to record lower averages. Nevertheless, the observed differences between territories remain limited, suggesting that Kwilu District is characterized by a relatively homogeneous solar regime at the district scale.

From a theoretical perspective, astronomical SD would normally indicate seasonal variations due to solar declination. However, the observed distribution of SD clearly shows that

cloud cover exerts a stronger control than astronomical factors in shaping seasonal variability within this equatorial context.

Appendix A.3 Maï-Ndombe

Territories analtzed: Bolobo, Inongo, Kutu, Kwamouth, Mushie et Yumbi. Table A.3 presents the monthly sunshine duration values for the main territories of Maï-Ndombe District, along with their geographical characteristics and weighted averages.

Table 3.3.: Monthly Averages SD for Maï-Ndombe District (h/day)

Latitude (°)	2°09'S	1°55'39"S	2°43'S	3°10'S	3°01'S	1°54'S	Weighted averages (h/d)
Longitude	16°14'E	18°17'08"E	18°05'E	16°12'E	16°55'E	16°34'E	
Area (Km²)	4 056	24 149	18 674	14 552	11 860	2 549	
Cities/Towns	Bolobo	Inongo	Kutu	Kwamouth	Mushie	Yumbi	
January	6.6	6.9	6.2	6.0	6.4	6.6	6.5
February	6.6	6.8	6.1	6.1	6.4	6.6	6.4
March	6.5	6.5	5.8	6.0	6.2	6.5	6.2
April	5.9	6.1	5.2	5.5	5.6	5.9	5.6
May	6.0	6.4	5.3	5.6	5.7	5.9	5.9
June	6.8	7.1	6.5	6.7	6.9	6.8	6.8
July	6.9	7.3	6.8	6.8	7.1	6.9	7.0
August	6.3	6.8	6.3	6.2	6.5	6.4	6.5
September	6.2	6.4	5.8	5.9	6.2	6.2	6.1
October	5.9	6.3	5.4	5.3	5.6	5.9	5.8
November	5.8	6.3	5.3	5.3	5.6	5.9	5.7
December	6.0	6.4	5.6	5.5	5.8	6.1	5.9
Anual	6.3	6.6	5.9	5.9	6.2	6.3	6.2

The results indicate an annual mean SD of approximately 6.2 h/day, positioning Maï-Ndombe between Kwango and Kwilu. The data also reveal moderate spatial variability between territories, with slightly higher values observed in Inongo and lower values in Kutu and Kwamouth. This suggests the influence of localized environmental factors such as vegetation cover and proximity to water bodies.

Figure A.3 shows the temporal trend of monthly sunshine duration in Maï-Ndombe District.

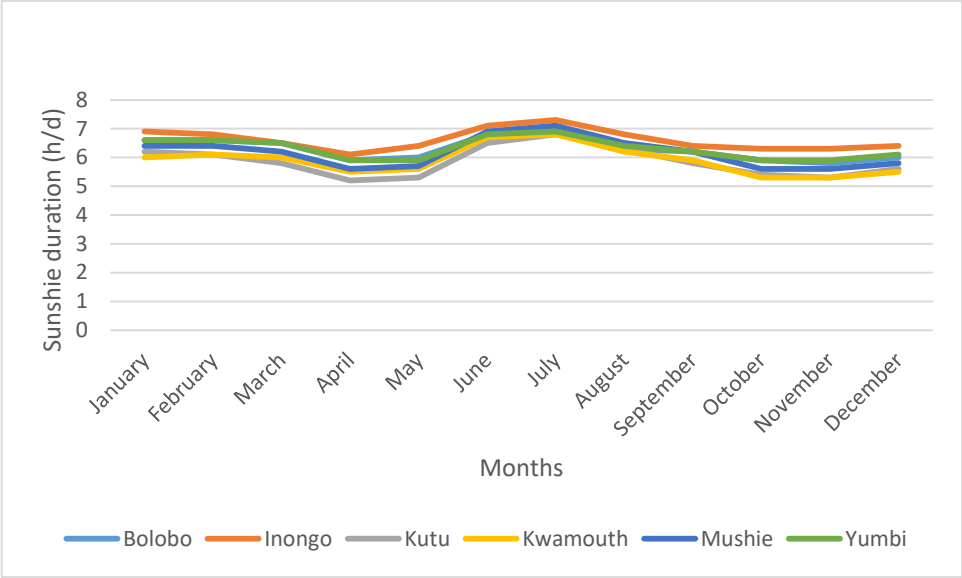

Figure A.3: Temporal Trend of Monthly SD in the Maï-Ndombe District

The figure confirms a relatively stable seasonal pattern, with a peak in July and lower values during the rainy season. The limited amplitude of variation reflects the equatorial context, where seasonal contrasts are primarily driven by atmospheric conditions rather than solar geometry.

A. Analytical Observations

The annual mean SD in Maï-Ndombe District is approximately 6.2 h/day, positioning it between Kwango and Kwilu. This intermediate value can be explained by its geographical location within the central basin, where forest cover and atmospheric humidity remain relatively significant.

The highest monthly SD is recorded in July, while the lowest values are generally observed in October and November, in direct correspondence with peak rainfall periods. The seasonal amplitude remains moderate, which confirms the limited astronomical variation associated with equatorial latitudes.

Among the territories, Inongo records the highest annual average (≈6.6 h/day), whereas Kutu and Kwamouth show comparatively lower averages (≈5.9 h/day). These variations may be attributed to microclimatic factors, including proximity to water bodies, vegetation density, and local atmospheric circulation patterns.

Overall, the SD regime in Maï-Ndombe confirms that cloudiness, rather than latitude, constitutes the dominant controlling factor of solar availability within the province.

APPENDIX B:

EQUATEUR-SPECIFIC SOLAR DATA RESULTS

8.1 Appendix B.1 Equateur District

SD data analysis was conducted for the city of Mbandaka and the territories of Basankusu, Bikoro, Lukolela, and Makanza. Table B.1 presents the monthly averages of SD for the main localities of Equateur District, together with their weighted averages.

Table B.1: Monthly SD in the Equateur District

Latitude	1°14'N	0°45'S	1°04'S	1°36'N	0°02'52"N	Weighted averages
Longitude	19°47'E	18°°7'E	17°12'E	17°09'E	18°15'21"E	
Area (Km²)	21 239	13 274	17 952	7 570	460	
Cities/Towns	Basankusu	Bikoro	Lukolela	Makanza	Mbandaka	(h/d)
January	6.9	6.7	6.4	7.1	6.4	6.6
February	6.6	6.5	6.2	6.7	6.5	6.4
March	6.2	6.2	5.9	6.5	6.3	6.1
April	5.5	5.8	5.5	5.8	5.6	5.7
May	5.3	5.7	5.4	5.6	5.9	5.5
June	5.6	6.5	6.2	5.7	7.3	6.2
July	5.4	6.6	6.5	5.6	7.7	6.4
August	5.0	6.1	6.1	5.3	7.2	6.0
September	4.9	5.7	5.6	5.2	6.4	5.6
October	4.7	5.8	5.6	5.0	5.5	5.5
November	4.7	5.6	5.4	5.0	5.5	5.4
December	5.9	6.2	5.8	6.2	5.9	6.0
Averages	5.5	6.1	5.9	5.8	6.4	6.0

The tabulated data indicate a moderate annual SD level, with a weighted average of approximately 6.0 h/day. A relatively limited spatial dispersion is observed between localities, although Mbandaka exhibits slightly higher values. The seasonal structure remains evident, with a gradual decrease from the beginning of the year toward a minimum during the peak rainy season.

Figure B.1 illustrates the temporal evolution of monthly sunshine duration in Equateur District.

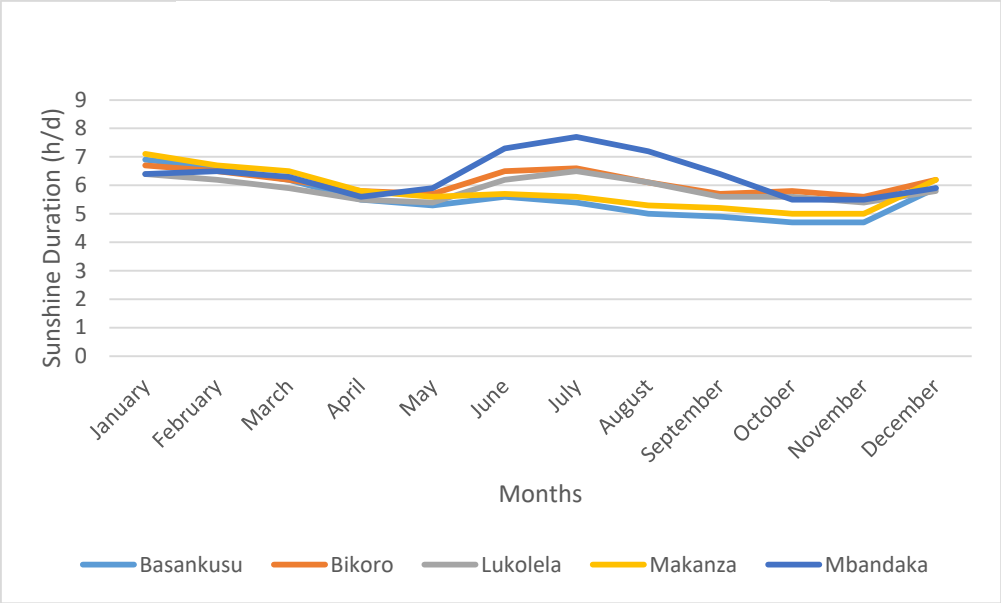

Figure B.1: Temporal Trend of monthly SD in the Equateur District

The figure B.11 highlights a smooth and coherent seasonal pattern, with a peak occurring around mid-year and a decline toward October–November. Compared to the tabular data, the graphical representation emphasizes the temporal continuity of SD variations and confirms the dominant role of cloud cover in shaping solar availability in this equatorial environment

A. Analytical Observations

The weighted annual mean SD for Equateur District is 6.0 h/day. Seasonally, SD values increase during the middle of the year, with a clear maximum reached in July, corresponding to the dry season period. June and August also exhibit relatively high values. Conversely, lower SD values are observed between September and November, in direct relation to increased cloud cover and rainfall activity. At the territorial level, Mbandaka records the highest annual mean SD (6.4 h/day), while Basankusu presents the lowest value (5.5 h/day). The inter-territorial range remains moderate, suggesting a relatively coherent solar regime within the district. The observed seasonal profile could be explained by cloud dynamics, which constitute the dominant regulating factor of sunshine availability in this equatorial environment, overriding purely astronomical considerations.

Appendix B.2 Mongala District

The analysis covers the city of Lisala and the territories of Bumba and Bongandanga. Table B.2 presents the monthly averages of sunshine duration for the main territories of Mongala District

Table B.2: Monthly Averages of SD for Mongala District

Latitude	1°31'N	2°10'N	2°09'N	Weighted averages (h/d)
Longitude	21°00^{E}	22°32'E	21°31'E	
Area (Km²)	33 912	15 598	14 733	
Cities/Towns	Bongandan.	Bumba	Lisala	
January	6.9	7.1	7.1	7.0
February	6.6	6.8	6.7	6.7
March	6.2	6.4	6.4	6.3
April	5.6	5.8	5.8	5.7
May	5.2	5.6	5.6	5.4
June	5.5	5.6	5.6	5.6
July	5.6	5.6	5.7	5.6
August	5.0	5.3	5.2	5.1
September	4.9	5.2	5.1	5.0
October	4.7	4.9	4.9	4.8
November	4.7	4.7	4.8	4.7
December	6.0	6.2	6.2	6.1
Averages	5.6	5.8	5.8	5.7

Source: Compiled from [15]

The data reveal a relatively lower annual SD (≈5.7 h/day) compared to other districts of the province. The spatial variability remains weak, suggesting a uniform solar regime. However, a more pronounced during the last quarter of the year indicates a stronger influence of seasonal atmospheric conditions.

Figure B.2 shows the temporal variation of monthly sunshine duration in Mongala District.

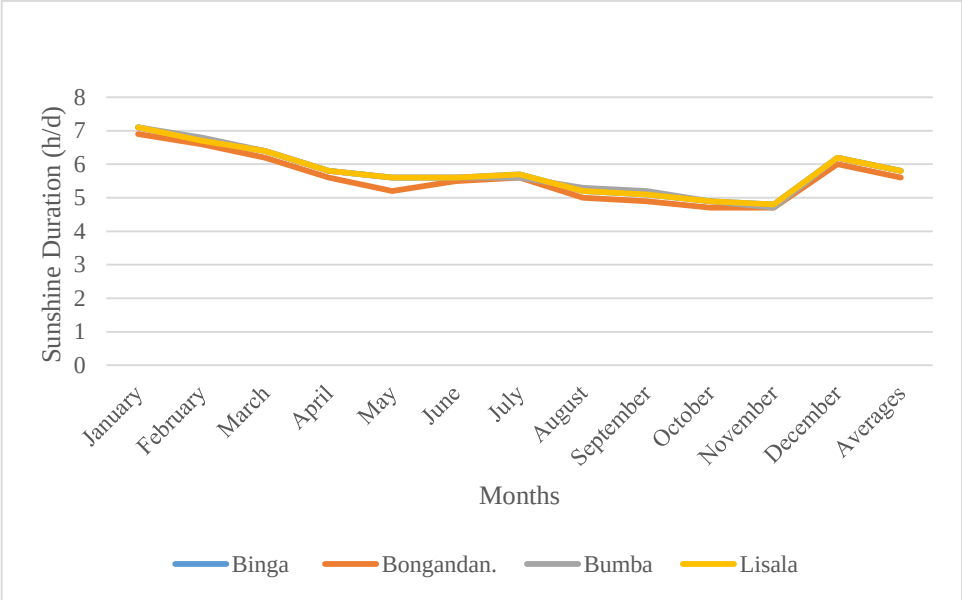

Figure B.2: Temporal Trend of Monthly SD in the Mongala District

The figure clearly illustrates a progressive decline in SD from the beginning of the year toward a minimum in November, followed by a recovery in December. This asymmetric seasonal pattern reflects the persistence of cloud cover during the extended rainy period.

A. Analytical Observations

The annual weighted mean SD for Mongala District is approximately 5.7 h/day, which is slightly lower than that of Equateur District. SD remains above 6.0 h/day during the first quarter of the year, then progressively decreases, reaching a minimum of 4.7 h/day in November. The seasonal amplitude is therefore more pronounced compared to Equateur District. However, among the territories, Bongandanga receives the lowest annual average sunshine (5.6 h/day), while Bumba and Lisala both exhibit higher values (5.8 h/day).

The seasonal decline toward October–November is clearly associated with intensified rainfall and cloud density. Once again, atmospheric conditions dominate over astronomical factors in shaping the SD profile. The Mongala's SD is practically uniform anywhere. It's above 6.0h/d during the first quarter of the year, then bottomed out at 4.7h/d in November. In general, the territory of Bongandanga receives the least sunlight throughout the year, with an yearly mean of daily SD equal to 5.6h while the territories of Bumba and Lisala exhibit an average annual daily sunshine duration of 5.8h.

Appendix B.3: Nord Ubangi District

Data analysis was carried out for the City of Gbadolite and the territories of Bosobolo, Businga and Yakoma . Table B.3 summarizes the monthly SD values for selected territories of Nord-Ubangi District.

Table B.3.: Monthly Averages of SD for Nord Ubangi District

Latitude	4°11'N	3°21'N	4°14'42"N	3°52'32"	Weighted average of SD(h/d)
Longitude	19°53'E	20°53^{E}	20°54'51"E	22°18'01"	
Area (Km²)	13 277	17 441	278	15 397	
Cities/Towns	Bosobolo	Businga	Gbadolite	Yakoma	
January	7.7	7.3	7.7	7.6	7.5
February	7.4	6.9	7.4	7.3	7.2
March	7.2	6.5	7.1	6.8	6.8
April	6.8	5.9	6.5	6.2	6.3
May	6.5	5.6	6.2	5.8	5.9
June	6.6	5.7	6.3	5.8	6.0
July	6.5	5.7	6.2	5.7	5.9
August	5.9	5.1	5.6	5.1	5.3
September	5.6	4.9	5.4	5.0	5.1
October	5.6	4.6	5.2	4.5	4.9
November	6.0	4.9	5.8	5.2	5.3
December	7.2	6.5	7.1	7.0	6.9
Averages (h/d)	6.6	5.8	6.4	6.0	6.1

Source: Compiled from [14].

The results indicate relatively high SD values, with an annual average of approximately 6.1 h/day. Compared to other districts, Nord-Ubangi exhibits higher sunshine levels during the first quarter of the year, suggesting a more favorable solar regime influenced by its northern geographical position.

Figure 3.15 presents the temporal trend of monthly sunshine duration in Nord-Ubangi District.

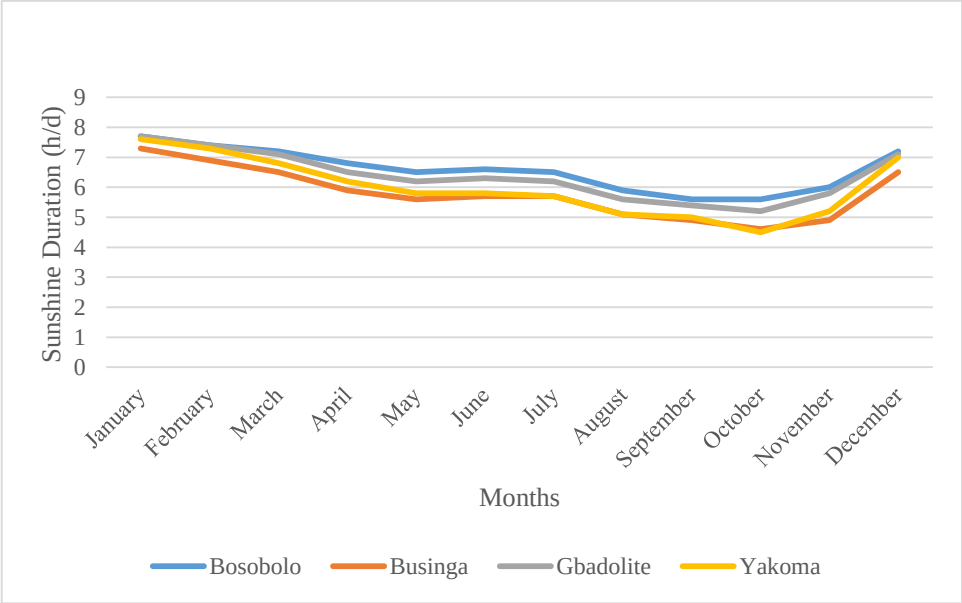

Figure 3.1: Temporal Trend of Monthly SD for Nord Ubangi District

The graphical trends reveal a marked seasonal gradient, with high SD values at the beginning and end of the year and a noticeable gradient during the mid-to-late rainy season. This pattern reflects a transition between equatorial and sub-equatorial climatic influences.

Analytical observations

Nord-Ubangi exhibits the highest annual weighted average SD among the four districts, estimated at 6.1 h/day. The highest monthly values are recorded in January (≈7.5 h/day), while the lowest occur in October (≈4.9 h/day). Unlike Equateur District, the maximum SD occurs at the beginning of the year rather than mid-year. At the territorial level, Bosobolo presents the highest annual average (6.6 h/day), while Businga records the lowest (5.8 h/day). This northward district, located farther from the equatorial forest core, benefits from relatively higher sunshine availability. The seasonal pattern still reflects rainfall-driven modulation

Appendix B. 4: Sud Ubangi

The analysis includes the city of Gemena and the territories of Kungu, Libenge, and Zongo. Table B.4 presents the monthly averages of SD for the main territories of Sud-Ubangi District.

Table B.4: Monthly averages of SD for Sud-Ubangi District

Latitude	3°15'N	2°47'09"N	3°39'N	4°20'36"N	Weighted Average of SD (h/d)
Longitude	19°47'E	19°12'19"E	18°38'E	18°35'34"E	
Area (Km²)	11,488	12,848	12,833	495	
Cities/Towns	Gemena	Kungu	Libenge	Zongo	
January	7.3	7.3	7.5	7.7	7.4
February	7.0	7.0	7.2	7.4	7.1
March	6.7	6.7	6.9	7.1	6.8
April	6.2	6.0	6.5	6.7	6.2
May	5.9	5.7	6.2	6.6	5.9
June	5.9	5.8	6.4	6.7	6.0
July	5.9	5.6	6.2	6.5	5.9
August	5.3	5.0	5.6	5.9	5.3
September	5.0	4.9	5.3	5.6	5.1
October	4.7	4.7	5.2	5.5	4.9
November	5.0	5.0	5.4	5.6	5.1
December	6.5	6.4	6.8	7.1	6.6
Averages	6.0	5.8	6.3	6.5	6.0

Source: Compiled from [14].

The annual mean SD is approximately 6.0 h/day, with moderate spatial variability between territories. Zongo exhibits relatively higher values, while Kungu records lower averages, indicating localized climatic influences within the district.

Figure B.4 illustrates the temporal evolution of monthly sunshine duration in Sud-Ubangi District.

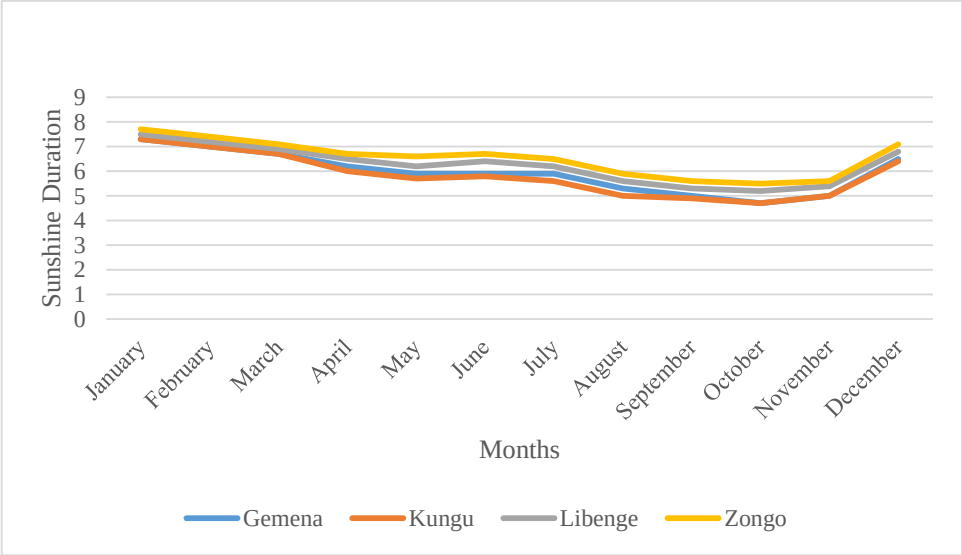

Figure B.4: Temporal Trend of Monthly SD for Sud Ubangi District

The figure B.4 shows a clear decreasing trend from January to November, followed by a recovery in December. This pattern suggests a strong seasonal control driven by rainfall intensity and cloud persistence, which significantly reduce solar availability during the late rainy season.

Analytical observations

The annual weighted average SD for Sud-Ubangi is 6.0 h/day. The SD decreases progressively from January to November, reaching its minimum before increasing again in December. The seasonal behavior is therefore relatively monotonic.

At the territorial level, Zongo records the highest annual average (6.5 h/day), while Kungu shows the lowest value (5.8 h/day).

The intra-district variability remains moderate, confirming spatial coherence of the solar regime. The average SD of Sud-Ubangi is 6.0h/d. The SD decreases continuously from January to November, when it reaches its low value before rising again in December. Zongo is exposed to the highest SD : 6.5h/d while Kungu shows the lowest in this province : 5.8h/d.

Appendix B.5: Tshuapa

The analysis includes the territories of Befale, Boende, Bokungu, Djolu, Ikela and Monkoto. Table B.5 presents the monthly averages of SD for these territories.

Table B.5: Monthly averages of SD for Tshuapa District

Area (Km²)	33 200	31 000	52 800	25 000	46 000	Weighted Average of
Cities/Towns	Befale	Bokungu	Boende	Djolu	Ikela	
January	6,6	6,2	6,4	6,6	6,4	6,2
February	6,5	6,1	6,2	6,3	6,2	5,9
March	6	5,7	5,9	6	5,9	5,6
April	5,2	5	5,1	5,3	5,1	4,9
May	5,1	5	5	5,1	5	5
June	5,6	5,8	5,7	5,6	5,9	6,1
July	5,8	6,2	6	5,8	6,2	6,5
August	5,2	5,3	5,4	5	5,6	5,7
September	5	5,2	5,1	5	5,3	5,4
October	4,8	4,9	5	4,8	5	5,1
November	4,6	4,7	4,7	4,6	4,8	4,8
December	5,7	5,3	5,4	5,7	5,4	5,2
Averages	5,5	5,5	5,5	5,5	5,6	5,5

Source: Compiled from [14].

Table B.5 highlights a remarkably homogeneous SD regime across the territories of Tshuapa, with annual averages tightly clustered around 5.5–5.6 h/day. The monthly distribution reveals a bimodal seasonal pattern:

— A primary maximum in January–February (~6.2–6.6 h/day),
— A secondary increase in June–July (~5.8–6.2 h/day),
— A pronounced minimum in October–November (~4.6–5.1 h/day).

This limited inter-territorial variability indicates a strong spatial coherence, suggesting that SD is predominantly controlled by large-scale atmospheric dynamics rather than local effects. The slight enhancement observed in Ikela (5.6 h/day) may reflect localized microclimatic advantages or reduced cloud persistence.

Figure B.5 illustrates the temporal evolution of monthly SD (h/day) in Tshuapa District.

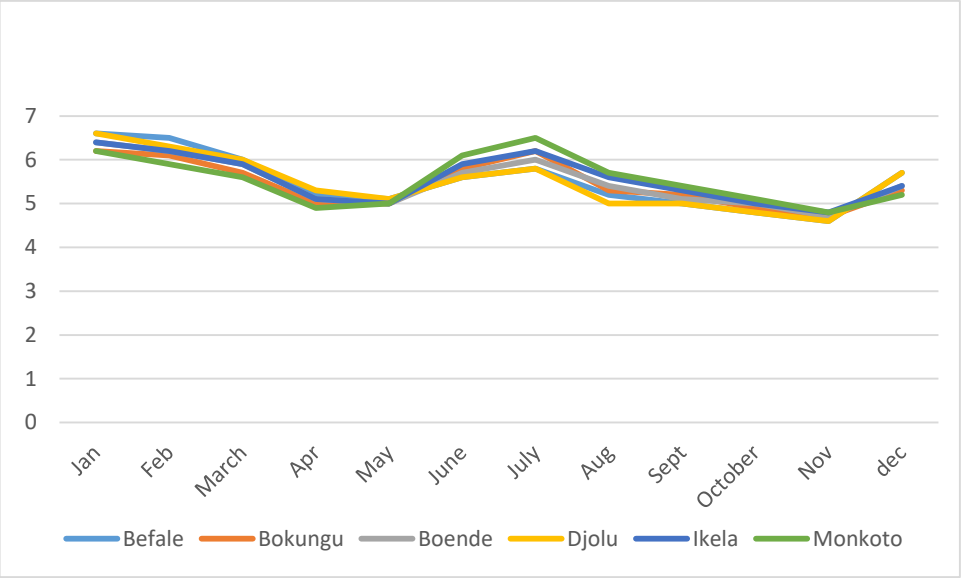

Figure B.5: Temporal Trend of Monthly SD for Tshuapa

Analytical observations

Figure 3.17 confirms and dynamically extends the results of Table 3.11 by illustrating the temporal structuring of SD variability across the annual cycle in Tshuapa. Unlike a monotonic interpretation, the curve clearly exhibits a nonlinear seasonal regime characterized by two distinct phases:

1. A progressive decline from the major peak in January toward a transitional minimum around April–May,
2. A secondary recovery phase in June–July, followed by a steady decrease toward the minimum in October–November, before a final rebound in December.

This temporal behavior suggests the influence of interacting atmospheric mechanisms, likely linked to the latitudinal migration of the ITCZ, and the seasonal modulation of cloud cover and convective activity.

APPENDIX C:

KASAÏ ORIENTAL-SPECIFIC SOLAR DATA RESULTS

Appendix C.1: Kasaï Oriental (New Province)

The analysis concerns the city of Mbuji-Mayi and the territories of Lupatapata and Tshilenge. Table C.1 provides the monthly sunshine duration averages for key locations in the Kasaï-Oriental province.

Table C.1: Monthly SD for Kasaï Oriental [4]

Latitude	6°08'13"S	6°10'39"	6°15'S	Weighted Average of SD
Longitude	23°35'23"E	23°32'E	23°46'E	
Area (Km²)	135	2 397	2 021	
City/Town	Mbuji-Mayi	Lupatapata	Tshilenge	
January	6.2	5.9	5.9	5.9
February	6.4	6.2	5.9	6.1
March	6.0	5.9	5.4	5.7
April	6.0	6.2	4.9	5.6
May	6.9	7.3	5.2	6.3
June	7.6	7.7	6.5	7.2
July	7.7	7.8	7.1	7.5
August	7.1	7.3	5.8	6.6
September	5.6	6.0	5.4	5.7
October	5.1	5.3	5.1	5.2
November	5.2	5.1	4.9	5.0
December	5.7	5.6	5.1	5.4
Averages	6.0	5.8	5.5	5.6

Source: Compiled from [14].

The results indicate a high degree of consistency between locations, with average SD values around 5.5–6.0 h/d. Seasonal variability remains pronounced, with peak values in June–July and minimum values in October–November, reflecting typical equatorial climatic dynamics.

Figure C.1 shows the monthly variation of sunshine duration across the studied locations in Kasaï-Oriental.

[4] In this context, Kasaï-oriental refers to the new province rather the former province bearing the same name.

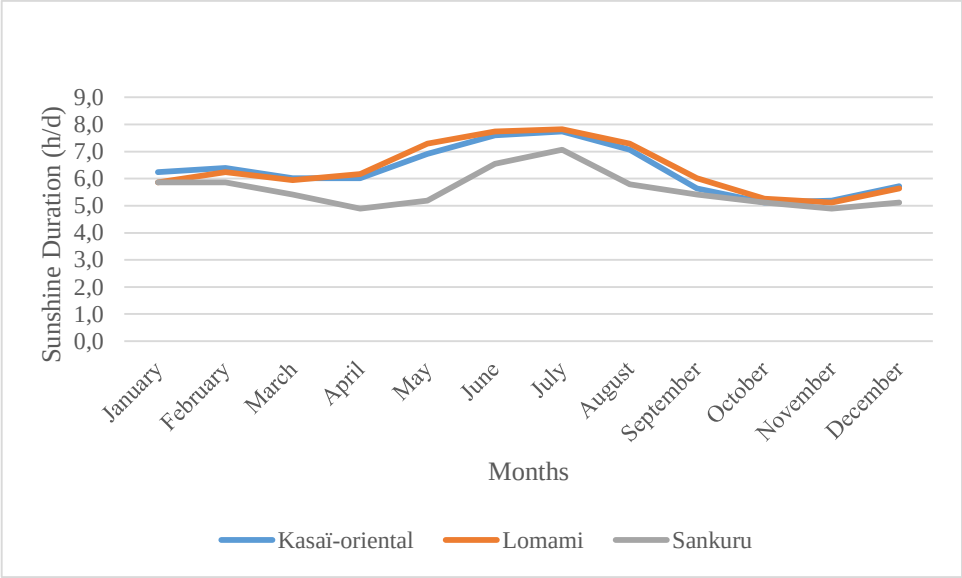

Figure C.1: Temporal Trend of Monthly SD for the (new) Kasaï-Oriental

The graphical representation confirms the uniformity observed in the tabulated data while emphasizing the smooth seasonal transitions. The alignment of curves suggests that spatial interpolation or regional modeling approaches are appropriate for this province.

Analytical Observations

— The annual weighted mean SD for the new Kasaï Oriental province is approximately 5.6 h/day.

— The maximum SD values are observed in June and July, with a peak of approximately 7.5 h/day.

— The minimum values occur in October and November, reaching approximately 5.0 h/day.

— Spatial variability between Mbuji-Mayi, Lupatapata and Tshilenge remains limited (range ≈0.5 h/day), suggesting a relatively homogeneous solar regime at this spatial scale.

The seasonal behavior follows a classical inter-tropical pattern: progressive increase toward the dry season peak (June–July), and sharp decrease during the rainy season (October–November). Astronomical factors alone cannot explain this amplitude; cloud cover and rainfall remain the dominant regulating variables.

Appendix C.2: Lomami Province (New-Province)

Data were analysed for the following territories : Kabinda, Ngandajika and Lubao. Table C.2 presents the monthly sunshine duration averages for selected cities in Lomami province.

Table C.2: Monthly SD for Lomami

Latitude	6°08'S	6°45'00"S	5°18'S	7°00'00"S	Weighted Average of SD
Longitude	24°29^{E}	23°58'01"E	25°43'E	23°46"E	
Area (Km²)	14 273	5 726	22 480	150	
City/Town	Kabinda	Ngandajika	Lubao	Mwene-Ditu	
January	6.0	6.2	5.6	6.2	5.8
February	6.2	6.4	6.3	6.3	6.3
March	5.9	6.0	5.9	5.9	5.9
April	6.1	6.2	6.2	6.2	6.2
May	7.2	7.4	7.4	7.4	7.3
June	7.7	7.7	7.7	7.7	7.7
July	7.8	7.8	7.8	7.8	7.8
August	7.1	7.3	7.4	7.4	7.3
September	5.8	6.0	6.1	6.1	6.0
October	5.2	5.3	5.3	5.3	5.2
November	5.0	5.3	5.2	5.2	5.1
December	5.5	5.7	5.7	5.7	5.6
Averages	6.3	6.4	6.4	6.4	6.4

Source: Compiled from [14].

The data exhibit very limited spatial dispersion, with nearly identical SD values across all locations (≈6.3–6.4 h/d annually). This indicates a highly uniform solar regime, making Lomami particularly suitable for generalized solar modeling without significant loss of accuracy.

Figure C.2 depicts the temporal evolution of sunshine duration in Lomami province.

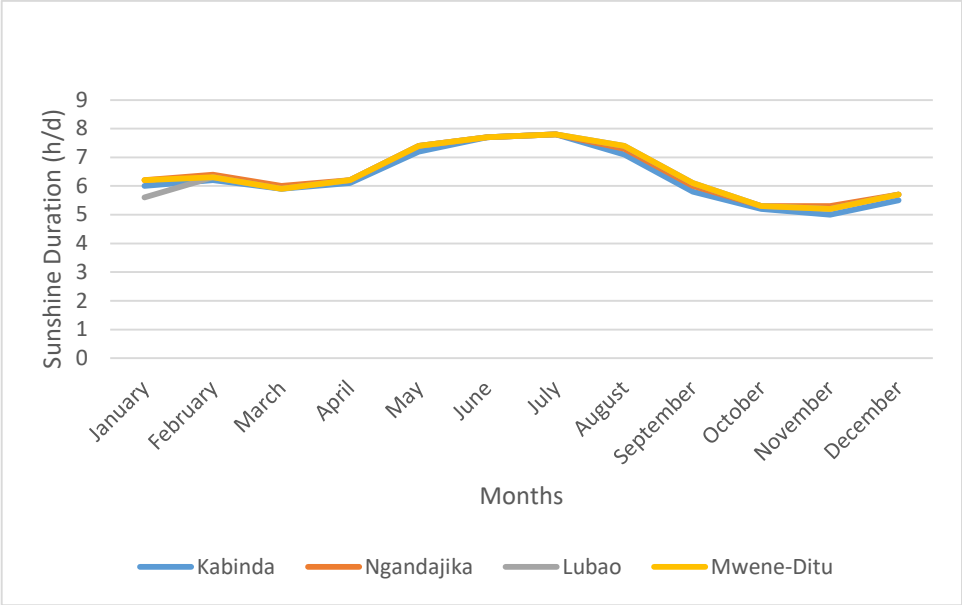

Figure C.2: Trend of monthly average of SD for Lomami (New province)

The near-perfect overlap of the curves further confirms the spatial homogeneity of SD. This strengthens the validity of using aggregated datasets and supports the robustness of regression-based solar radiation models in the Lomami province.

Analytical observations

- It is noticed that Lomami exhibits a higher annual mean SD compared to Kasaï Oriental, with a weighted average of approximately 6.4 h/day.
- The peak SD is consistently recorded in July (≈7.8 h/day), while the minimum is observed in November (≈5.1 h/day).
- One of the most striking characteristics of Lomami is the remarkable uniformity of SD across territories. The inter-territorial differences are almost negligible, indicating a stable regional solar regime.
- The seasonal amplitude remains moderate and well-defined, reinforcing the dominant influence of dry-season atmospheric stability on solar availability.

Appendix C.3: Sankuru

Data analysis in the Sankuru covers the following territories: Katako-Kombe, Kole, Lodja, Lomela, Lubefu, and Lusambo, while table C.3 presents monthly SD values for these territories.

Table C.3: Monthly SD for Sankuru

Latitude	3°24'S	3°28'S	3°29'S	2°17'S	4°44'S	4°58'S	Averages
Longitude	24°25'E	22°27'	23°26'E	23°16'E	24°26'E	23°26"E	
Area (Km²)	25,942	16,192	12,054	26,346	12,229	16,508	
City/Town	Katakokombe	Kole	Lodja	Lomela	Lubefu	Lusambo	
January	5.9	5.8	5.8	5.9	6.0	5.7	5.9
February	5.9	5.7	5.8	5.9	6.1	5.7	5.9
March	5.4	5.3	5.3	5.5	5.7	5.4	5.4
April	5.0	4.7	4.7	4.6	5.6	5.0	4.9
May	5.3	5.0	5.0	4.7	6.2	5.6	5.2
June	6.6	6.5	6.5	5.9	7.2	7.1	6.5
July	7.1	7.0	7.1	6.5	7.5	7.5	7.0
August	6.1	6.1	6.0	5.4	6.6	6.5	6.0
September	5.6	5.5	5.3	5.0	5.6	5.5	5.4
October	5.3	5.2	5.1	4.9	5.3	5.0	5.1
November	5.0	4.9	4.8	4.7	5.1	4.9	4.9
December	5.2	5.0	5.0	5.0	5.5	5.2	5.1
Averages	5.7	5.6	5.5	5.3	6.0	5.8	5.6

Source: Compiled from [14].

Compared to other districts of the Province Kasaï-Oriental, Sankuru exhibits slightly lower SD values and greater spatial variability (≈5.3–6.0 h/d). This suggests a stronger influence of localized climatic conditions, possibly linked to higher cloud persistence or humidity levels. Figure C.3 illustrates the monthly evolution of SD across Sankuru territories.

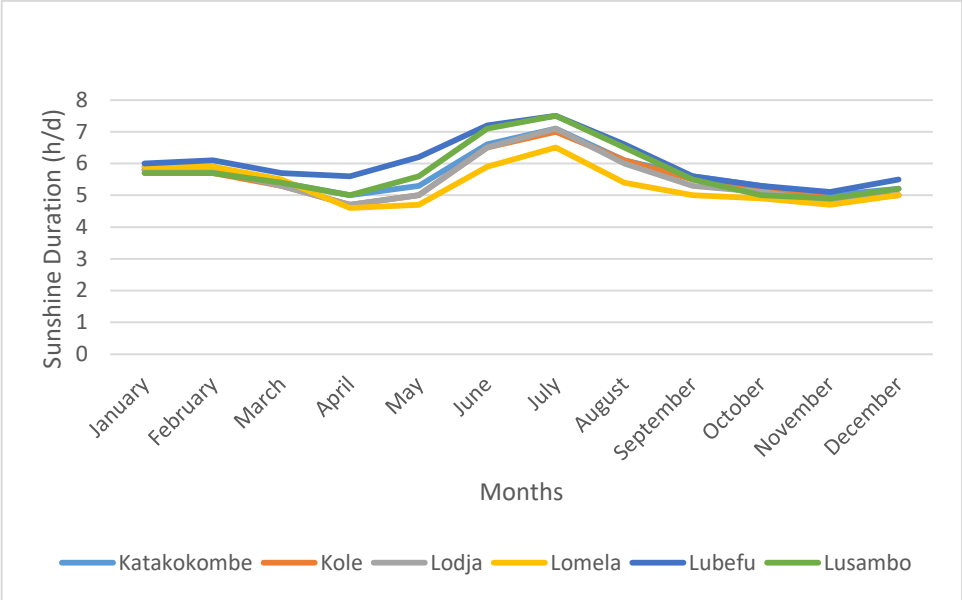

Figure C.3: Temporal Trend of monthly SD for Sankuru

The dispersion between curves is more pronounced than in other regions, indicating reduced spatial uniformity. This suggests that localized calibration may be necessary when modeling solar radiation in Sankuru

Analytical Observations

The analytical observations for Sankuru can be summarized as follows:

- Sankuru presents the lowest annual SD among the three daughter provinces, with a weighted average of approximately 5.6 h/day.
- The highest annual SD is observed in Lubefu (≈6.0 h/day), while the lowest is recorded in Lomela (≈5.3 h/day).
- The monthly peak occurs in July (≈7.0 h/day), whereas the minimum is reached in November (≈4.9 h/day).

Compared to Lomami, Sankuru exhibits slightly greater spatial dispersion, which may be attributed to the higher forest density, the increased atmospheric humidity, the central basin climatic influence.

APPENDIX D:

KATANGA-SPECIFIC SOLAR DATA RESULTS

Appendix D.1: Haut-Katanga

The analysis includes Lubumbashi, Kasumbalesa, Kipushi, Likasi, Pweto, and Sakania. Table 4.1 presents the monthly averages of SD across selected locations in Haut-Katanga.

Table 4.1: Monthly SD for Haut Katanga

Latitude	10°52'S	10°24'S	11°46'S	10°59'00"S	11°40'00"S	8°38'S	10°52S	Weighted Average of SD
Longitude	26°38'E	28°36'E	27°14'E	26°44'00"E	27°29"00E	28°54'E	26°38'E	
Area (Km²)	22,235	24,691	8,969	280	747	24,933	22,421	
Cities/Towns	Kambo.	Kasenga	Kipushi	Likasi	Lubum.	Mitwaba	Pweto	
January	5.6	6.5	5.8	6.1	6.0	5.5	6.8	6.1
February	5.6	6.4	5.7	6.1	5.9	5.8	6.7	6.1
March	5.0	6.0	5.2	5.5	5.4	5.3	6.3	5.6
April	5.5	6.3	5.8	5.9	5.9	5.9	6.6	6.1
May	7.0	7.6	7.4	7.5	7.4	7.4	7.7	7.4
June	7.7	7.7	7.6	7.7	7.6	7.7	7.8	7.7
July	7.7	7.8	7.7	7.7	7.7	7.8	7.8	7.8
August	7.9	7.9	7.9	7.9	7.9	7.9	7.9	7.9
September	8.0	8.1	8.1	8.1	8.1	7.7	7.9	7.9
October	7.8	8.2	8.1	8.0	8.1	6.7	7.6	7.6
November	6.5	7.4	7.0	7.1	7.4	5.6	6.6	6.6
December	5.6	6.5	5.7	6.2	6.0	5.3	6.5	5.9

The data reveal relatively high SD values with moderate spatial variability across the district. Peak values occur between August and September, reflecting the dry-season maxima typical of this tropical continental region. Localized divergences indicate altitude and land cover effects, but large-scale atmospheric conditions primarily control SD.

Figure D.1 illustrates the temporal evolution and inter-site variability of MASD across Haut Katanga.

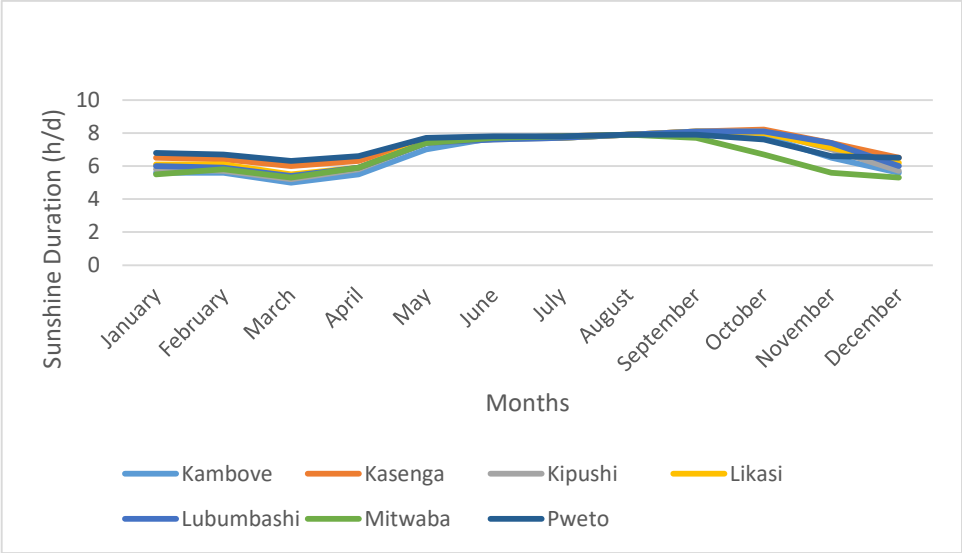

Figure D.1:Temporal Trend of Monthly SD for Haut-Katanga

Figure D.1 highlights a strong seasonal signal and confirms the coherence of SD patterns among sites. Minor differences between curves suggest local modulation by topography, reinforcing the importance of considering both regional and local factors for solar resource assessment.

Analytical Observations

The results for Haut-Katanga may be summarized as follows:

- Haut-Katanga records one of the highest SD regimes in the country.
- The annual weighted mean SD is approximately 6.8 h/day, corresponding to nearly 2,482 sunshine hours per year.
- The maximum monthly SD occurs in July (≈8.1 h/day), while the minimum is observed in December (≈5.4 h/day).

The seasonal structure is clearly marked by strong increase toward the dry season (May–July) and pronounced stability during peak dry months. Gradual decline toward the rainy season (November–January). Spatial variability across territories remains moderate (≈0.6 h/day range), indicating a coherent regional solar regime dominated by dry subtropical atmospheric conditions.

Annexe D.2: Haut Lomami

The SD data for the folloing locations were analyzed: the City of Bukama and the territories of Kabongo, Kamina, Kaniama and Malemba-Nkulu. The findings are summarized in the table 4.2.

Table 4.2: Monthly SD for Haut Lomami

Latitude	9°12'S	7°22'S	8°23'55"S	7°31'S	8°00'S	Avergaes
Longitude	25°50'E	25°35'E	24°39'32"E	24°11'E	26°50'E	
Area (Km²)	19 398	20 898	41 887	13 894	15 298	
Cities/Towns	Bukama	Kabongo	Kamina	Kaniama	Malemba-Nkulu	
January	5.1	7.1	5.4	5.6	4.9	5.6
February	5.4	7.1	5.9	6.1	5.4	5.7
March	5.0	6.5	5.8	5.8	5.6	5.3
April	6.5	6.5	6.7	6.5	6.9	6.4
May	7.8	7.4	7.7	7.7	7.8	7.8
June	7.7	7.8	7.7	7.8	7.7	7.8
July	7.8	7.9	7.8	7.8	7.8	7.8
August	8.0	8.0	8.0	8.0	8.0	7.9
September	7.8	8.0	8.0	8.0	8.0	7.5
October	7.0	7.4	7.6	7.4	7.3	6.5
November	5.3	6.3	6.5	6.3	5.9	5.3
December	4.9	5.6	5.3	5.6	4.9	5.2
Averages	6.5	7.1	6.9	6.9	6.7	6.6

The curves are nearly overlapping, indicating a highly homogeneous solar regime. SD peaks during June–September, characteristic of the dry season, supporting the suitability of generalized solar modeling.

Figure D.2 presents the temporal trends of SD across Haut-Lomami.

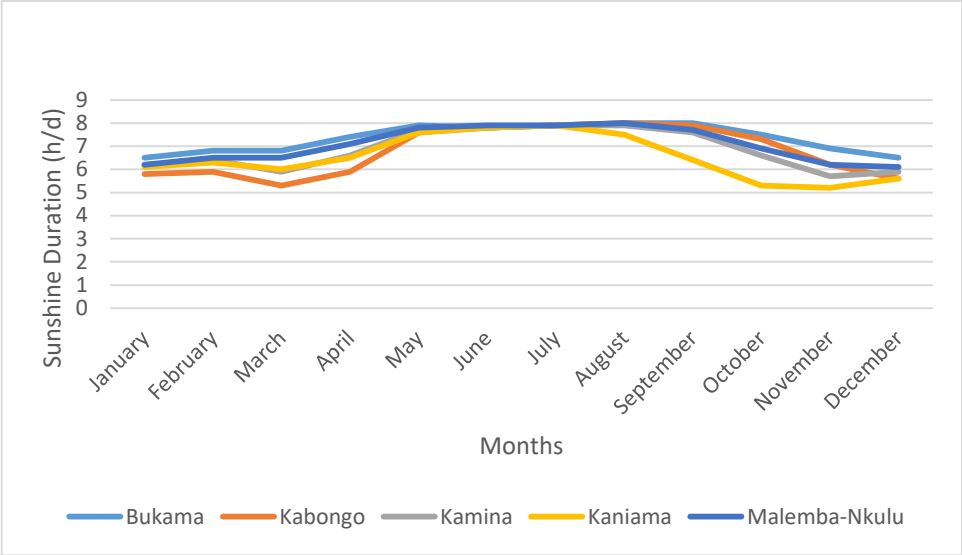

Figure D.2: Temporal Trend of monthly SD for Haut Lomami

Figure D.2 confirms uniform seasonal behavior with minimal spatial deviation. This suggests that regional climatic control dominates, providing stable conditions for PV system planning.

Analytical Observations

Analytical findings for Haut Lomami are outlined as follows:

— Haut-Lomami presents an annual weighted SD of approximately 6.6 h/day.
— The highest monthly SD is recorded in July (≈8.0 h/day), while the lowest occurs in November (≈4.9 h/day).
— Compared to Haut-Katanga, the seasonal amplitude remains similar but slightly attenuated.
— Spatial dispersion between territories is minimal, suggesting strong climatic homogeneity across the province.
— The upward concavity of the SD curve during the dry season again confirms the dominance of atmospheric transparency rather than astronomical declination effects.

Appendix D.3: Lualaba

The SD data for these locations were analyzed: the City of Kolwezi and the territories of Dilolo, Kapanga, Lubudi, Mutshathsa and Sandoa. These SD are presented in Table D.3.

Table D.3: Monthly SD for Lualaba (h/day)

Latitude	10°41'12"S	10°42'S	10°43"00"S	9°55'S	10°39'S	9°42'S	Averages
Longitude	22°20'37"E	22°39'E	25°28'00^{E}	25°58'E	24°27'E	22°52'E	
Area (Km²)	25,648	25,509	213	18,939	18,859	25,557	
Cities/Towns	Dilolo	Kapanga	Kolwezi	Lubudi	Mutshatsha	Sandoa	
January	5.1	7.1	5.4	5.6	4.9	5.6	5.7
February	5.4	7.1	5.9	6.1	5.4	5.7	6.0
March	5.0	6.5	5.8	5.8	5.6	5.3	5.6
April	6.5	6.5	6.7	6.5	6.9	6.4	6.5
May	7.8	7.4	7.7	7.7	7.8	7.8	7.7
June	7.7	7.8	7.7	7.8	7.7	7.8	7.8
July	7.8	7.9	7.8	7.8	7.8	7.8	7.8
August	8.0	8.0	8.0	8.0	8.0	7.9	8.0
September	7.8	8.0	8.0	8.0	8.0	7.5	7.8
October	7.0	7.4	7.6	7.4	7.3	6.5	7.1
November	53	6.3	6.5	6.3	5.9	5.3	5.8
December	4.9	5.6	5.3	5.6	4.9	5.2	5.2
Averages	6.5	7.1	6.9	6.9	6.7	6.6	6.8

Spatial variability is slightly higher than in Haut-Lomami but remains limited. SD maxima occur in August–September, minima in December, reflecting the transition between wet and dry seasons. Figure D.3 shows the temporal evolution of SD across Lualaba.

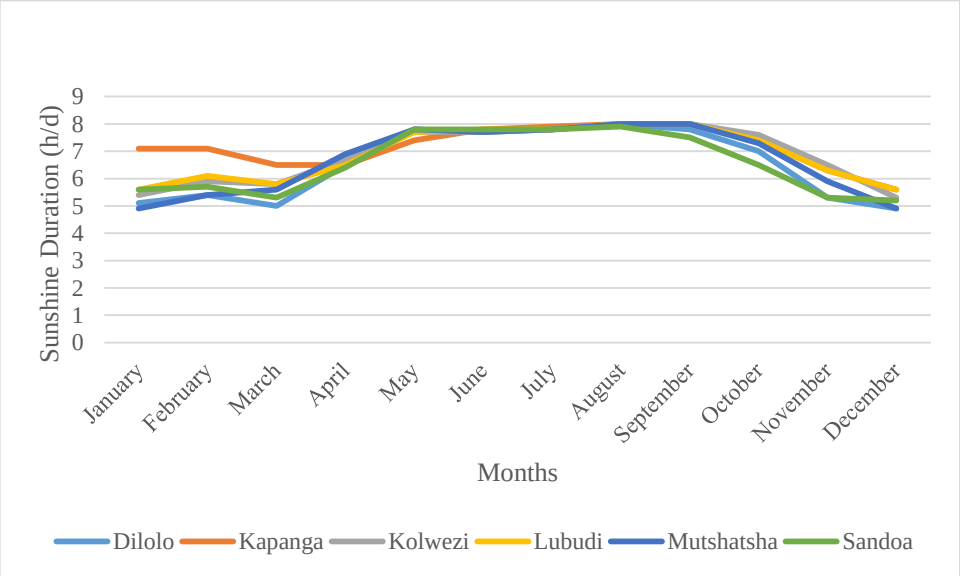

Figure D.3: Temporal Trend of monthly SD for Lualaba

Figure D.3 confirms consistent seasonal behavior and indicates cloud cover variability as the main driver of SD fluctuations. This reinforces the need for temporal modeling adjustments in PV simulations.

Analytical Observations

- Lualaba exhibits an annual weighted SD of approximately 6.5 h/day.
- The peak SD is reached in July (≈8.0 h/day), while the minimum is observed in December (≈4.9 h/day).
- The province shows slightly higher variability between western (Dilolo, Kapanga) and central zones (Kolwezi), possibly reflecting localized moisture dynamics.

  Nevertheless, the overall SD regime remains highly favorable for solar exploitation.

District of Tanganyika

The territories analyzed include Kalemie, Kongolo, Kabalo, Manono, Moba, and Nyunzu. Table 3.21 presents SD values for selected locations in Tanganyika.

Table 3.21: Monthly SD for Tanganyika

Latitude	6°03'S	5°56'S	5°24'S	7°18'S	7°04'S	5°57'S	Averages
Longitude	26°55'E	29°11'E	27°00'E	27°25'E	29°43'E	28°01'E	
Area (Km²)	14 779	21 155	13 171	34 615	23 079	15 471	
Cities/Towns	Kabalo	Kalemie	Kongolo	Manono	Moba	Nyunzu	
January	5.4	7.1	5.4	5.4	7.1	5.7	6.1
February	5.8	7.2	5.9	5.9	7.1	6.0	6.4
March	5.6	6.8	5.6	5.9	6.5	5.9	6.1
April	6.3	6.5	6.2	6.9	6.5	6.5	6.6
May	7.5	7.4	7.2	7.7	7.4	7.6	7.5
June	7.8	7.9	7.7	7.9	7.8	7.8	7.8
July	7.9	8.0	7.8	7.9	7.9	7.9	7.9
August	7.5	8.0	7.3	7.8	8.0	7.7	7.8
September	6.5	8.0	6.2	7.1	8.0	6.8	7.2
October	5.8	7.7	5.4	6.2	7.8	6.0	6.6
November	5.2	7.2	5.0	5.3	7.1	5.1	5.9
December	5.0	7.0	5.0	5.1	6.8	5.2	5.7
Averages	6.4	7.4	6.2	6.6	7.3	6.5	6.8

Source: Compiled from [14].

SD values are relatively high with noticeable spatial contrasts. Maxima are slightly earlier compared to other districts, reflecting local climatic influences.

Figure D.3 illustrates the seasonal dynamics of SD in Tanganyika.

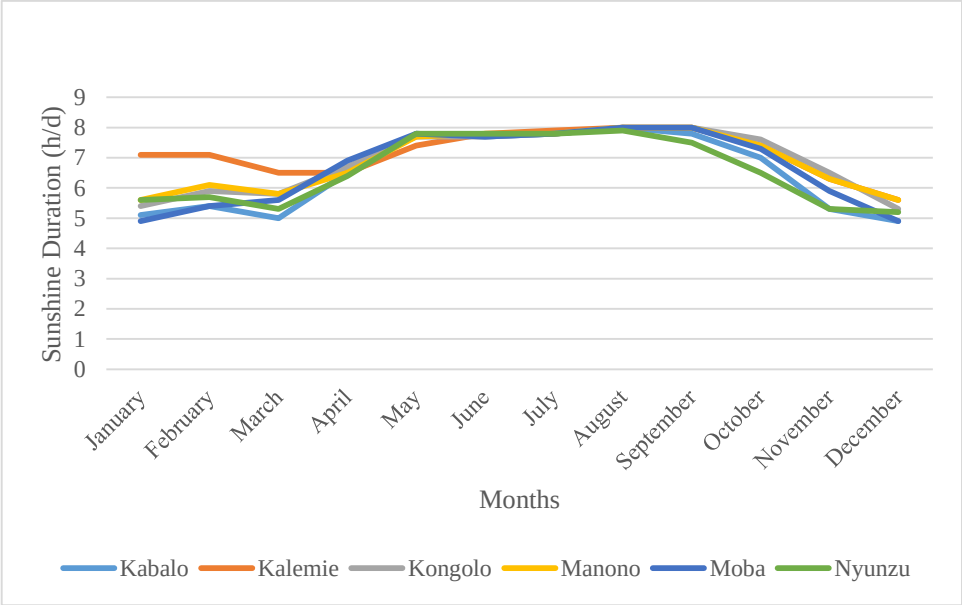

Figure D.3: Temporal Trend of monthly SD for Haut Tanganika

The figure highlights the modulation of SD by proximity to Lake Tanganyika, suggesting that local humidity and cloud formation must be considered in solar resource assessments for PV deployment.

Analytical Observations

- Kalemie is the territory in Tanganyika receiving the highest annual sunshine, with a yearly mean daily SD of 7.4 h/day.
- Kongolo is the territory with the lowest annual sunshine, with a yearly mean daily SD of 6.2 h/day.
- The maximum daily SD occurs in July, reaching 8.0 h/day.
- The minimum daily SD occurs in December, dropping to 5.0 h/day

APPENDIX E:

PROVINCE ORIENTALE-SPECIFIC SOLAR DATA RESULTS

Appendix E.1: Bas-Uele

Data analysis was conducted for the territories of Aketi, Ango, Bambesa, Bondo, Buta and Poko. Table E.1 reports the monthly SD across these territories, providing the empirical basis for assessing spatial uniformity and its implications for solar resource modeling.

Table E.1: Monthly SD for Bas Uele

Latitude	2°45'N	4°01'N	3°28'N	3°49'N	2°49'N	3°06'N
Longitude	23°46'E	25°42'E	25°42'E	23°41'N	24°44'E	26°58'E
Area (Km²)	25,417	34,304	9,130	38,075	8,098	22,909
City/Town	Aketi	Ango	Bambesa	Bondo	Buta	Poko
January	7.1	7.4	7.2	7.3	7.0	7.2
February	6.8	7.2	7.0	7.1	6.8	7.0
March	6.3	6.7	6.3	6.3	6.2	6.3
April	5.6	6.0	5.5	5.6	5.3	5.4
May	5.2	5.4	5.0	5.2	5.0	4.7
June	5.3	5.4	5.0	5.3	5.0	4.7
July	5.5	5.6	5.2	5.3	5.3	4.8
August	5.0	5.1	4.8	4.8	4.8	4.6
September	4.7	4.7	4.5	4.6	4.6	4.3
October	4.4	4.4	4.1	4.2	4.2	4.0
November	4.6	5.3	4.8	4.7	4.4	4.7
December	6.2	6.8	6.5	6.5	6.0	6.5
Averages	5.6	5.9	5.5	5.6	5.4	5.3

Source: Compiled from [14].

The narrow SD range (≈5.3–5.9 h/day) indicates weak spatial gradients and a quasi-homogeneous radiative regime. This suggests that cloud cover persistence and convective activity operate at a mesoscale level, leading to spatially consistent solar attenuation. From a

modeling perspective, such homogeneity is advantageous, as it reduces the need for complex spatial parameterization when estimating GSI from SD-based models.

Figure E.1 illustrates the temporal evolution of SD across Bas-Uele, highlighting seasonal variability relevant for irradiance reconstruction.

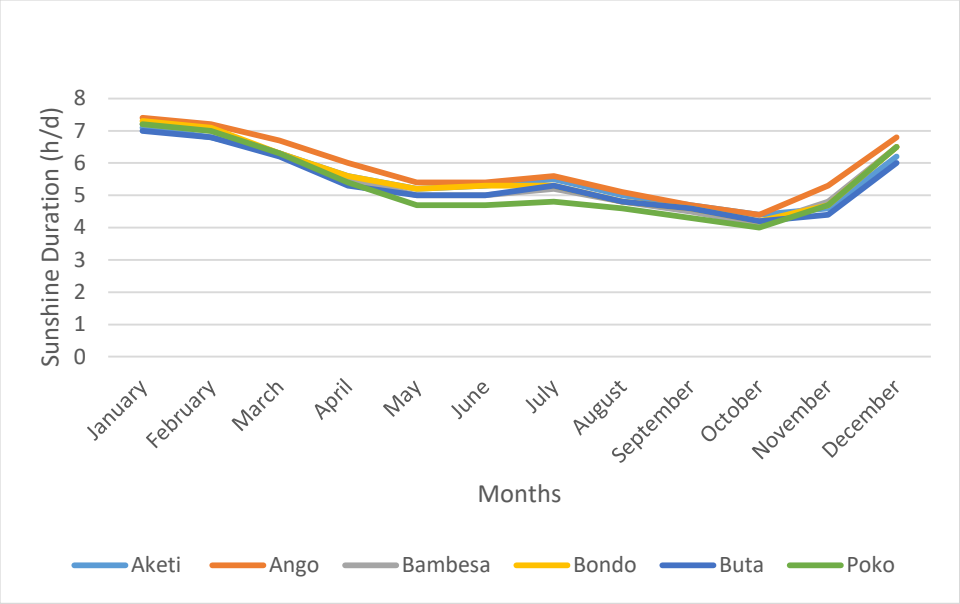

Figure E.1: Temporal Trend of monthly SD for Bas-Uele

The highly synchronized seasonal pattern, with maxima in January–February and minima in October, reflects the dominant control of the ITCZ on cloud dynamics. This temporal regularity provides a robust basis for calibrating empirical SD–irradiance relationships, as it ensures predictable seasonal modulation of atmospheric transmissivity.

Appendix E2: Haut-Uele

Table E.2 presents the monthly SD distribution across Haut-Uele, enabling the assessment of spatial variability and its implications for solar resource estimation.

Table E.2: Monthly averages of SD for Haut-Uele District

Latitude	3°37'N	3°44'N	2°46'N	3°40'N	2°09'N	3°02'N
Longitude	28°34'E	29°43'E	27°37'07"E	27°53'E	28°00'E	29°31'E
Area (Km²)	32,446	12,702	9,406	9,369	9,838	16,463
January	7.6	8.0	7.0	7.7	6.8	7.7
February	7.4	7.8	6.7	7.4	6.5	7.5
March	6.8	7.4	5.9	6.9	5.6	6.9
April	6.2	6.5	5.0	6.2	4.9	6.3
May	5.3	6.2	4.5	5.3	4.4	5.8
June	5.0	6.4	4.4	5.0	4.3	5.6
July	5.2	6.2	4.4	5.3	4.4	5.6
August	5.1	5.6	4.3	5.1	4.3	5.6
September	4.7	5.6	4.1	4.7	4.1	5.1
October	4.5	5.5	3.9	4.5	4.0	5.0
November	5.5	6.5	4.4	5.5	4.3	5.9
December	7.1	7.7	6.1	7.1	5.5	7.3
Averages	5.9	6.6	5.1	5.9	4.9	6.2

Source: Table compiled by ourselves on basis of data taken from [14].

The higher SD levels (up to 6.6 h/day) and moderate dispersion suggest improved atmospheric clarity relative to Bas-Uele. This indicates reduced cloud persistence and enhanced solar transmissivity. For irradiance modeling, this implies higher expected global solar radiation and potentially lower model bias when using SD-based empirical correlations.

Figure E.2 depicts the temporal variability of SD in Haut-Uele, emphasizing both seasonal forcing and spatial differentiation.

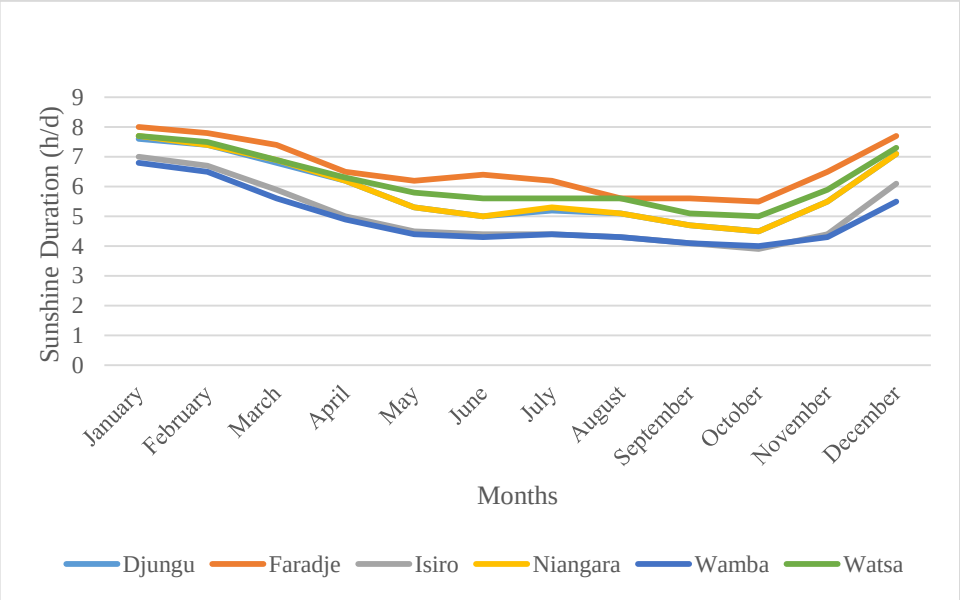

Figure E.2: Trend of monthly SD for Haut Uele District

The increased amplitude of seasonal variation compared to Bas-Uele suggests stronger radiative contrast between wet and dry periods. This enhances the sensitivity of SD-based irradiance models, making Haut-Uele a suitable region for validating model responsiveness to seasonal atmospheric changes.

Appendix E.3: Ituri

In Ituri, data analysis was carried out for the territories of Aru, Djugu, Irumu, Mahagi, Mambassa. Table E.3 provides monthly SD values across the Ituri District, highlighting spatial heterogeneity relevant to solar resource modeling.

Table E.3: Monthly SD for Ituri

Latitude	2°53'N	1°564N	1°27'N	2°18'N	1°22'N
Longitude	30°51'E	30°29'E	29°52'E	30°59'E	29°03'E
Area (Km²)	6,740	8,184	8,730	5,221	36,783
City/Town	Aru	Djugu	Irumu	Mahagi	Mambasa
January	7.9	6.8	7.2	8.0	6.8
February	7.9	6.7	7.1	8.0	6.7
March	7.6	5.4	6.4	7.8	5.7
April	7.1	5.1	6.1	7.5	5.0
May	6.9	5.6	5.8	7.6	4.4
June	6.8	5.7	5.4	7.9	4.2
July	6.8	5.6	5.4	7.8	4.2
August	6.4	5.2	5.2	7.7	4.1
September	6.3	4.7	4.9	7.6	3.8
October	6.3	4.4	4.7	7.4	3.8
November	6.9	4.6	5.1	7.4	4.1
December	7.6	5.9	6.5	7.8	5.7
Averages	7.0	5.5	5.8	7.7	4.9

Source: Compiled from [14].

The wide SD range (≈4.9–7.7 h/day) reveals strong spatial heterogeneity, likely driven by topographic complexity and localized convective processes. This variability introduces significant challenges for irradiance estimation, as uniform SD–irradiance relationships may not hold across the district without spatial calibration.

Figure E.3 shows the temporal evolution of SD across Ituri, illustrating the coexistence of distinct local regimes.

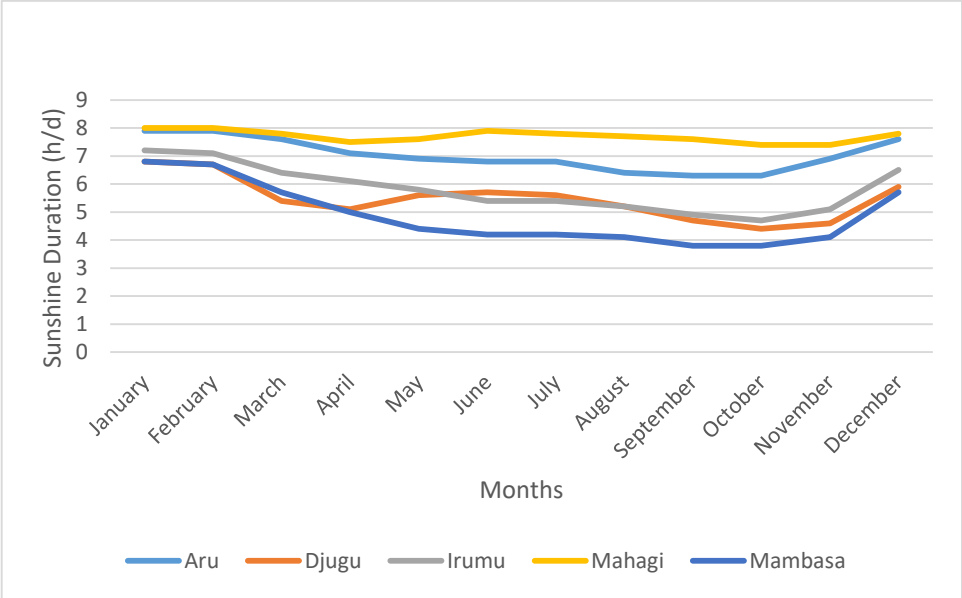

Figure E.3: Temporal Trend of Monthly SD for Ituri

The divergence between curve patterns indicates multiple microclimatic regimes within the same district. This suggests that irradiance modeling in Ituri requires region-specific parameterization, as a single empirical model may fail to capture localized atmospheric effects influencing solar radiation.

Appendix E. 4: Tshopo

For Tshopo District, Kisangani and the territories of Bafwasende, Banalia, Basoko, Isangi, Opala, and Yahuma were selected. Table E.4 summarizes their monthly SD values, representing the most cloud-affected regime within Province Orientale.

Table E.4: Monthly SD for Tshopo

Latitude	1° 01′ N	1° 32′ N	1° 14′ N	0° 47′ N	0° 31′ 09″N	0° 37′ SUD	0° 21′ SUD
Longitude	27° 10′ E	25° 20′ EST	23° 36′ EST	24° 14′ EST	25° 11′ 46″	24° 21′ EST	25° 25′ EST
Area (Km²)	48 818	23 631	22 677	13 769	1 910	26 453	41 537
City/Town	Bafwasende	Banalia	Basoko	Isangi	Kisangani	Opala	Ubundu
January	6.7	6.3	7.0	6.5	6.0	6.1	5.9
February	6.5	6.3	6.8	6.4	6.1	6.1	5.9
March	5.7	5.7	6.4	5.9	5.6	5.7	5.4
April	4.9	5.0	5.6	5.3	4.8	4.9	4.7
May	4.3	4.5	5.4	4.9	4.4	4.6	4.4
June	4.1	4.7	5.6	5.3	4.7	5.3	4.7
July	4.3	5.0	5.8	5.6	5.0	5.7	5.1
August	4.1	4.5	5.2	5.0	4.5	5.0	4.7
September	4.1	4.5	5.3	5.0	4.5	4.9	4.5
October	4.2	4.3	5.0	4.7	4.4	4.7	4.4
November	4.1	4.0	4.7	4.4	4.1	4.5	4.2
December	5.6	5.3	6.1	5.5	5.0	5.0	4.9
Averages	4,9	5.0	5.7	5.4	4.9	5.2	4.9

Source: Compiled from [14].

The persistently low SD values (≈4.9–5.7 h/day) indicate strong atmospheric attenuation due to continuous cloud cover and high humidity. This implies reduced solar irradiance levels and highlights the limitations of SD-based models, which may underestimate the impact of diffuse radiation under such conditions.

Figure E.4 illustrates the temporal SD dynamics in Tshopo, with implications for low-irradiance environments.

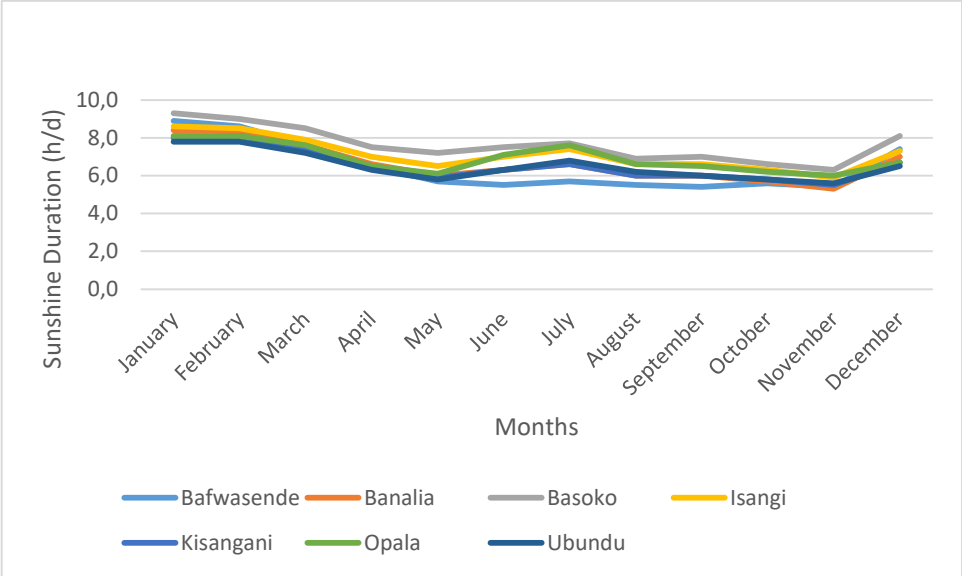

Figure E.4: Temporal Trend of monthly SD for Tshopo

The flattened seasonal profile confirms limited variability in atmospheric transmissivity throughout the year. For modeling purposes, this suggests a relatively stable but low irradiance regime, where model calibration must account for persistent cloud-induced attenuation rather than seasonal extremes.